

1 **Evolutionary ecology of ungulates ~~Ecological evolution~~ in northern Iberia**
2 **(~~SW Europe~~) during the Late Pleistocene through isotopic analysis on**
3 **~~ungulate teeth~~**

4
5 **Mónica Fernández-García^{1,2,3} (*), Sarah Pederzani^{2,3,4}, Kate Britton^{3,5}, Lucía Agudo-Pérez¹,**
6 **Andrea Cicero¹, Jeanne Marie Geiling¹, Joan Daura^{6,4}, Montserrat Sanz-Borrás^{4,6}, Ana B.**
7 **Marín-Arroyo^{1(*)}**

8 1 Grupo de I+D+i EVOADAPTA (Evolución Humana y Adaptaciones durante la Prehistoria), Departamento de Ciencias Históricas,
9 Universidad de Cantabria, 44. 39005 Santander, Spain

10 [2 Departament de Prehistòria, Arqueologia i Història Antiga, Universitat de València, Av. Blasco Ibañez 28, 46010 Valencia, Spain.](#)

11 [3 Institut Català de Paleoecologia Humana i Evolució Social \(IPHES-CERCA\), zona Educacional 4 Edifici W3, Campus Sescelades](#)
12 [URV, 43007 Tarragona, Spain.](#)

13 [2 3 4 Archaeological Micromorphology and Biomarkers Laboratory \(AMBI Lab\), Instituto Universitario de Bio-Orgánica- "Antonio](#)
14 [González", Universidad de La Laguna, 38206 San Cristóbal de La Laguna, Tenerife, Spain](#)

15 [5 Department of Archaeology, University of Aberdeen, Aberdeen AB24 3UF, United Kingdom](#)

16 [6 4 Grup de Recerca del Quaternari \(GRQ-SERP\), Department of History and Archaeology, Universitat de Barcelona, Grup de](#)
17 [Recerca del Quaternari \(GRQ-SERP\), C/Montalegre 6-8, 08001 Barcelona-08004, Spain.](#)

18 (*) Corresponding authors: anabelen.marin@unican.es, monica.fernandez.garcia.90@gmail.com

Field Code Changed

Field Code Changed

19
20 **Abstract**

21 During the Late Pleistocene, stadial and interstadial fluctuations affected vegetation, fauna, and human
22 groups that were forced to cope with these pronounced ~~spatial and temporal~~ climatic and environmental
23 changes ~~in time and space~~. These changes were especially abrupt during the Marine Isotopic Stage (MIS)
24 3. ~~However, little is still known about the local and regional climatic conditions experienced by hominins in~~
25 ~~Europe.~~ Here, we reconstruct the climatic trends in northern Iberia considering the stable isotopic
26 composition of ungulate skeletal tissues found in archaeological deposits dated between 80 to 15 ~~ka-000~~
27 cal BP. The carbon and oxygen isotopic composition preserved in the carbonate fraction of tooth enamel
28 provides a reliable and high-resolution proxy of the food and water consumed by these animals, which is
29 indirectly related to the local vegetation, environment, and climate, allowing us to estimate
30 paleotemperatures and rainfall ~~data intensity~~. This study presents ~~new isotope data from~~ 44 bovine, equid,
31 and cervid teeth from five archaeological sites in the Vasco-Cantabrian region (El Castillo, ~~El Otero~~, Axlor,
32 Labeko Koba, Aitzbitarte III ~~interior and El Otero~~.) and one in ~~the Mediterranean area~~ northeastern Iberia
33 (Canyars), where human evidence is attested from the Mousterian to the Magdalenian. The carbon isotope
34 values reflect animals feeding on ~~diverse~~ C3 plants ~~with a mix-feeder diet mainly developed~~ in open
35 environments, ~~and point to. However, carbon isotope value ranges point to~~ differentiated ecological niches
36 for equids and bovines, especially during the Aurignacian in the Vasco-Cantabrian region. Temperature
37 estimations based on oxygen isotopic compositions and rainfall obtained from carbon isotopic compositions
38 indicate colder and more arid conditions than nowadays ~~for the human occupations~~ from the Late Mousterian
39 to the Aurignacian. The contemporary ~~Mediterranean-northeastern Iberia~~ site shows slightly lower
40 temperatures related to an arid period when animals mainly graze in open landscapes. In the Vasco-
41 Cantabrian region, during the MIS2, the Gravettian data reflect a landscape opening, whereas the
42 Magdalenian points to warmer ~~conditions~~ (but still arid) ~~conditions~~.

43 **Keywords:** Middle and Upper Palaeolithic; Neanderthal; Homo sapiens, palaeoecology; geochemistry

44 1. Introduction

45 Understanding ~~the~~ local and regional climatic ~~evolution-variability~~ during the Late Pleistocene in southern
46 Europe is crucial for assessing the potential impact of climate on the adaptation and decline of Neanderthals,
47 ~~as well as~~ ~~and~~ the subsequent expansion and resilience of Anatomically Modern Humans during the Upper
48 Paleolithic (e.g., D'Errico and Sánchez Goñi, 2003; Finlayson and Carrión, 2007; Sepulchre et al., 2007;
49 Staubwasser et al., 2018). During the Late Pleistocene, the climatic records demonstrate stadial and
50 interstadial continuous fluctuations during the Marine Isotope Stage 3 (MIS 3, ca. 60-27 ka) and MIS 2 (ca.
51 27-11 ka). Human groups had to face those episodes, which affected ~~different~~ vegetation and fauna ~~to~~
52 ~~different extents~~, depending on the region. Northern Iberia is a key study area due to the abundance of well-
53 preserved archaeological caves and rock shelters where, in the last decade, an updated and
54 multidisciplinary approach has been applied to disentangle how changing environmental conditions affected
55 the subsistence dynamics of Middle and Upper Paleolithic hominins. Recent chronological, technological,
56 ~~and~~ subsistence studies ~~and~~ ~~ecological reconstructions~~ are revealing a ~~wider regional circumstance~~ more
57 complex ~~regional panorama~~ than previously known (e.g., Klein et al., 2023; Sánchez Goñi, 2020;
58 Timmermann, 2020; Vidal-Cordasco et al., 2022, 2023).

59 The Vasco-Cantabrian region, located in northwestern Iberia, is subject to the influence of Atlantic climatic
60 conditions, ~~and has~~ ~~where~~ ~~been widely~~ ~~recently~~ ~~has been~~ ~~evaluated~~ ~~debated~~ ~~as a region that was~~
61 ~~significantly~~ ~~the~~ impacted ~~of by~~ the glacial-interglacial oscillations during ~~the~~ MIS3 (Vidal-Cordasco et al.,
62 2022). Modelling of traditional environmental proxies (small vertebrates and pollen) ~~associated to~~ ~~from~~
63 archaeo-paleontological deposits show a progressive shift in the climatic conditions with decreasing
64 temperatures and rainfall levels detected during the late Mousterian (Fernández-García et al., 2023).
65 Ecological alterations have been observed in large mammals, such as niche partitioning between horses
66 and cervids (Jones et al., 2018), a decrease in the available biomass for secondary consumers, and
67 consequently, ~~a decrease~~ ~~reduction~~ in ~~the~~ ~~ungulate~~ ~~herbivores~~ carrying capacity ~~with regards to~~ ~~ungulates~~
68 ((Jones et al., 2018; Vidal-Cordasco et al., 2022). Cold and arid conditions are ~~maintained~~ ~~observed~~ during
69 the Aurignacian and the Gravettian until the onset of MIS2. Afterwards, during the Last Glacial Maximum
70 (LGM, 23-19 ka), the global climatic deterioration associated with this glacial phase results in colder and
71 more arid conditions in the region, with a predominance of open landscapes. However, this region still
72 provided resources for human ~~exploitation~~ survival acting as a refugia ~~area~~ with more humid conditions in
73 comparison to the Mediterranean area (Cascalheira et al., 2021; Fagoaga, 2014; Fernández-García et al.,
74 2023; Garcia-Ibaibarriaga et al., 2019a; Lécuyer et al., 2021; Posth et al., 2023). By the end of the LGM, a
75 climate amelioration and a moderate expansion of the deciduous forest are documented from the late
76 Solutrean through the Magdalenian (Garcia-Ibaibarriaga et al., 2019a; Jones et al., 2021).

77 In contrast, northeastern Iberia is influenced by the Mediterranean climate. ~~During~~ ~~The~~ MIS 3, ~~human~~
78 ~~settlement in this region have been linked this period in~~ ~~temperatures in this region has frequently been~~
79 ~~described as~~ ~~often~~ ~~were~~ ~~characterised as being to by~~ ~~cooler~~ temperatures ~~and with~~ ~~and with~~ ~~higher~~
80 ~~rainfall~~, ~~higher~~ ~~rainfall~~ compared to the present, ~~but~~ ~~and~~ ~~less~~ ~~with~~ ~~climatic~~ ~~fluctuations~~ ~~described as being~~
81 ~~less~~ pronounced ~~climatic~~ ~~fluctuations~~ ~~when~~ compared to the Vasco-Cantabrian region ~~in the same period~~
82 (López-García et al., 2014; Fernández-García et al., 2020; Vidal-Cordasco et al., 2022). ~~Archaeobotanical~~
83 ~~and small vertebrate evidence~~ ~~Small vertebrate communities and archaeobotanical evidence~~ indicate
84 relatively stable climatic conditions, but also ~~suggest~~ the persistence of open forests during the Middle to
85 Upper Paleolithic transition, as ~~found~~ in northwestern Iberia (Allué et al., 2018; Ochando et al., 2021).
86 However, certain ~~archaeological~~ records indicate specific climatic ~~excursion~~ ~~episodes~~, such as increased
87 aridity and landscape opening during Heinrich Events 4 and 5 (e.g., Álvarez-Lao et al., 2017; Daura et al.,
88 2013; López-García et al., 2022; Ruffi et al., 2018).

89 ~~These multi-proxy studies have significantly expanded our understanding of the environmental evolution in~~
90 ~~Iberia, alongside proxies derived from marine core records in Iberia margins~~ (Fourcade et al., 2022; Martrat
91 et al., 2004; Naughton et al., 2007; Roucoux et al., 2001; Sánchez-Goñi et al., 1999, 2009) ~~and other regional~~
92 ~~paleoclimatic records sourced from local natural deposits~~ (e.g., Pérez-Mejías et al., 2019; Moreno et al.,

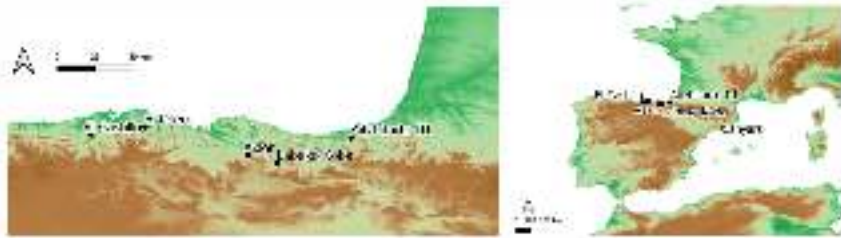
93 2010, 2012; González-Sampérez et al., 2020; Ballesteros et al., 2020) ~~thereby providing a valuable~~
94 ~~framework for understanding environmental evolution.~~ However, the availability of proxies enabling the
95 ~~establishment of direct connections between these environmental shifts and human activities remains~~
96 ~~limited.~~

97

98 ~~These~~ While multi-proxy studies have significantly expanded our understanding of the environment in Iberia.
99 ~~However,~~ there is still limited availability of high-resolution proxies directly linked ~~directly~~ to human activity.
100 In this study, we ~~propose to~~ investigate the ~~palaeo~~ecologically and ~~palaeo~~environmental dynamics of ~~past~~
101 ~~ungulates of this region in northern Iberia~~ during the late Middle and Upper Paleolithic by measuring the
102 carbon and oxygen isotopic composition ($\delta^{13}\text{C}$, $\delta^{18}\text{O}$) of bioapatite carbonates ($\delta^{13}\text{C}_{\text{carb}}/\delta^{18}\text{O}_{\text{carb}}$) preserved
103 in archaeological mammal teeth. ~~These analyses provide high-resolution snapshots of ecological~~
104 ~~information from animals accumulated during human occupations at the cavesites.~~ Tooth enamel forms
105 incrementally and does not biologically remodel (Kohn, 2004; Passey and Cerling, 2002), in contrast to other
106 ~~body~~ tissues such as bone, which implies that the isotope values measured on them reflect the animal
107 diet and water sources consumed during its mineralisation, around one to two years of ~~animal life in our~~
108 ~~study-species~~ life for the species included in our study (bovids, equids, cervids) (e.g., Hoppe et al., 2004;
109 Pederzani and Britton, 2019; Ambrose and Norr, 1993; Luz et al., 1984). ~~The preserved carbon and oxygen~~
110 ~~isotope composition in the carbonate fraction of tooth enamel offers a high-resolution record of the dietary~~
111 ~~choices of the plants and water animals consume, which indirectly reflects the vegetation, environmental~~
112 ~~conditions, and climate.~~ The preserved carbon isotope composition ~~rely on dietary choices of animals~~
113 ~~reflecting mainly the type of plant consumed (C3/C4), exposition to light and levels of humidities~~ on animal
114 ~~dietary choices reflecting mainly the type of plant consumed (C3/C4), exposition to light and humidity levels.~~
115 ~~Otherwise, the oxygen isotope composition reflects mainly the environmental water consumed by animals,~~
116 ~~directly by drinking or through diet, which reflects isotopic information derived from water sources as well as~~
117 ~~changes in climatic conditions. Both indirectly provide information on the vegetation and climate that~~ This
118 allows ~~us to estimate~~ past temperatures, rainfall, and moisture ~~levels~~ on a sub-annual scale, returning
119 isotopic ~~information data~~ of the foraging areas where animals were feeding during ~~teeth-teeth~~ formation.

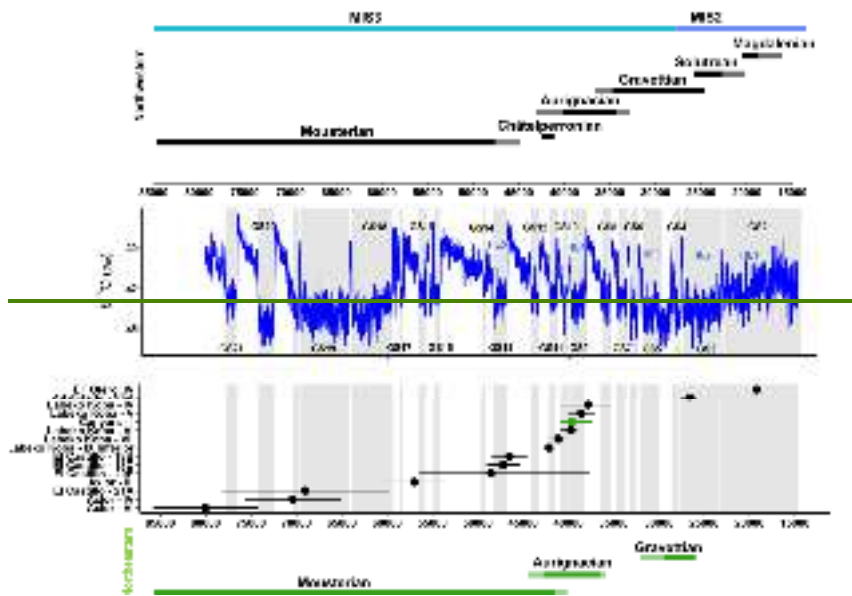
120 By analysing the stable isotopic composition of 44 ungulate teeth obtained from 15 archaeological levels
121 ~~directly~~ associated with human occupation, including El Castillo, ~~El Otero,~~ Axlor, Labeko Koba, Aitzbitarte
122 ~~III interior and El Otero~~ in northwestern Iberia, and Terrasses de la Riera dels Canyars in northeastern Iberia,
123 this study presents novel insights into local and regional environmental and climatic trends ~~associated to~~
124 ~~human presence~~ during the Late Pleistocene (Fig.1; Fig.2; Appendix A). Specifically, it focuses on the Middle
125 to Upper Paleolithic transition in both areas and the post-LGM period in the Vasco-Cantabrian region.

126 The main objectives of this work are: 1) to assess how regional environmental conditions, including changes
127 in moisture and vegetation cover, but also temperatures and rainfall, are recorded ~~in tooth enamel in the~~
128 ~~stable isotopic composition of tooth enamel~~; 2) to ~~approach~~ ~~characterize~~ animal diet and their ecological
129 niches; 3) to obtain quantitative temperature data to compare with available proxies; 4) to characterise
130 seasonal patterns of animals found in the archaeological sites by identifying winter and summer fluctuations.
131 ~~The chronological resolution information in associated to the study studied areas levels for this period allows~~
132 ~~us to correlate regional paleoenvironmental changes with global records.~~



133
134
135
136

Figure 1. Location of the archaeological sites included in this [workstudy](#). From west to east, in the autonomous community of Cantabria, El Castillo, and El Otero; in the Basque Country, Axlor and Aitzbitarte III interior; in Catalonia, Canyars.



137

167 **3.1 Methods: Dating methods**

168 Individual Bayesian age models were built for Canyars, El Castillo, Labeko Koba and Aitzbitarte III interior
169 based on radiocarbon dates (AMS UF and non-UFUF, ABOx-SC and ABA ~~pretreatmentspretreatments on~~
170 ~~bones and charcoal remains with ultrafiltration treatment~~) using OxCal4.4 software (Ramsey, 2009),
171 considering the INTCAL20 calibration curve (Reimer et al., 2020) (Appendix C). The Bayesian model
172 enables the modification of the calibrated Probability Distribution Function (PDF) of individual dates based
173 on the existing relative stratigraphic and other relative age information. A resolution of 20 years was
174 assumed, being a reasonable balance between required accuracy and computational costs. An order
175 function in the OxCal was used to calculate the probability that one PDF predated another, providing
176 information to assess synchronicity and temporal overlap of individual archaeological levels and cultural
177 phases in each of the four separate sites modelled. Dates were organised into a 'Sequence,' and
178 chronological information for each level was grouped into a single 'Phase' with start and end 'boundaries' to
179 bracket each archaeological level. The interval between the start of each level and its end provided the
180 duration of each level. In all cases, convergence was greater than 95%. CQL codes, individual Bayesian
181 models and modelled dates per site are reported in Appendix C.

182 No chronological models were built for El Otero because only a single date was obtained for level IV and El
183 Castillo levels 20E and 21 (ESR dated) and Axlor levels III, IV and VI (OSL dated) because dates go beyond
184 the limit of the radiocarbon. To show the duration of these levels in combination with the other sites and
185 levels, each of these dates was estimated by adding and subtracting the sigma (68% Confidence Interval)
186 from the uncalibrated date. In this way, we estimated the duration of these levels to be beyond 55 ka cal
187 BP.

188 **3.2.4 Tooth sampling**

189 All teeth included were sequentially sampled to reconstruct the complete $\delta^{18}\text{O}_{\text{carb}}$ and $\delta^{13}\text{C}_{\text{carb}}$ intratooth
190 profiles based on enamel carbonate bioapatite. Intratooth sequential sampling was applied to the second
191 and third molars and third and fourth premolars. Bovine and horse teeth sampled exceeded 3-4 cm of crown
192 height to ensure that at least a one-year isotopic record of animal life was obtained (Britton et al., 2019;
193 Hoppe et al., 2004). Samples were taken perpendicular to the growth axis on the tooth where the enamel
194 was best preserved, avoiding, whenever possible taphonomic alterations such as cracks or postdepositional
195 damages. Samples were performed in the ~~labial-buccal~~ face for the lower teeth and the lingual part for the
196 upper ones. The outermost enamel surface was abraded to remove the superficial enamel, calculus,
197 cementum, or concretions adhering to the surface to avoid contaminations. The sequential sampling
198 consisted of straight strips (ca. 8 x 1.5 x 1 mm) covering the width of the selected lobe, approximately every
199 2-3 mm, from the crown to the Enamel-Root-Junction (ERJ). The sample depth covered around 75% of the
200 enamel depth, and dentine inclusion was avoided. A low-revolution variable-speed manual drill was used,
201 equipped with 1 mm diamond-coated drill bits of conical and cylindrical shape. About 10-15mg of enamel
202 powder was collected in each subsample, generating 693 subsamples for IRMS measurements (see
203 complete intratooth profiles in Appendix D).

Formatted: Subscript
Formatted: Subscript

Site	Level - Cultural period	Bovines	Horses	Red deer	Teeth	Subsamples
Axlor	VI - Mousterian	2			2	32
	IV - Mousterian	1			1	12
	III - Mousterian	4			4	62
El Castillo	21 A - Mousterian	2	1		3	47
	20 E - Mousterian	2	2		4	56
	18C - Trans. Aurignacian	4			4	66
	18B - Trans. Aurignacian	3	2	1	6	93
	IX - Châtelperronian		1	1	2	24
Labeko Koba	VII - ProtoAurignacian	3			3	68
	VI - Aurignacian		1		1	16
	V - Aurignacian	1	1		2	39
	IV - Aurignacian		1		1	16
Canyars	I - Aurignacian	2	3		5	76
Aitzbitarte III	V - Gravettian	1			1	18
El Otero	IV - Magdalenian		2	3	5	68
TOTAL		25	14	5	44	693

204

Site	Level - Cultural period	Bovines	Horses	Red deer	Teeth	Subsamples
Axlor	VI - Mousterian	2			2	32
	IV - Mousterian	1			1	12
	III - Mousterian	4			4	62
El Castillo	21A - Mousterian	2	1		3	47
	20E - Mousterian	2	2		4	56
	18C - Trans. Aurignacian	4			4	66
	18B - Trans. Aurignacian	3	2	1	6	93
	IX - Châtelperronian		1	1	2	24
Labeko Koba	VII - ProtoAurignacian	3			3	68
	VI - Aurignacian		1		1	16
	V - Aurignacian	1	1		2	39
	IV - Aurignacian		1		1	16
Canyars	I - Aurignacian	2	3		5	76
Aitzbitarte III	V - Gravettian	1			1	18
El Otero	IV - Magdalenian		2	3	5	68
TOTAL		25	14	5	44	693

205

206 Table 1. Number of teeth sampled by species, archaeological sites and cultural periods.

206

207

208 **3.3.2 Sample treatment and stable isotope mass spectrometry**

209 Several authors have debated the necessity of chemical pre-treatments to remove organic matter and
210 secondary carbonates from bioapatite carbonates before stable isotopic analysis. Some chemical
211 treatments can introduce secondary carbonates, increase carbonate content, and alter the original isotopic
212 signal (Pellegrini and Snoeck, 2016; Snoeck and Pellegrini, 2015). The "side effects" of these pre-treatments
213 can compromise the final isotopic signal measured. For this reason, in this work, most of the samples were
214 not pretreated, except for the equids and cervids samples from Labeko Koba, and Aitzbitarte III interior, and
215 the cervids and equids from El Otero and El Castillo that were sampled and pretreated in the context of the
216 initial project in an earlier phase of the project. The absence of pretreatment can elevate the risk of secondary
217 carbonates (Chesson et al., 2021; France et al., 2020). Nonetheless, any pretreatment method cannot
218 guarantee their complete removal, and the 'side effects' may compromise the final isotopic signal to a greater
219 extent. While variations in pretreatment methods exist among samples in this study, the lack of a universally
220 accepted protocol necessitates careful consideration of any potential isotopic effects resulting from these
221 differences.

222 Pretreatment was followed for above-mentioned samples of this work from fourteen teeth was established by
223 Balasse et al. (2002), where around 7 mg of powdered enamel was prepared and pretreated with 3% of
224 sodium hypochlorite (NaOCl) at room temperature for 24 h (0.1 ml/mg sample); and thoroughly rinsed with
225 deionised water, before a reaction with 0.1M acetic acid for 4_h (0.1 ml/mg sample) (Balasse et al., 2002;
226 equivalent protocol in Jones et al., 2019). Samples were then thoroughly rinsed, frozen, and freeze-dried.
227 NaOCl is one of the most common agents used for pretreating carbonates and works as a base that removes
228 organic matter by oxidation. Although it is considered one of the most efficient agents for removing organic
229 matter, it can induce the absorption of exogenous carbonates, such as atmospheric CO₂ and secondary
230 carbonates (Pellegrini and Snoeck, 2016; Snoeck and Pellegrini, 2015). It is argued that using acetic acid
231 after NaOCl pretreatment can remove exogenous carbonates absorbed during NaOCl application. However,
232 it is unclear if all newly introduced carbonates are finally released and which effect they produce on the
233 original isotopic composition. While variations in pretreatment methods exist among samples in this study,
234 the lack of a universally accepted protocol necessitates careful consideration of any potential isotopic effects
235 resulting from these differences. These samples were analysed in the Godwin Laboratory (Department of
236 Earth Sciences, University of Cambridge). Enamel powder samples were reacted with 100%
237 orthophosphoric acid for 2_h at 70°C in individual vessels in an automated Gasbench interfaced with a
238 Thermo Finnigan MAT253 isotope ratio mass spectrometer. Results were reported in reference to the
239 international standard VPDB and calibrated using the NBS-19 standard (limestone, δ¹³C = +1.95‰ and δ¹⁸O
240 = -2.2‰; Coplen, 2011) for which the precision is better than 0.08‰ for δ¹³C and 0.11‰ for δ¹⁸O.

241 For the non-pre-treated samples, carbon and oxygen stable isotopic ratios were measured using continuous
242 flow-isotope ratio mass spectrometry, specifically a Europa Scientific 20-20 IRMS coupled to a
243 chromatograph, at the Iso-Analytical laboratory in Cheshire, UK. The samples were weighed into clean
244 exetainer tubes after being flushed with 99.995% helium. Phosphoric acid was then added to the samples,
245 and they were allowed to react overnight to ensure the complete conversion of carbonate to CO₂, following
246 the method outlined by Coplen et al. (1983). The reference materials used for VPDB calibration and quality
247 control of the analysis included: IA-R022 (calcium carbonate, δ¹³C = -28.63‰, δ¹⁸O = -22.69‰), NBS-18
248 (carbonate, δ¹³C = -5.01‰, δ¹⁸O = -23.2‰), IA-R066 (chalk, δ¹³C = +2.33‰; δ¹⁸O = -1.52). The accepted
249 values of the in-house standards IA-R022 and IA-R066 were obtained by calibrating against IAEA
250 international reference materials, NBS-18 and NBS-19, and NBS-18 and IAEA-CO-1 (Carrara marble, δ¹³C
251 = 2.5‰, and δ¹⁸O = -2.4‰), respectively. Additionally, in-house standards long-term measured were used:
252 ILC1 (calcite, δ¹³C = 2.13, δ¹⁸O = -3.99‰), and Y-02 (calcite, δ¹³C = 1.48, δ¹⁸O = -9.59‰). The analytical
253 precision of quality control standard replicates was better than 0.09‰ for δ¹³C and better than 0.12‰ for
254 δ¹⁸O. The calcium carbonate content test on of these samples, ranging between 3.9% and 8.9%, does
255 not indicate a substantial presence of secondary carbonates, considering (Chesson et al., 2021).
256 Additionally, phosphate results on samples from Axlor showed δ¹⁸O_{carb}-δ¹⁸O_{phos} offsets within the expected
257 range for well-preserved samples (Pederzani et al., 2023).

258 3.4.3 Carbon stable isotopic compositions as environmental and ecological tracers

259 To unravel animal diet and to compare the different species, in standardised terms, it is necessary to
260 consider the fractionation-enrichment factor (ε*) between δ¹³C obtained by the animal on its diet (δ¹³C_{diet})
261 and δ¹³C recorded on enamel carbonates (δ¹³C_{carb}) (Bocherens, 2003; Cerling and Harris, 1999). The ε*
262 estimated for large ruminant mammals results in an offset of around 14.1‰ between diet and dental enamel,
263 which is commonly applied generally commonly applied to medium-sized herbivores. However, it is well-
264 known that this offset varies between species, considering animals' different physiological parameters.
265 Recently, a formal model to predict species-specific diet-consumer isotopic offsets has been proposed,
266 which uses body mass (BM) and digestive physiology as the main factors that regulating-regulate the ε*

Formatted: Subscript

Formatted: Subscript

267 (Tejada-Lara et al., 2018). This model proposes the following prediction equations for ruminant or foregut
268 fermenters (Equation 1: Eq.1) and hindgut fermenters (Eq. 2):-

269 (Eq. 1) $\epsilon^* = 2.34 + 0.05 \text{ (BM)}$ $[r^2=0.78; \text{p-value}=0.008]$

270 (Eq. 2) $\epsilon^* = 2.42 + 0.032 \text{ (BM)}$ $[r^2=0.74; \text{p-value}=0.003]$

271 ~~In this work, we compare~~This work compares species with different digestive physiology, ruminants for
272 bovines and cervids, and non-ruminants for equids. The ϵ^* value was adjusted ~~to for~~ each animal to avoid
273 bias from digestive physiology when comparing these species. The following ~~fractionation-enrichment~~
274 factors have been used: 14.6‰ for *Bos taurus* (Passey et al., 2005a), 13.7‰ for *Equus caballus* (Cerling
275 and Harris, 1999), and 13.2‰ for *Cervus elaphus* (Merceron et al. (2021) following (Eq. 1) for ruminants
276 with a mean body mass of 125 kg.

277 In body tissues, carbon isotopic composition in body tissues is considered a combination of diet
278 (understood as consumed food), environment openness (and associated exposure to light), and the amount
279 of precipitation. Assuming that $\delta^{13}\text{C}$ of past vegetation is close to $\delta^{13}\text{C}_{\text{diet}}$ of ungulates, Having the
280 precipitation in mind, Lécuyer et al. (2021) proposed to estimate Mean Annual Precipitations (MAP) from
281 $\delta^{13}\text{C}_{\text{carb}}$ preserved in enamel carbonates, derived from diets based on C3 plants. After transforming ~~$\delta^{13}\text{C}$~~
282 from enamel carbonate ($\delta^{13}\text{C}_{\text{carb}}$) to $\delta^{13}\text{C}$ of the diet ($\delta^{13}\text{C}_{\text{diet}}$) using the ~~fractionation-enrichment~~ factors
283 established above, this work suggested transforming this value to $\delta^{13}\text{C}$ from vegetation ($\delta^{13}\text{C}_{\text{leaf}}$). However,
284 the isotopic composition of animals' diet may not directly reflected vegetation cover, but rather the food
285 preference of the animal and this approach should be discussed alongside other environmental data.

286 The MAP estimation is based on least square regression developed by Rey et al. (2013) and based on Kohn
287 (2010) dataset (Eq.4), which requires first to estimate the $\delta^{13}\text{C}_{\text{leaf}}$ (Eq. 3). The $\delta^{13}\text{C}$ values of atmospheric
288 CO_2 ($\delta^{13}\text{C}_{\text{atm}}$) are fixed in -7‰ (Lécuyer et al., 2021; Leuenberger et al., 1992; Schmitt et al., 2012).
289 Atmospheric CO_2 levels have varied throughout the Late Pleistocene, with $\delta^{13}\text{C}_{\text{atm}}$ range between -7 to -
290 6.4‰ (Eggleson et al., 2016), favouring an age-specific correction approach. However, maintaining general
291 corrections is preferred considering the chronological uncertainty of the studied levels.

292 (Eq.3) $\delta^{13}\text{C}_{\text{leaf}} \text{ (VPDB)} = (\delta^{13}\text{C}_{\text{atm}} - \delta^{13}\text{C}_{\text{diet}}) / [1 + (\delta^{13}\text{C}_{\text{diet}} / 1000)]$

293
294 (Eq.4) $\text{Log1}(\text{MAP}+300) = 0.092(\pm 0.004) \times \delta^{13}\text{C}_{\text{leaf}} + 1.148(\pm 0.074)$

295
296 Additionally, The Lécuyer et al. (2021) equation ~~also incorporates accounts for the consideration of~~ the pCO_2
297 effect on $\delta^{13}\text{C}_{\text{leaf}}$ estimation, which is expected to result in an offset of +1‰ from current levels (considering
298 that pCO_2 was 180 ppm during the LGM, which is lower than ~~the~~ 300 ppm experienced during the post
299 ~~post~~ after the deglaciation period around 15 ka). If this correction was not applied, MAP results ~~will~~ could
300 be underestimated by -150mm. In agreement with Lécuyer et al. (2021) appreciation, these MAP estimations
301 are a preliminary approximation and should be cross-validated with other environmental proxies. The
302 associated uncertainties range from ± 100 to 200 mm, influencing the interpretation of the final values.

303
304

305 3.54 Oxygen stable isotope compositions as environmental tracers

306 ~~Intratooth profiles are known to provide a time-averaged signal compared to the input isotopic signal ($\delta^{13}\text{C}$ / $\delta^{18}\text{O}_{\text{carb}}$)~~
307 ~~during enamel formation (Passey et al., 2005b). This signal attenuation is caused both by time-~~
308 ~~averaging effects incurred through the extended nature of amelogenesis and tooth formation, and through~~

309 the sampling strategy. During mineralisation, the maturation zone, which is time-averaged, often affects a
 310 large portion of the crown height and might affect the temporal resolution of the input signal of the sample
 311 taken. To obtain climatically informative seasonal information on the analysed tooth, the application of the
 312 inverse modelling method proposed by (Passey et al., 2005b) is, therefore, required applied in this work.
 313 This method allows us to computationally estimate the time-averaging effects of sampling and tooth
 314 formation to obtain more accurately the original amplitude of the isotopic input signal, thus the original
 315 amplitude of the isotopic input signal more accurately, thus, to summer and winter extremes (Appendix D).
 316 This method considers parameters based on the amelogenesis trends of each species and sampling
 317 geometry, which are critical for a meaningful interpretation of intratooth isotope profiles. To evaluate the
 318 data's reproducibility and precision, the model also estimates the error derived from the uncertainty of the
 319 sampling and the mass spectrometer measurements the model also estimates the error derived from the
 320 sampling uncertainty and the mass spectrometer measurements to evaluate the data's reproducibility and
 321 precision. This method was initially developed for continuously growing teeth, taking into account a constant
 322 growth rate within a linear maturation model, which with a progressive time average increment as sampling
 323 advances along the teeth profile. The species studied in this research exhibit non linear tooth enamel
 324 formation, particularly in later-forming molars (Bendrey et al., 2015; Zazzo et al., 2012; Passey and Cerling,
 325 2002; Kohn, 2004; Blumenthal et al., 2014). Although the aforementioned model model mentioned above is
 326 not ideal, as it does not account for non-linear enamel formation and certain growth parameters for the
 327 species included are unknown, it is the best estimation based on the current state of the field and remains
 328 widely used (Pederzani et al., 2023, 2021a, b). Flat and less sinusoidal profiles are less suitable for the
 329 application of the model, given its inherent assumption of an approximately sinusoidal form. Therefore, we
 330 chose not to apply this methodology in the analysis of intratooth $\delta^{13}\text{C}$ profiles, and it is recommended to
 331 approach the interpretation of model outcomes for non sinusoidal $\delta^{18}\text{O}$ curves with caution. Further details
 332 on the application of this method can be found in Appendix D.

333 Stable oxygen isotopes from meteoric water (mainly derived from rainfall) have a strong relationship strongly
 334 correlate with mean air temperatures in mid to high latitudes (Dansgaard, 1964; Rozanski et al., 1992) on a
 335 regional-to-local scale. Obligate drinkers, such as like bovines and horses, acquire this water and record its
 336 isotopic composition in their teeth and bones with a fixed, but species-specific offset (Pederzani and Britton,
 337 2019). Considering this two-step relationship, past climatic conditions can be estimated. However, most of
 338 the temperature reconstructions based on $\delta^{18}\text{O}$ have considered the $\delta^{18}\text{O}$ from the phosphate fraction of
 339 bioapatite enamel ($\delta^{18}\text{O}_{\text{phos}}$) to build linear correlations between tooth enamel and drinking water $\delta^{18}\text{O}$ and
 340 obtain climatic information. For this reason, the $\delta^{18}\text{O}_{\text{carb}}$ from carbonates values obtained in this work
 341 ($\delta^{18}\text{O}_{\text{carb}}$) were converted into $\delta^{18}\text{O}_{\text{phos}}$ from phosphates ($\delta^{18}\text{O}_{\text{phos}}$). To do so, first, to express in VSMOW
 342 notation, the $\delta^{18}\text{O}_{\text{carb}}$ was corrected using the following correlation (Brand et al., 2014; Coplen et al., 1983):

$$(Eq.5) \delta^{18}\text{O}_{\text{carb}} (\text{VSMOW}) = 1.0309 \times \delta^{18}\text{O}_{\text{carb}} (\text{VPDB}) + 30.91$$

344 Second, considering the relationship existent in tooth enamel between the carbonate and phosphate fraction
 345 (Iacumin et al., 1996; Pellegrini et al., 2011), from a compilation of the existent bibliography of modern
 346 animals measurements (Bryant et al., 1996; Pellegrini et al., 2011; Trayler and Kohn, 2017), Pederzani et
 347 al. (2023) proposed the following correlation:

$$(Eq.6) \delta^{18}\text{O}_{\text{phos}} (\text{VSMOW}) = 0.941 \times \delta^{18}\text{O}_{\text{carb,C}} (\text{VSMOW}) - 7.16$$

349 Once the isotopic information is expressed in $\delta^{18}\text{O}_{\text{phos}}$ (VSMOW), we can estimate the $\delta^{18}\text{O}$ on meteoric
 350 waters ($\delta^{18}\text{O}_{\text{mw}}$). It is known that different physiological factors will condition how oxygen isotope composition
 351 is fixed in each mammalian group. Thus, usually, the correlations are usually species-specific and
 352 developed considering the particular physiology of each animal group. The obligate drinkers heavily rely on
 353 consuming large amounts of liquid drinking water, being the relative contribution of water from plants

Formatted: English (United Kingdom)

Formatted: English (United Kingdom)

Field Code Changed

Formatted: English (United Kingdom)

Formatted: English (United Kingdom)

negligible and then minimizing the possible impact of isotopic enrichment through evapotranspiration in plants (Hoppe, 2006; Maloy, 1973; Pederzani and Britton, 2019). However, certain types of drinking behaviours can impact $\delta^{18}\text{O}$, such as systematic consumption of certain highly buffered water sources (rivers or lakes), can significantly attenuate the final signal recorded. The correlation employed by this work relies on recent data compilations (Pederzani et al., 2021b, 2023). In the case of horses (Eq. 7), it has been considered the data combination of Blumenthal et al. (2019); Chillón et al. (1994); Bryant et al., 1994; Delgado Huertas et al., 1995), whereas for bovines (Eq. 8) the data from D'Angela and Longinelli (1990) and Hoppe (2006) have been put together in Eq. 4. To estimate $\delta^{18}\text{O}_{\text{mw}}$ from red deer remains, we selected D'Angela and Longinelli (1990) correlation (Eq. 9):

$$\text{(Eq.7) } \delta^{18}\text{O}_{\text{mw}} (\text{VSMOW}) = (\delta^{18}\text{O}_{\text{phos}} (\text{VSMOW}) - 22.14) / 0.6287$$

$$\text{(Eq.8) } \delta^{18}\text{O}_{\text{mw}} (\text{VSMOW}) = (\delta^{18}\text{O}_{\text{phos}} (\text{VSMOW}) - 22.436) / 0.785$$

$$\text{(Eq.9) } \delta^{18}\text{O}_{\text{mw}} (\text{VSMOW}) = (\delta^{18}\text{O}_{\text{phos}} (\text{VSMOW}) - 24.39) / 0.91$$

Finally, paleotemperatures estimations from $\delta^{18}\text{O}_{\text{mw}}$ are typically approached using a geographically adjusted linear regression, which can vary from precise adjustments (aimed at reducing errors) to broader geographical adjustments that encompass more variability and but also introduce greater uncertainty but are less precise (e.g., Pryor et al., 2014; Skrzypek et al., 2011; Tütken et al., 2007). The mean annual temperatures (MAT) were calculated from $\delta^{18}\text{O}_{\text{mw}}$. In this work, temperatures were calculated considering the linear regression model relating $\delta^{18}\text{O}_{\text{mw}}$ and air temperatures from Iberia proposed by Pederzani et al. (2021) Fernández-García et al. (2019). This correlation is based on monthly climatic records (monthly mean $\delta^{18}\text{O}_{\text{mw}}$ and monthly mean air temperatures) from Western, Southern and Central Europe all Iberian stations from the Global Network of Isotopes in Precipitation, operated by the International Atomic Energy Association and the World Meteorological Organization (IAEA/ WMO, 2018/2020). Considering current IAEA data sets from northern Iberia, there is a strong positive relationship between $\delta^{18}\text{O}_{\text{mw}}$ and annual or monthly temperatures (Moreno et al., 2021). However, it is known that Iberia is under a mixed influence between Atlantic and Mediterranean moisture sources that affects the isotopic composition of rainfall (Araguas-Araguas and Diaz Teijeiro, 2005; Garcia-Alix et al., 2021; Moreno et al., 2021). Given uncertainties in past atmospheric circulation patterns and the limited availability of reference stations, it was deemed most appropriate to select an equation that extends beyond the borders of Iberia and incorporates higher variability. Different correlations were for mean annual temperature (Eq. 10), summer (Eq. 11), and winter (Eq. 12) temperatures (T):

$$\text{(Eq.10) } \delta^{18}\text{O}_{\text{mw}} (\text{VSMOW}) = (0.50 \times T) - 13.64$$

$$\text{(Eq.11) } \delta^{18}\text{O}_{\text{mw}} (\text{VSMOW}) = (0.46 \times T) - 14.70$$

$$\text{(Eq.12) } \delta^{18}\text{O}_{\text{mw}} (\text{VSMOW}) = (0.52 \times T) - 11.26$$

$$\text{(Eq. 10) } \text{MAT } (^{\circ}\text{C}) = 2.38(\pm 0.10) \times \delta^{18}\text{O}_{\text{mw}} + 28.19(\pm 0.58)$$

$$[r^2 = 0.65; n = 304; p\text{-value} < 0.0001]$$

Nonetheless, oscillations between glacial and interglacial conditions in the past have influenced global ice volume and sea level fluctuations (Dansgaard, 1964; Shackleton, 1987), impacting seawater oxygen isotope composition and the surface hydrological cycle on a global/worldwide scale, including $\delta^{18}\text{O}_{\text{mw}}$ (Schrag et al., 2002). Prior studies have used sea level information to correct $\delta^{18}\text{O}_{\text{mw}}$ (e.g., Fernández-García et al., 2019; Schrag et al., 2002). Given the chronological uncertainty in the studied levels, a general correction was applied to $\delta^{18}\text{O}_{\text{mw}}$ before temperatures estimations, following Fernández-García et al. (2020) approach. Considering the mean sea level descent for the MIS 3 period (50 meters below present-day sea

Formatted: Superscript

Formatted: Subscript

396 level)(Chappell and Shackleton, 1986), this may have contributed to a potential increase in the global $\delta^{18}\text{O}_{\text{mw}}$
397 value by $\approx 0.56\%$, inferring a bias in calculated air temperatures of $\approx 1^\circ\text{C}$.

398 Following (Pederzani et al., 2021b), mean annual temperatures (MAT) were deduced from the $\delta^{18}\text{O}$ mean
399 average of $\delta^{18}\text{O}_{\text{carb}}$ values between summer and winter detected in original sinusoidal intratooth profiles
400 (Appendix C) in each tooth before modeling to reduce associated error and maximise number of usable data
401 records. This work shows that comparable results can be obtained before and after model application, but
402 doing it beforehand avoids the associated errors induced by the inverse model. Summer and winter
403 estimations were extracted from the obtained $\delta^{18}\text{O}$ values after inverse modeling application, to identify
404 seasonal variation. To maximize data, in non-sinusoidal teeth profiles, MAT was deduced from the average
405 of all points within a tooth. However, this approach is less reliable when complete annual cycles are not
406 recorded. When possible, summer and winter estimations were derived from the obtained $\delta^{18}\text{O}_{\text{carb}}$ values
407 after inverse modelling application, aiming to identify the seasonal amplitude, which is dampened in the
408 original $\delta^{18}\text{O}_{\text{carb}}$ signal.

409 Due to the uncertainties incurred from converting stable isotope measurements to palaeotemperature, the
410 final estimations in this work should be considered exploratory and as a method of standardisation to make
411 results comparable with among different sites, data from different species, and other non-isotopic
412 palaeoclimatic records. In these estimations, the associated error from converting $\delta^{18}\text{O}_{\text{phos}}$ to MAT is
413 enlarged by the uncertainty derived from the transformation of $\delta^{18}\text{O}_{\text{carb}}$ (VPDB) to $\delta^{18}\text{O}_{\text{phos}}$ (VSMOW) (see
414 Pryor et al., 2014; Skrzypek et al., 2016 for further discussion). However, Pryor et al. (2014) and Pederzani
415 et al. (2023) concluded that the impact of this conversion is negligible compared to the error propagation in
416 subsequent calibrations used for temperature estimations from $\delta^{18}\text{O}_{\text{phos}}$. These associated errors were
417 quantified following the methodology outlined by Pryor et al. (2014) (Appendix B).

418 3.6 Inverse modelling applied to intratooth profiles

419 Intratooth profiles frequently provide a time-averaged signal compared to the input isotopic signal ($\delta^{13}\text{C}/$
420 $\delta^{18}\text{O}_{\text{carb}}$) during enamel formation (Passey et al., 2005b). This signal attenuation is caused by time-averaging
421 effects incurred through the extended nature of amelogenesis and tooth formation, and through the sampling
422 strategy. During mineralisation, the maturation zone, which is time-averaged, often affects a large portion of
423 the crown height and might affect the temporal resolution of the input signal of the sample taken. To obtain
424 climatically informative seasonal information on the analysed teeth, the inverse modelling method
425 proposed by (Passey et al. (2005b) is applied in this work. This method computationally estimates the time-
426 averaging effects of sampling and tooth formation to obtain the original amplitude of the isotopic input signal
427 more accurately, thus, to summer and winter extremes (Appendix E). This method considers parameters
428 based on the amelogenesis trends of each species and sampling geometry, which are critical for a
429 meaningful interpretation of intratooth isotope profiles. The model also estimates the error derived from the
430 sampling uncertainty and the mass spectrometer measurements to evaluate the data's reproducibility and
431 precision. This method was initially developed for continuously growing teeth, taking into account a constant
432 growth rate within a linear maturation model, with a progressive time-average increment as sampling
433 advances along the teeth profile. The species studied in this research exhibit non-linear tooth enamel
434 formation, particularly in later-forming molars (Bendrey et al., 2015; Blumenthal et al., 2014; Kohn, 2004;
435 Passey and Cerling, 2002; Zazzo et al., 2012). Although the model mentioned above is not ideal, as it does
436 not take into account for non-linear enamel formation and certain specific growth parameters for the species
437 included are unknown, it is the best estimation based on the current state of the field and remains widely
438 used (Pederzani et al., 2021a, b, 2023). Flat and less sinusoidal profiles are less suitable for the application
439 of the model, given its inherent assumption of an approximately sinusoidal form. Therefore, we chose not to
440 apply this methodology in the analysis of intratooth $\delta^{13}\text{C}$ profiles, and it is recommended to approach the

441 [interpretation of model outcomes for non-sinusoidal \$\delta^{18}\text{O}\$ curves with caution. Further details on the](#)
442 [application of this method can be found in Appendix E.](#)

443 [Following Pederzani et al. \(2021b\), mean annual temperatures \(MAT\) were deduced from the average of](#)
444 [\$\delta^{18}\text{O}_{\text{carb}}\$ values between summer and winter detected in original sinusoidal intratooth profiles \(Appendix D\).](#)
445 [This work shows that comparable results for annual means can be obtained before and after model](#)
446 [application, but doing it beforehand avoids the associated errors induced by the inverse model. To maximize](#)
447 [data, in non-sinusoidal teeth profiles, MAT was deduced from the average of all points within a tooth.](#)
448 [However, this approach is less reliable when complete annual cycles are not recorded. When possible,](#)
449 [summer and winter temperature estimations were derived from the obtained \$\delta^{18}\text{O}_{\text{carb}}\$ values after inverse](#)
450 [modelling application, aiming to identify the corrected seasonal amplitude, which is dampened in the original](#)
451 [\$\delta^{18}\text{O}_{\text{carb}}\$ signal.](#)

452

453 **3.647 Present-day isotopic and climatic data**

454 Present-day climatic conditions surrounding each site have been considered, allowing an inter-site
455 comparison, essential for [compare our this study but also a regional to a with other regional and global](#)
456 [perspective data](#). Considering current MATs and MAPs, estimated climatic data is expressed in relative
457 terms as MAT and MAP anomalies. Present-day summer and winter temperatures were also considered.
458 Present-day temperatures and precipitation values were obtained from the WorldClim Dataset v2 (Fick and
459 Hijmans, 2017) (Appendix B). This dataset includes the average of bioclimatic variables between 1970-2000
460 in a set of raster files with a spatial resolution every 2.5 minutes. The exact location of the selected archeo-
461 palaeontological sites was used, using geographical coordinates in the projection on modern climatic maps
462 with QGIS software.

463 Present-day $\delta^{18}\text{O}_{\text{mw}}$ values from the analysed sites' areas were obtained using the Online Isotopes in
464 Precipitation Calculator (OIPC Version 3.1 (4/2017); Bowen, 2022) based on datasets collected by the
465 Global Network for Isotopes in Precipitation from the IAEA/WMO (Appendix B).

Formatted: Subscript

Site	Level	Culture	Species	Tooth type	Code	CCE (%)	n	$\delta^{13}\text{Ccarb}$ VPDB (‰)	min	max	SD	Range	$\delta^{18}\text{Ocarb}$ VPDB (‰)	min	max	SD	Range
Axlor	III	Mousterian	<i>Bos/Bison</i> sp.	LRM3	AXL59	5.6	14	-8.9	-9.6	-8.2	1.4	0.4	-6.0	-7.3	-5.2	0.7	2.1
Axlor	III	Mousterian	<i>Bos/Bison</i> sp.	LRM2	AXL60	5.5	18	-9.7	-10.0	-8.9	1.1	0.3	-5.7	-6.8	-4.6	0.7	2.2
Axlor	III	Mousterian	<i>Bos/Bison</i> sp.	LRM3	AXL65	6.2	13	-8.9	-9.3	-8.1	1.2	0.4	-6.0	-7.2	-4.6	0.8	2.6
Axlor	III	Mousterian	<i>Bos/Bison</i> sp.	LRM2	AXL66	5.6	16	-8.9	-8.8	-8.3	1.5	0.5	-4.8	-6.1	-3.8	0.7	2.3
Axlor	IV	Mousterian	<i>Bos/Bison</i> sp.	LRM2	AXL70	5.7	12	-9.1	-9.4	-8.6	0.7	0.3	-5.3	-7.3	-3.9	1.2	3.4
Axlor	VI	Mousterian	<i>Bos/Bison</i> sp.	LLM3	AXL77	5.9	14	-9.7	-10.2	-9.2	1.0	0.4	-6.2	-7.9	-5.0	0.9	2.9
Axlor	VI	Mousterian	<i>Bos/Bison</i> sp.	LLM3	AXL86	5.5	18	-9.9	-10.2	-9.3	0.9	0.3	-5.4	-6.5	-3.8	0.7	2.6
El Castillo	20E	Mousterian	<i>Equus</i> sp.	LRP3/LRP4	CAS50	14		-11.9	-12.5	-11.5	1.0	0.3	-3.3	-4.1	-2.4	0.4	1.6
El Castillo	20E	Mousterian	<i>Equus</i> sp.	LRP3/LRP4	CAS51	14		-12.2	-12.4	-12.1	0.3	0.1	-4.9	-5.8	-4.3	0.4	1.5
El Castillo	20E	Mousterian	<i>Bos/Bison</i> sp.	LLM2	CAS139	6.7	16	-11.6	-12.2	-11.2	0.9	0.3	-5.6	-6.3	-4.9	0.5	1.4
El Castillo	20E	Mousterian	<i>Bos/Bison</i> sp.	LLM2	CAS140	5.7	12	-11.5	-11.9	-11.1	0.8	0.3	-5.5	-6.3	-4.6	0.6	1.7
El Castillo	21A	Mousterian	<i>Bos/Bison</i> sp.	LLM3	CAS141	5.7	15	-11.2	-11.5	-10.9	0.6	0.2	-5.4	-6.5	-4.3	0.6	2.2
El Castillo	21A	Mousterian	<i>Bison priscus</i>	LLM3	CAS142	6.1	15	-11.2	-11.7	-10.9	0.7	0.2	-5.0	-5.7	-4.4	0.4	1.3
El Castillo	21A	Mousterian	<i>Equus</i> sp.	LLM3	CAS143	6.5	17	-12.6	-12.9	-12.5	0.4	0.1	-6.2	-7.2	-5.4	0.5	1.8
El Castillo	18B	Transitional Aurignacian	<i>Bos/Bison</i> sp.	ULM2	CAS132	6.2	13	-11.3	-11.5	-10.9	0.6	0.2	-6.2	-7.4	-4.9	0.7	2.6
El Castillo	18B	Transitional Aurignacian	<i>Bos/Bison</i> sp.	ULM2	CAS133	6.8	18	-10.9	-11.6	-10.5	1.1	0.3	-5.4	-6.5	-4.2	0.7	2.2
El Castillo	18B	Transitional Aurignacian	<i>Bos/Bison</i> sp.	ULM2	CAS134	6.6	18	-12.4	-12.8	-11.6	1.2	0.3	-5.4	-6.3	-4.5	0.5	1.8
El Castillo	18C	Transitional Aurignacian	<i>Bos/Bison</i> sp.	LLM3	CAS135	6	17	-11.3	-11.5	-11.0	0.5	0.2	-6.1	-6.6	-5.5	0.3	1.1
El Castillo	18C	Transitional Aurignacian	<i>Bos/Bison</i> sp.	LLM3	CAS136	5.8	17	-12.0	-12.5	-11.7	0.9	0.2	-5.8	-6.7	-5.0	0.6	1.7
El Castillo	18C	Transitional Aurignacian	<i>Bos/Bison</i> sp.	LLM3	CAS137	6.6	14	-10.2	-10.6	-9.9	0.7	0.2	-5.8	-6.5	-4.1	0.7	2.4
El Castillo	18C	Transitional Aurignacian	<i>Bos/Bison</i> sp.	LLM3	CAS138	6.1	18	-11.6	-11.8	-11.4	0.4	0.1	-5.3	-5.9	-4.8	0.3	1.2
El Castillo	18B	Transitional Aurignacian	<i>Cervus elaphus</i>	ULM2+ULM3	CAS8	11		-13.0	-14.9	-12.1	2.8	1.0	-6.8	-10.4	-4.1	2.1	6.3
El Castillo	18B	Transitional Aurignacian	<i>Equus</i> sp.	ULP3/ULP4	CAS58	19		-11.7	-11.8	-11.5	0.3	0.1	-6.6	-7.5	-5.6	0.5	1.8
El Castillo	18B	Transitional Aurignacian	<i>Equus</i> sp.	LLP3/LLP3	CAS59	14		-11.5	-11.7	-11.0	0.7	0.2	-4.0	-4.7	-3.5	0.4	1.2
Labeko Koba	IX inf	Chateauperronian	<i>Equus</i> sp.	URM3	LAB38	17		-12.0	-12.2	-11.9	0.3	0.1	-6.6	-7.7	-5.9	0.5	1.9
Labeko Koba	IX inf	Chateauperronian	<i>Cervus elaphus</i>	LLM2	LAB02	7		-12.3	-12.4	-12.1	0.3	0.1	-4.7	-6.0	-3.7	1.0	2.3
Labeko Koba	VI	Aurignacian	<i>Equus</i> sp.	URM2	LAB20	16		-12.0	-12.2	-11.8	0.4	0.1	-5.3	-6.1	-4.4	0.6	1.7
Labeko Koba	V	Aurignacian	<i>Equus</i> sp.	LRM3	LAB42	17		-11.9	-12.3	-11.5	0.2	0.7	-5.7	-6.6	-5.0	0.5	1.6
Labeko Koba	IV	Aurignacian	<i>Equus</i> sp.	LRM2	LAB36	17		-11.6	-11.8	-11.3	0.6	0.2	-5.9	-6.2	-5.5	0.2	0.7
Canyars	I	Aurignacian	<i>Equus</i> sp.	URM3	CAN01	7.8	12	-10.0	-10.4	-9.5	0.9	0.3	-4.8	-5.3	-4.3	0.3	1.1
Canyars	I	Aurignacian	<i>Equus ferus</i>	URM3	CAN02	6.2	17	-10.5	-10.7	-10.3	0.4	0.1	-4.4	-5.0	-3.6	0.5	1.4
Canyars	I	Aurignacian	<i>Equus ferus</i>	URP3/URP4	CAN03	6.4	17	-10.7	-11.2	-10.4	0.8	0.2	-4.8	-5.3	-4.0	0.4	1.4
Labeko Koba	VII	Aurignacian	<i>Bos primigenius</i>	LRM3	LAB53	5.2	23	-9.5	-10.1	-8.7	1.4	0.3	-5.7	-7.0	-4.2	0.9	2.8
Labeko Koba	VII	Aurignacian	<i>Bos primigenius</i>	LRM3	LAB55	5.6	23	-10.4	-11.5	-9.8	1.6	0.3	-5.1	-7.0	-2.7	1.2	4.3
Labeko Koba	VII	Aurignacian	<i>Bos/Bison</i> sp.	LRM3	LAB62	6.5	21	-9.7	-10.2	-9.1	1.2	0.3	-7.2	-8.1	-6.2	0.6	2.0
Labeko Koba	V	Aurignacian	<i>Bos primigenius</i>	LRM3	LAB59	5.5	21	-9.3	-10.3	-7.3	3.0	0.9	-7.2	-8.8	-5.5	0.9	3.3
Canyars	I	Aurignacian	<i>Bos primigenius</i>	ULM3	CAN04	6.8	14	-9.3	-9.8	-8.7	1.1	0.3	-3.6	-4.2	-2.6	0.5	1.6
Canyars	I	Aurignacian	<i>Bos primigenius</i>	ULM3	CAN05	6.6	14	-9.0	-9.5	-8.5	0.9	0.3	-5.5	-6.2	-5.0	0.4	1.2
Atxibartze III	V (int)	Gravettian	<i>Bos/Bison</i> sp.	LLM3	ATI10	5.5	17	-9.2	-9.6	-8.7	0.9	0.3	-5.5	-6.5	-4.3	0.5	2.2
El Otero	IV	Magdalenian	<i>Cervus elaphus</i>	LLM2+LLM3	OTE1	11		-11.4	-11.6	-11.2	0.4	0.1	-4.4	-5.8	-2.9	1.0	2.9
El Otero	IV	Magdalenian	<i>Cervus elaphus</i>	LLM2+LLM3	OTE5	10		-11.3	-11.5	-11.0	0.5	0.2	-5.1	-5.7	-3.8	0.6	1.9
El Otero	IV	Magdalenian	<i>Cervus elaphus</i>	LLM2+LLM3	OTE6	14		-11.4	-11.8	-10.6	1.2	0.3	-4.6	-5.4	-4.0	0.4	1.4
El Otero	IV	Magdalenian	<i>Equus</i> sp.	LLP3/LLP4	OTE11	17		-11.6	-11.8	-11.4	0.5	0.1	-5.0	-6.3	-3.9	0.7	2.4
El Otero	IV	Magdalenian	<i>Equus</i> sp.	LLP3/LLP4	OTE12	16		-11.3	-11.5	-10.9	0.6	0.1	-3.9	-4.9	-3.3	0.6	1.6

Site	Level	Culture	Species	Tooth type	Code	n	$\delta^{13}\text{C}_{\text{carb}}$ VPDB (‰)	min	max	SD	Range	$\delta^{18}\text{O}_{\text{carb}}$ VPDB (‰)	min	max	SD	Range
Axlor	III	Mousterian	<i>Bos/Bison</i> sp.	LRM3	AXL59	14	-8.9	-9.6	-8.2	1.4	0.4	-6.0	-7.3	-5.2	0.7	2.1
Axlor	III	Mousterian	<i>Bos/Bison</i> sp.	LRM2	AXL60	18	-9.7	-10.0	-8.9	1.1	0.3	-5.7	-6.8	-4.6	0.7	2.2
Axlor	III	Mousterian	<i>Bos/Bison</i> sp.	LRM3	AXL65	13	-8.9	-9.3	-8.1	1.2	0.4	-6.0	-7.2	-4.6	0.8	2.6
Axlor	III	Mousterian	<i>Bos/Bison</i> sp.	LRM2	AXL66	16	-8.9	-9.8	-8.3	1.5	0.5	-4.8	-6.1	-3.8	0.7	2.3
Axlor	IV	Mousterian	<i>Bos/Bison</i> sp.	LRM2	AXL70	12	-9.1	-9.4	-8.6	0.7	0.3	-5.3	-7.3	-3.9	1.2	3.4
Axlor	VI	Mousterian	<i>Bos/Bison</i> sp.	LLM3	AXL77	14	-9.7	-10.2	-9.2	1.0	0.4	-6.2	-7.9	-5.0	0.9	2.9
Axlor	VI	Mousterian	<i>Bos/Bison</i> sp.	LLM3	AXL86	18	-9.9	-10.2	-9.3	0.9	0.3	-5.4	-6.5	-3.8	0.7	2.6
El Castillo	20E	Mousterian	<i>Equus</i> sp.	LRP3/LRP4	CAS60	14	-11.9	-12.5	-11.5	1.0	0.3	-3.3	-4.1	-2.4	0.4	1.6
El Castillo	20E	Mousterian	<i>Equus</i> sp.	LRP3/LRP4	CAS61	14	-12.2	-12.4	-12.1	0.3	0.1	-4.9	-5.8	-4.3	0.4	1.5
El Castillo	20E	Mousterian	<i>Bos/Bison</i> sp.	LLM2	CAS139	16	-11.6	-12.2	-11.2	0.9	0.3	-5.6	-6.3	-4.9	0.5	1.4
El Castillo	20E	Mousterian	<i>Bos/Bison</i> sp.	LLM2	CAS140	12	-11.5	-11.9	-11.1	0.8	0.3	-5.5	-6.3	-4.6	0.6	1.7
El Castillo	21A	Mousterian	<i>Bos/Bison</i> sp.	LLM3	CAS141	15	-11.2	-11.5	-10.9	0.6	0.2	-5.4	-6.5	-4.3	0.6	2.2
El Castillo	21A	Mousterian	<i>Bison priscus</i>	LLM3	CAS142	15	-11.2	-11.7	-10.9	0.7	0.2	-5.0	-5.7	-4.4	0.4	1.3
El Castillo	21A	Mousterian	<i>Equus</i> sp.	LLM3	CAS143	17	-12.6	-12.9	-12.5	0.4	0.1	-6.2	-7.2	-5.4	0.5	1.8
El Castillo	19B	Transitional Aurignacian	<i>Bos/Bison</i> sp.	ULM2	CAS132	13	-11.3	-11.5	-10.9	0.6	0.2	-6.2	-7.4	-4.9	0.7	2.6
El Castillo	19B	Transitional Aurignacian	<i>Bos/Bison</i> sp.	ULM2	CAS133	18	-10.9	-11.6	-10.5	1.1	0.3	-5.4	-6.5	-4.2	0.7	2.2
El Castillo	19B	Transitional Aurignacian	<i>Bos/Bison</i> sp.	ULM2	CAS134	18	-12.4	-12.8	-11.6	1.2	0.3	-5.4	-6.3	-4.5	0.5	1.8
El Castillo	19C	Transitional Aurignacian	<i>Bos/Bison</i> sp.	LLM3	CAS135	17	-11.3	-11.5	-11.0	0.5	0.2	-6.1	-6.6	-5.5	0.3	1.1
El Castillo	19C	Transitional Aurignacian	<i>Bos/Bison</i> sp.	LLM3	CAS136	17	-12.0	-12.5	-11.7	0.9	0.2	-5.8	-6.7	-5.0	0.6	1.7
El Castillo	19C	Transitional Aurignacian	<i>Bos/Bison</i> sp.	LLM3	CAS137	14	-10.2	-10.6	-9.9	0.7	0.2	-5.8	-6.5	-4.1	0.7	2.4
El Castillo	19C	Transitional Aurignacian	<i>Bos/Bison</i> sp.	LLM3	CAS138	18	-11.6	-11.8	-11.4	0.4	0.1	-5.3	-5.9	-4.8	0.3	1.2
El Castillo	19B	Transitional Aurignacian	<i>Equus elaphus</i>	ULM2+ULM3	CAS8	11	-13.0	-14.9	-12.1	2.8	1.0	-6.8	-10.4	-4.1	2.1	6.3
El Castillo	19B	Transitional Aurignacian	<i>Equus</i> sp.	ULP3/ULP4	CAS58	19	-11.7	-11.8	-11.5	0.3	0.1	-6.6	-7.5	-6.6	0.5	1.8
El Castillo	19B	Transitional Aurignacian	<i>Equus</i> sp.	LLP3/LLP3	CAS59	14	-11.5	-11.7	-11.0	0.7	0.2	-4.0	-4.7	-3.5	0.4	1.2
Labelo Koba	IX inf	Chalcolithic	<i>Equus</i> sp.	URM3	LAB38	17	-12.0	-12.2	-11.9	0.3	0.1	-6.6	-7.7	-5.9	0.5	1.9
Labelo Koba	IX inf	Chalcolithic	<i>Equus elaphus</i>	LLM2	LAB02	7	-12.3	-12.4	-12.1	0.3	0.1	-4.7	-6.0	-3.7	1.0	2.3
Labelo Koba	VI	Aurignacian	<i>Equus</i> sp.	URM2	LAB20	16	-12.0	-12.2	-11.8	0.4	0.1	-5.3	-6.1	-4.4	0.6	1.7
Labelo Koba	V	Aurignacian	<i>Equus</i> sp.	LRM3	LAB42	17	-11.9	-12.3	-11.5	0.2	0.7	-5.7	-6.6	-5.0	0.5	1.6
Labelo Koba	IV	Aurignacian	<i>Equus</i> sp.	LRM2	LAB36	17	-11.6	-11.8	-11.3	0.6	0.2	-5.9	-6.2	-5.5	0.2	0.7
Canyars	I	Aurignacian	<i>Equus</i> sp.	URM3	CAN01	12	-10.0	-10.4	-9.5	0.9	0.3	-4.8	-5.3	-4.3	0.3	1.1
Canyars	I	Aurignacian	<i>Equus ferus</i>	URM3	CAN02	17	-10.5	-10.7	-10.3	0.4	0.1	-4.4	-5.0	-3.6	0.5	1.4
Canyars	I	Aurignacian	<i>Equus ferus</i>	URP3/URP4	CAN03	17	-10.7	-11.2	-10.4	0.8	0.2	-4.8	-5.3	-4.0	0.4	1.4
Labelo Koba	VII	Aurignacian	<i>Bos primigenius</i>	LRM3	LAB53	23	-9.5	-10.1	-8.7	1.4	0.3	-5.7	-7.0	-4.2	0.9	2.8
Labelo Koba	VII	Aurignacian	<i>Bos primigenius</i>	LRM3	LAB55	23	-10.4	-11.5	-9.8	1.6	0.3	-5.1	-7.0	-2.7	1.2	4.3
Labelo Koba	VII	Aurignacian	<i>Bos/Bison</i> sp.	LRM3	LAB62	21	-9.7	-10.2	-9.1	1.2	0.3	-7.2	-8.1	-6.2	0.6	2.0
Labelo Koba	V	Aurignacian	<i>Bos primigenius</i>	LRM3	LAB69	21	-9.3	-10.3	-7.3	3.0	0.9	-7.2	-8.8	-5.5	0.9	3.3
Canyars	I	Aurignacian	<i>Bos primigenius</i>	ULM3	CAN04	14	-9.3	-9.8	-8.7	1.1	0.3	-3.6	-4.2	-2.6	0.5	1.6
Canyars	I	Aurignacian	<i>Bos primigenius</i>	ULM3	CAN05	14	-9.0	-9.5	-8.5	0.9	0.3	-5.5	-6.2	-5.0	0.4	1.2
Atxibiltarte III	V (int)	Gravettian	<i>Bos/Bison</i> sp.	LLM3	AIT110	17	-9.2	-9.6	-8.7	0.9	0.3	-5.5	-6.5	-4.3	0.5	2.2
El Otero	IV	Magdalenian	<i>Equus elaphus</i>	LLM2+LLM3	OTE1	11	-11.4	-11.6	-11.2	0.4	0.1	-4.4	-5.8	-2.9	1.0	2.9
El Otero	IV	Magdalenian	<i>Equus elaphus</i>	LLM2+LLM3	OTE5	10	-11.3	-11.5	-11.0	0.5	0.2	-5.1	-5.7	-3.8	0.6	1.9
El Otero	IV	Magdalenian	<i>Equus elaphus</i>	LLM2+LLM3	OTE6	14	-11.4	-11.8	-10.6	1.2	0.3	-4.6	-5.4	-4.0	0.4	1.4
El Otero	IV	Magdalenian	<i>Equus</i> sp.	LLP3/LLP4	OTE11	17	-11.6	-11.8	-11.4	0.5	0.1	-5.0	-6.3	-3.9	0.7	2.4
El Otero	IV	Magdalenian	<i>Equus</i> sp.	LLP3/LLP4	OTE12	16	-11.3	-11.5	-10.9	0.6	0.1	-3.9	-4.9	-3.3	0.6	1.6

Table 2. Mean, maximum value (Max), minimum value (Min), and standard deviation (SD) of $\delta^{13}\text{C}$ and $\delta^{18}\text{O}$ values per archaeological site and level organised by cultural periods. CCE, calcium carbonate equivalent; n_i = number of intratooth subsamples measured. In tooth type: position (U, upper; L, lower); laterality (R, right; L, left); tooth (M, molar; P, premolar).

4. Results

In northwestern Iberia, specifically in the Vasco-Cantabrian region, the mean $\delta^{13}\text{C}_{\text{carb}}$ values range from -13.8‰ to -8.94‰, with a mean value of -11‰ (SD = 1.2‰) (Table 2; Table 3). Considering species' different fractionation-enrichment factors, the $\delta^{13}\text{C}_{\text{carb}}$ were transformed in $\delta^{13}\text{C}_{\text{diet}}$, resulting in mean values that extend from -27.235‰ to -23.527‰ (Fig. 4). It must be considered that average values may reflect slightly different periods or be affected by seasonal bias because different teeth encompass different diverse periods, but it has been verified in our teeth that the variations are limited when the seasonal information of the sequential sampling is incorporated (± 0.2 ; Appendix B). The carbon isotopic composition varies between species. The bovines have generally higher mean $\delta^{13}\text{C}_{\text{carb}}$ (from -12.489‰ to -8.9424‰) than the horses (from -12.6413‰ to -11.3426‰), whereas the red deer samples fall within the horses' range (from -14.3‰ to -11.3‰). Average values of $\delta^{18}\text{O}_{\text{carb}}$ in all Vasco-Cantabrian individuals extend between -7.233‰ and -3.372‰ (mean = -5.5‰; SD = 0.8‰). When transformed to $\delta^{18}\text{O}$ expected from meteoric waters ($\delta^{18}\text{O}_{\text{mw}}$), with species-adapted correlations, the $\delta^{18}\text{O}_{\text{mw}}$ values range from -10.639‰ to -5.599‰. Less clear patterns in $\delta^{18}\text{O}_{\text{carb}}$ are observed between bovines and horses, with mean values of -5.7‰ and -5.2‰, respectively. In the Mediterranean-northeastern Iberia area, the site of Canyars, both species have relatively high $\delta^{18}\text{O}_{\text{carb}}$ values that fall inside the range of variation observed in the Cantabria region, between -5.536‰ and -3.655‰ in bovines and between -4.84‰ and -4.48‰ in case of horses.

	Vasco-Cantabrian region (NW Iberia)				Mediterranean region (NE Iberia)			
	$\delta^{13}\text{C}_{\text{carb}}$ VPDB (‰)	$\delta^{13}\text{C}_{\text{diet}}$ VPDB (‰)	$\delta^{18}\text{O}_{\text{carb}}$ VPDB (‰)	$\delta^{18}\text{O}_{\text{mw}}$ VSMOW (‰)	$\delta^{13}\text{C}_{\text{carb}}$ VPDB (‰)	$\delta^{13}\text{C}_{\text{diet}}$ VPDB (‰)	$\delta^{18}\text{O}_{\text{carb}}$ VPDB (‰)	$\delta^{18}\text{O}_{\text{mw}}$ VSMOW (‰)
Mean	-11.0	-25.1	-5.5	-6.7	-9.9	-24.0	-4.6	-5.4
Max	-8.9	-23.5	-3.3	-3.9	-9.0	-23.6	-3.6	-4.3
Min	-13.0	-27.0	-7.2	-9.9	-10.7	-24.4	-5.5	-6.5
Range	4.1	3.5	3.9	6.0	1.7	0.8	1.9	2.2
SD	1.2	0.9	0.8	1.1	0.8	0.3	0.7	0.8
Mean	-10.4	-25.0	-5.7	-6.8	-9.1	-23.7	-4.5	-5.4
Max	-8.9	-23.5	-4.8	-5.7	-9.0	-23.6	-3.6	-4.3
Min	-12.4	-27.0	-7.2	-8.5	-9.3	-23.9	-5.5	-6.5
Range	3.5	3.5	2.4	2.7	0.3	0.3	1.9	2.2
SD	1.1	1.1	0.6	0.7	0.2	0.2	1.4	1.6
Mean	-11.8	-25.5	-5.2	-6.0	-10.4	-24.1	-4.7	-5.4
Max	-11.3	-25.0	-3.3	-3.9	-10.0	-23.7	-4.4	-5.1
Min	-12.6	-26.3	-6.6	-7.6	-10.7	-24.4	-4.8	-5.6
Range	1.4	1.4	3.3	3.7	0.7	0.7	0.5	0.5
SD	0.4	0.4	1.1	1.2	0.3	0.3	0.3	0.3

		Vasco-Cantabrian region (NW Iberia)				Northeastern Iberia			
		$\delta^{13}\text{C}_{\text{carb}}$ VPDB (‰)	$\delta^{13}\text{C}_{\text{diet}}$ VPDB (‰)	$\delta^{18}\text{O}_{\text{carb}}$ VPDB (‰)	$\delta^{18}\text{O}_{\text{mw}}$ VSMOW (‰)	$\delta^{13}\text{C}_{\text{carb}}$ VPDB (‰)	$\delta^{13}\text{C}_{\text{diet}}$ VPDB (‰)	$\delta^{18}\text{O}_{\text{carb}}$ VPDB (‰)	$\delta^{18}\text{O}_{\text{mw}}$ VSMOW (‰)
Total	Mean	-11.0	-25.1	-5.5	-6.0	-9.9	-24.0	-4.6	-7.1
	Max	-8.9	-23.5	-3.3	-5.5	-9.0	-23.6	-3.6	-5.0
	Min	-13.0	-27.0	-7.2	-10.6	-10.7	-24.4	-5.5	-7.9
	Range	4.1	3.5	3.9	5.1	1.7	0.8	1.9	2.9
	SD	1.2	0.9	0.8	1.2	0.8	0.3	0.7	1.2
Bovines	Mean	-10.4	-25.0	-5.7	-7.7	-9.1	-23.7	-4.5	-6.2
	Max	-8.9	-23.5	-4.8	-6.5	-9.0	-23.6	-3.6	-5.0
	Min	-12.4	-27.0	-7.2	-9.5	-9.3	-23.9	-5.5	-7.4
	Range	3.5	3.5	2.4	3.0	0.3	0.3	1.9	2.4
	SD	1.1	1.1	0.6	0.7	0.2	0.2	1.4	1.7
Horses	Mean	-11.8	-25.5	-5.2	-8.5	-10.4	-24.1	-4.7	-7.6
	Max	-11.3	-25.0	-3.3	-5.5	-10.0	-23.7	-4.4	-7.2
	Min	-12.6	-26.3	-6.6	-10.6	-10.7	-24.4	-4.8	-7.9
	Range	1.4	1.4	3.3	5.1	0.7	0.7	0.5	0.7
	SD	0.4	0.4	1.1	1.8	0.3	0.3	0.3	0.4

Table 3. Mean $\delta^{13}\text{C}$ from enamel carbonate ($\delta^{13}\text{C}_{\text{carb}}$) and diet ($\delta^{13}\text{C}_{\text{diet}}$), and $\delta^{18}\text{O}$ from enamel carbonate ($\delta^{18}\text{O}_{\text{carb}}$) and meteoric waters ($\delta^{18}\text{O}_{\text{mw}}$), by species on the Vasco-Cantabrian and Mediterranean-northeastern Iberia areas. Max: maximum value; Min: minimum value; SD: standard deviation.

4.1 Axlor (Mousterian, ca. 80 ka BP - 50 ka cal BP)

A total of seven bovine teeth were included from levels III (n = 4), IV (n = 1), and VI (n = 2) of Axlor cave (Pederzani et al., 2023). The mean $\delta^{13}\text{C}_{\text{carb}}$ range from -9.9‰ to -8.9‰ ($\delta^{13}\text{C}_{\text{diet}}$ = -24.3‰ to -24.5‰); whereas mean $\delta^{18}\text{O}_{\text{carb}}$ values are between -6.2‰ to -4.8‰ and -4.86‰ to -8.35‰ ($\delta^{18}\text{O}_{\text{mw}}$ = -8.35‰ to -6.57‰), indicating a range of variation around 1‰ and 1.4‰, respectively (Fig. 3; 4). Considering isotopic compositions by levels, mean $\delta^{13}\text{C}_{\text{carb}}$ decreases from level III to level IV, whereas mean $\delta^{18}\text{O}_{\text{carb}}$ remains stable through the sequence (Table 2; Appendix B). A range between 0.3‰ and 0.5‰ is observed in $\delta^{13}\text{C}_{\text{carb}}$ variation within tooth profiles. Individuals show clear $\delta^{18}\text{O}$ sinusoidal profiles, with peaks and troughs, and intratooth ranges from 2.1‰ to 3.4‰. The $\delta^{18}\text{O}_{\text{mw}}$ after inverse modelling intratooth profiles range from -9.15‰ to -7.36‰ (Appendix C; D; E). Mean Annual Temperatures (MATs), estimated from mean $\delta^{18}\text{O}_{\text{mw}}$ values, with seasonal control, oscillated between 10.1°C and 12.64°C (MATAs = -3.1/+0.4+1.8/-2.1°C) (Table 4). From sinusoidal profiles, summer temperatures were extracted from peaks, which are estimated to extend resulting from 15.4°C to 23.7°C, and winter temperatures from troughs provided values ranging from -7°C to 10.8°C. Mean Annual Precipitation (MAPs), extracted from $\delta^{13}\text{C}_{\text{carb}}$, extend between 204mm and 326mm (MAPAs = 843/241/721/843mm). Based on these estimations, a non-clear climatic trend is observed through these levels.

4.2 El Castillo (Mousterian and Transitional Aurignacian, 62.5 ka BP – 46.4 ka cal BP)

Formatted: Subscript

Formatted: Subscript

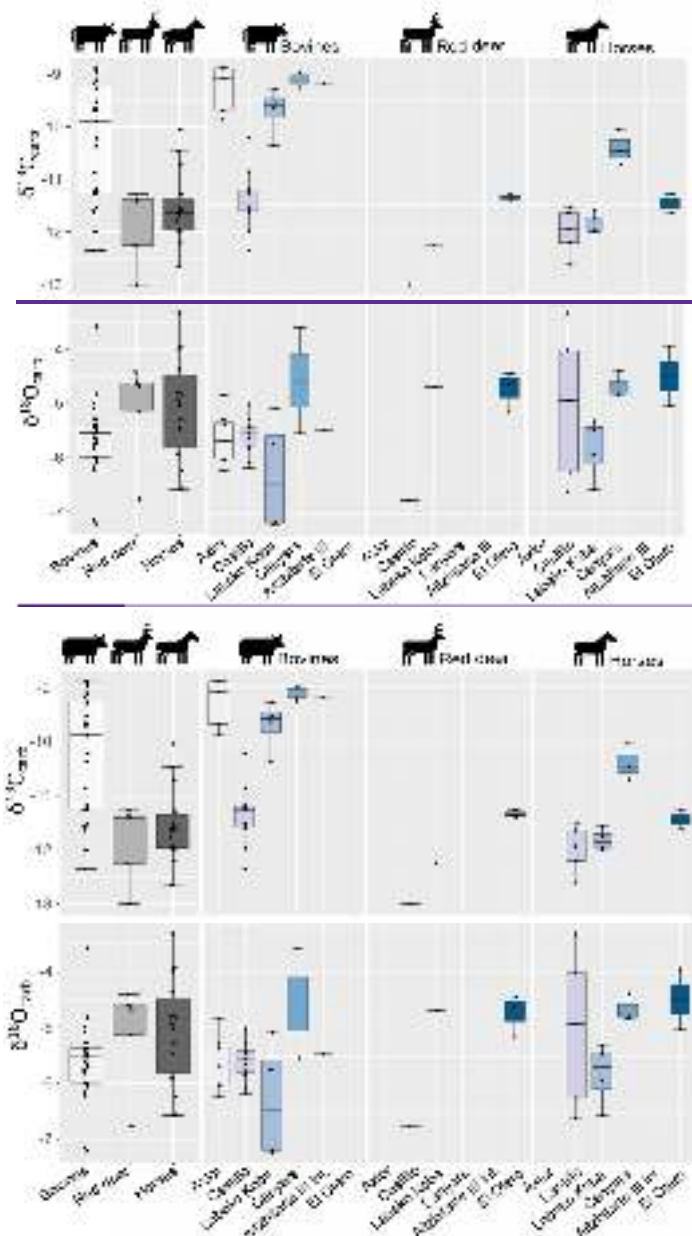
Formatted: Subscript

Formatted: Subscript

511

512 From El Castillo, this work includes bovines (n = 11), horses (n = 5), and red deer (n = 1) teeth from the
513 Mousterian (21 and 20E) and the Transitional Aurignacian levels (18B and 18C). The mean $\delta^{13}\text{C}_{\text{carb}}$ values
514 are lower for horses, bovines, and red deer (-13‰ to -10.2‰) than other sites. Between -12.4‰ and -10.2‰
515 for bovines ($\delta^{13}\text{C}_{\text{diet}} = -24.6‰$ to $-25.8‰$) and between -12.6‰ and -11.5‰ for horses ($\delta^{13}\text{C}_{\text{diet}} = -26.3‰$ to
516 -25.2‰) (Fig. 3). The mean $\delta^{18}\text{O}_{\text{carb}}$ values extend from -6.8‰ and -3.3‰. Horses and bovines overlap in
517 their isotopic niche (Fig. 4), mainly due to the notably lower $\delta^{13}\text{C}_{\text{carb}}$ reported by bovines. The mean $\delta^{13}\text{C}_{\text{carb}}$
518 (-13‰) of the single red deer tooth is inside the variation range of bovines and horses but with a lower
519 $\delta^{18}\text{O}_{\text{carb}}$ mean value (-6.8‰). Considering these isotopic compositions by levels, bovine mean $\delta^{13}\text{C}_{\text{diet}}$ values
520 highly increase the variation range from Mousterian levels (20E and 21A) to Transitional Aurignacian levels
521 (18C and 18B). In contrast, horses increase mean $\delta^{13}\text{C}_{\text{diet}}$ values (Fig. 5). Bovine mean $\delta^{18}\text{O}_{\text{mw}}$ values
522 decrease from level 21A to level 18B, while horses from 18B have a large intra-level amplitude.

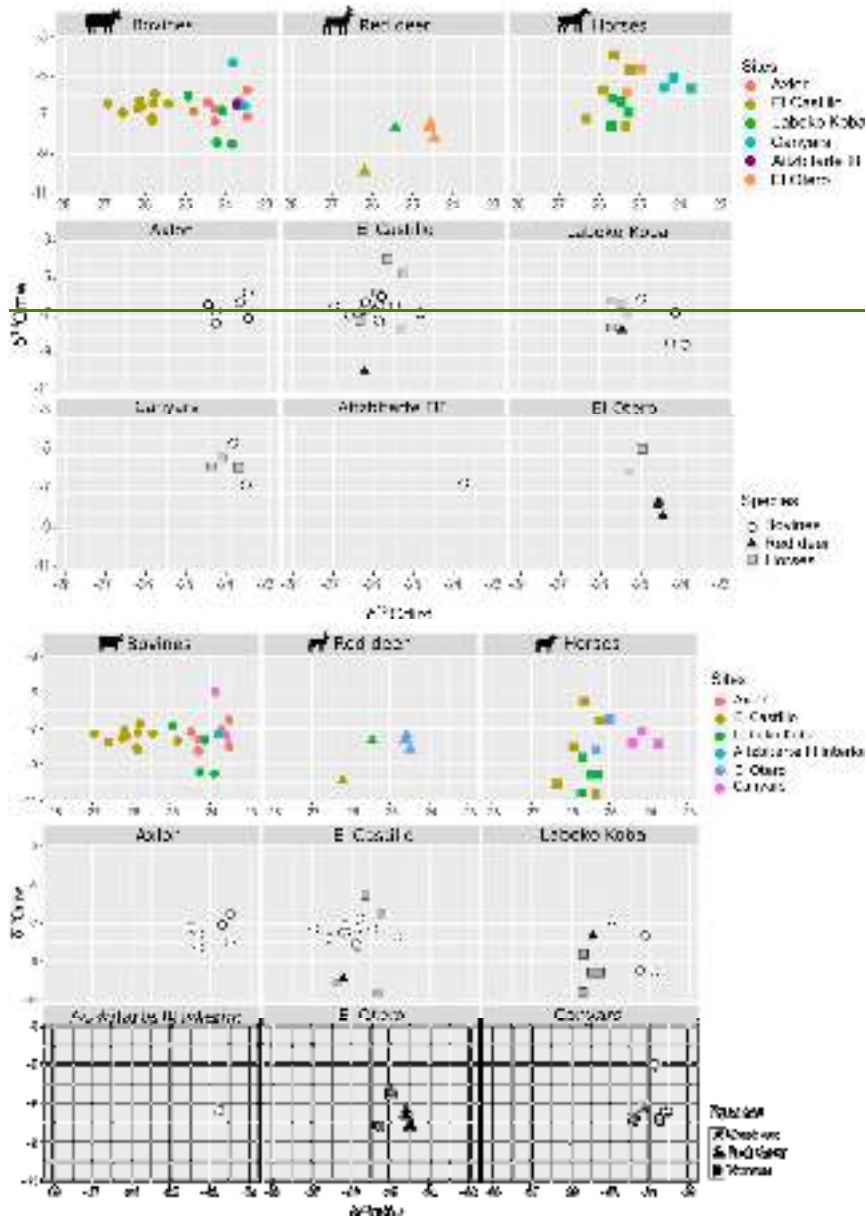
523 The mean $\delta^{18}\text{O}_{\text{carb}}$ values from horses have a more significant variation (range = 3.3‰) than bovines (range
524 = 2.2‰). All individuals show flat $\delta^{13}\text{C}_{\text{carb}}$ intratooth profiles (<0.4‰), except for red deer (1‰) (Appendix
525 DC). Intratooth $\delta^{18}\text{O}_{\text{carb}}$ ranges of individuals are around 1-2‰ for horses and 1-3‰ for bovines. Some of
526 the individuals analyzed do not show non-complete annual cycles. No precise $\delta^{18}\text{O}_{\text{carb}}$ sinusoidal profiles
527 are detected in three teeth; the other six have particularly unclear profiles. After modelling, individual $\delta^{18}\text{O}_{\text{carb}}$
528 ranges oscillated between 2.7‰ and 7.4‰ (Appendix ED). MATs oscillated between 4.6°C and 12.6°C
529 (MATAs = -8.8°C/-0.9°C), with mean summer temperatures from around 20.5°C and mean winter
530 temperatures around -1.1°C. MAPs extend between 376mm and 784mm (MAPAs = -656/-248mm) (Table
531 4). Non-important differences in rainfall estimations based on bovines and equids are noticed, probably
532 because they feed on similar ecological resources. Diachronic trends are unclear along the sequence, but
533 mean annual and winter temperatures from levels 18C and 18C seem slightly lower. MAPs estimations
534 oscillated more in the upper levels.



535

536

537 **Figure 3.** Distribution of mean carbon ($\delta^{13}\text{C}_{\text{carb}}$) and oxygen ($\delta^{18}\text{O}_{\text{carb}}$) isotopic values from of enamel carbonate for by species and
 538 archaeological site.



539

540

541 Figure 4. Biplot crossing- $\delta^{13}\text{C}$ from diet ($\delta^{13}\text{C}_{\text{diet}}$) and $\delta^{18}\text{O}$ from meteoric waters ($\delta^{18}\text{O}_{\text{mw}}$) by species and archaeological sites.

542 **4.3 Labeko Koba (Châtelperronian and Aurignacian, 45.1-36.3 ka cal BP)**

543 This work includes teeth of bovines (n = 4), horses (n = 4), and red deer (n = 1) teeth from levels related to
 544 Châtelperronian (IXb inf), ProtoAurignacian (VII), and Aurignacian (VI, V, and IV). Significant differentiation
 545 in mean $\delta^{13}\text{C}_{\text{carb}}$ between bovines and horses is observed, with higher values between -9.3‰ and -10.4‰

Formatted: Subscript

Formatted: Subscript

546 in bovines ($\delta^{13}\text{C}_{\text{diet}} = -25.23.8\text{‰}$ to $-23.8-25\text{‰}$) than equids, whose values extend from -1244.6‰ to $-$
547 4211.6‰ ($\delta^{13}\text{C}_{\text{diet}} = -25.82\text{‰}$ to -25.28‰) (Fig. 3;). These horses' values are within the ranges observed
548 from this species in the region. Red deer have similar $\delta^{13}\text{C}_{\text{carb}}$ values to those of horses ($\delta^{13}\text{C}_{\text{carb}} = -12.3\text{‰}$;
549 $\delta^{13}\text{C}_{\text{diet}} = -25.5\text{‰}$). Mean $\delta^{18}\text{O}_{\text{carb}}$ values are similar between species from $-7.24.7\text{‰}$ to $-4.77.2\text{‰}$ ($\delta^{18}\text{O}_{\text{mw}} =$
550 $-8.56.4\text{‰}$ to $-6.18.5\text{‰}$). However, bovines have a very high variation within mean $\delta^{18}\text{O}_{\text{carb}}$ values (2.1‰),
551 also reflected in the intratooth profiles. These $\delta^{18}\text{O}$ values are lower than in other Vasco-Cantabrian sites,
552 especially for two individuals in levels VII and V (Table 3). Differences in $\delta^{13}\text{C}_{\text{diet}}$ values between bovines
553 and horses result in isotopic niche differentiation between both species (Fig. 4). The red deer niche is placed
554 within the horses' niche. The evolution of ~~red this deer~~ niche over time cannot be evaluated by levels due to
555 the limited sample. Considering the isotopic compositions by levels (Fig. 5), both bovines and horses
556 experienced a slight increase in mean $\delta^{13}\text{C}_{\text{diet}}$ from levels IX_inf to IV_inf that is, from Châtelperronian to
557 Aurignacian. Mean $\delta^{18}\text{O}_{\text{mw}}$ values of bovines decrease from VII to V, whereas ~~in the case of horses increase~~
558 ~~from XIinf to VI to the horses increase from XIinf to VI to~~ decrease from VI to IV.

559 Variability of $\delta^{13}\text{C}_{\text{carb}}$ values in intratooth profiles is slightly higher (0.1-0.7‰), especially in bovines (0.3-
560 0.9‰), with more oscillating profiles than generally flat profiles observed in horses and red deer (Appendix
561 C-D; E). Intratooth profiles ranges of $\delta^{18}\text{O}_{\text{carb}}$ are also larger within bovines (2-4‰) than in horses (1-2‰).
562 Inverse-modelled individual $\delta^{18}\text{O}_{\text{carb}}$ ranges oscillated between 5-8‰ and 2-4‰, respectively. Sinusoidal
563 curves are observed ~~both~~ in horses and bovines, but bovine profiles are noisier. The red deer has a ~~large~~
564 ~~extensive~~ $\delta^{18}\text{O}_{\text{carb}}$ range (6.3‰) from summer peak to an incomplete winter trough. We detect an inverse
565 relation between $\delta^{13}\text{C}_{\text{carb}}$ and $\delta^{18}\text{O}_{\text{carb}}$ in some points of these individual profiles. MATs oscillated between
566 5.27°C and $11.43.7^\circ\text{C}$ (MATAs = $-5.6/+1.1^\circ\text{C}$), with summer temperatures from $14.5.3^\circ\text{C}$ to 27.35°C and
567 winter temperatures from 01.9°C to $-4.99.4^\circ\text{C}$. MAPs extend between 248mm and 521mm, ~~which are~~
568 ~~notable drier conditions~~ notably drier than nowadays (MAPAs = $-798/-525\text{mm}$) (Table 4). Lower rainfall levels
569 and higher seasonal amplitudes are recorded along the sequence, especially in samples from the
570 ProtoAurignacian level VII. Relevant differences are noticed between MAPs estimated from bovines and
571 equids, the first providing more arid conditions.

572 4.4 Aitzbitarte III interior (Gravettian, 27.9 ka cal BP)

573 A single bovine individual was analysed from Gravettian level V ~~located in the inner part of the cave, related~~
574 ~~to Gravettian~~. It has a high mean $\delta^{13}\text{C}_{\text{carb}}$ (-9.2‰) considering the observed range in bovines from the Vasco-
575 Cantabrian region, whereas the $\delta^{18}\text{O}_{\text{carb}}$ mean value (-5.5‰) is inside the common $\delta^{18}\text{O}_{\text{carb}}$ variation
576 observed (Fig. 3). The mean $\delta^{13}\text{C}_{\text{diet}}$ value of -23.8‰ is comparable with Canyars and some individuals from
577 Axlor, but different from Labeko Koba and El Castillo individuals. The individual $\delta^{13}\text{C}_{\text{carb}}$ fluctuation is ~~small~~
578 ~~slight~~ (0.3‰) (Appendix C; D; E). These teeth show not quite sinusoidal profile shape in $\delta^{18}\text{O}_{\text{carb}}$, with an
579 intratooth range of around 2.2‰. Climatic information is extracted but may be considered cautiously due to
580 the profile shape and the limited sample size. From the inverse modelled mean $\delta^{18}\text{O}_{\text{mw}}$ value (-5.4‰), we
581 estimate a MAT of 134.5°C (MATA = $-0.4+1.4^\circ\text{C}$) with a summer temperature of $19.7.5^\circ\text{C}$ and winter
582 temperature of -2.94°C . The MAP estimation reached 235mm (-1127mm to nowadays) (Table 4).

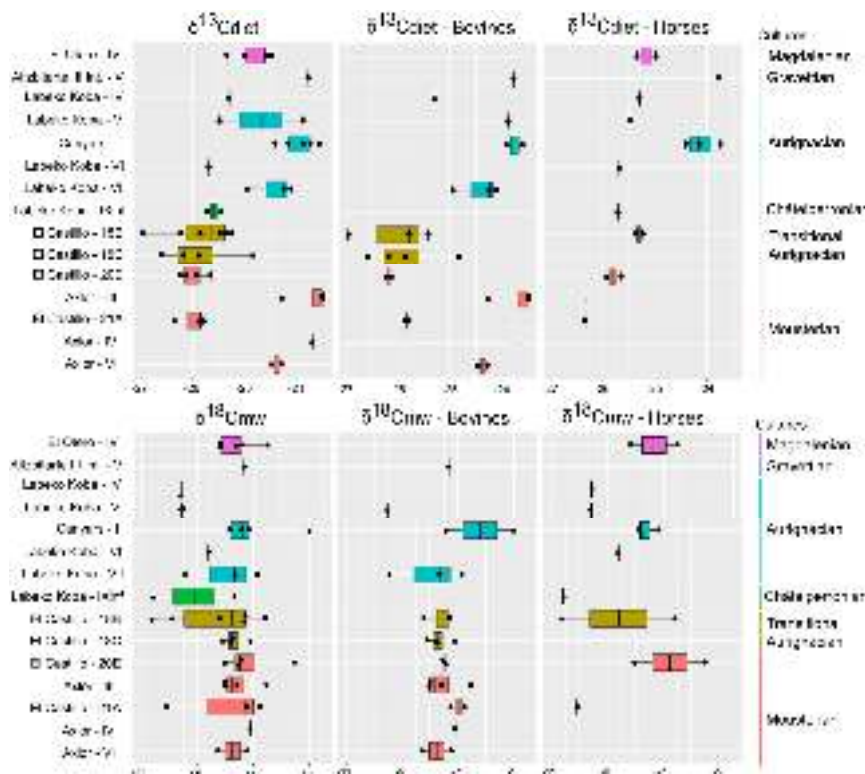
583 4.5 El Otero (Magdalenian, ca. 17.3 ka cal BP)

584 Two equids and three cervids are included from level IV from El Otero, ~~recently redated and chronologically~~
585 ~~related to the Magdalenian phase (Marín-Arroyo et al., 2018)~~. The mean $\delta^{13}\text{C}_{\text{carb}}$ values are close, between
586 -11.43‰ and -11.34‰ for red deer ($\delta^{13}\text{C}_{\text{diet}} = -24.4\text{‰}$ and -24.6‰) and -11.63‰ and -11.36‰ for horse
587 ($\delta^{13}\text{C}_{\text{diet}} = -25.3\text{‰}$ and -25.3‰) (Fig. 3). These $\delta^{13}\text{C}$ values for both species are relatively high concerning
588 other studied samples, especially for cervids (around $+1-2\text{‰}$). Both species have higher $\delta^{18}\text{O}_{\text{carb}}$ values
589 concerning the common range of variation observed in the Vasco-Cantabria region, between -53.9‰ and $-$
590 3.95‰ for horses and between $-5.14.4\text{‰}$ and $-4.45.4\text{‰}$ for red deer. When values are transformed to $\delta^{13}\text{C}_{\text{diet}}$
591 and $\delta^{18}\text{O}_{\text{mw}}$, equids and cervids isotopic niches are separated (Fig. 4). All individuals show low-amplitude

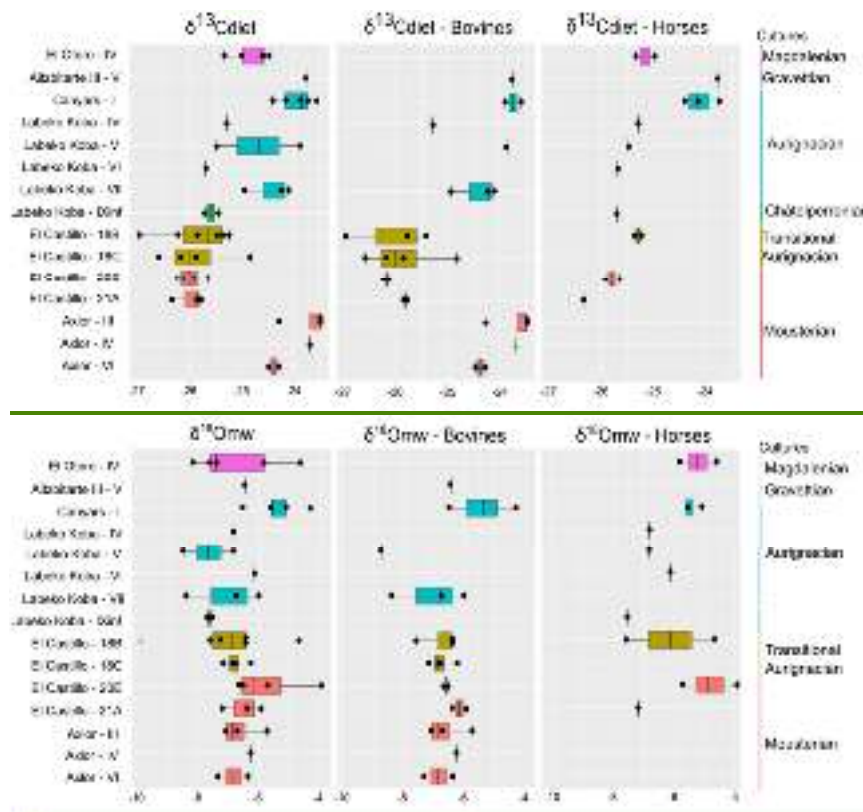
Formatted: Subscript

Formatted: Subscript

592 $\delta^{13}\text{C}_{\text{carb}}$ intratooth profiles (<0.3‰), but especially equids with an intratooth variation around 0.1‰ (Appendix
593 G; D; E). Equids and cervids show $\delta^{18}\text{O}_{\text{carb}}$ sinusoidal profiles, with intratooth ranges between 1.4‰ and
594 2.4‰. Climatic estimations are proposed only for equids, providing MATs estimations from $13.48.8^{\circ}\text{C}$ to
595 $12.6.7^{\circ}\text{C}$ (MATAs = $-4.90.3^{\circ}\text{C}/-1+3^{\circ}\text{C}$) and MAP between 400mm and 456mm (MAPAs = -755/-699mm)
596 (Table 4). A high-temperature seasonality can be seen, with summer temperatures between $19.7.4^{\circ}\text{C}$ and
597 $23.82.5^{\circ}\text{C}$ and winter temperatures from $0.7-10.4^{\circ}\text{C}$ to $-3.17.2^{\circ}\text{C}$.



598



599

600 **Figure 5.** Evolution of $\delta^{13}\text{C}$ in diet ($\delta^{13}\text{C}_{\text{diet}}$) and $\delta^{18}\text{O}$ in meteoric waters ($\delta^{18}\text{O}_{\text{mw}}$) by archaeological levels in a diachronic order.
 601 From right to left: all species, including cervids, bovines and horses. Colors correspond to different chrono-cultures.

602 **4.6 Canyars (Aurignacian, 39.7 ka cal BP)**

603 From the archaeological layer-level I at Canyars, corresponding to the Aurignacian, this work includes
 604 bovines (n = 2) and equids (n = 3) teeth. The mean $\delta^{13}\text{C}_{\text{carb}}$ values for bovines are between -9‰ to -9.3‰
 605 ($\delta^{13}\text{C}_{\text{diet}} = -23.6\text{‰}$ and -23.8‰), and for horses between -10‰ and -10.7‰ ($\delta^{13}\text{C}_{\text{diet}} = -23.7\text{‰}$ and -24.4‰)
 606 (Fig.3). In this site, the $\delta^{13}\text{C}_{\text{carb}}$ values for horses are notably higher than samples in the Vasco-Cantabrian
 607 region (around $+1\text{‰}$ to $+2\text{‰}$) (Table 3). Both species have relatively high $\delta^{18}\text{O}_{\text{carb}}$ values, but they fall inside the
 608 range of variation observed in the Vasco-Cantabrian region, between -5.5‰ to -3.6‰ and -5.5‰ to -3.6‰ in bovines
 609 and between -4.84‰ and -4.48‰ in horses. Different responses are seen in mean $\delta^{18}\text{O}$ values between the
 610 two bovines, with one high mean value, but with close $\delta^{13}\text{C}$ mean values. Bovine and equid isotopic
 611 niches overlap (Fig. 4), but different responses are seen in mean $\delta^{18}\text{O}_{\text{mw}}$ values between the two bovines,
 612 with one high mean value but close $\delta^{13}\text{C}_{\text{diet}}$ mean values.

613 All individuals show flat $\delta^{13}\text{C}_{\text{carb}}$ intratooth profiles ($<0.3\text{‰}$ variation). Some individuals analysed do not show
 614 $\delta^{18}\text{O}_{\text{carb}}$ sinusoidal profiles, with intratooth profiles moderately flat and ranging from 1.14‰ to 1.66‰ . We
 615 detect an inverse relation between $\delta^{13}\text{C}_{\text{carb}}$ and $\delta^{18}\text{O}_{\text{carb}}$ in some points of bovine individual isotopic profiles.
 616 MATs oscillated between 42.59°C and 114.98°C (MATAs = -5.42‰ to -30.32‰), with summer
 617 temperatures from 16.35°C to 27.5°C and winter temperatures from 7.3°C to 1.84°C (Table 4).

Formatted: Subscript

618 MAPs extend between 211mm and 316mm (MAPAs = -431/-326mm). No substantial differences are noticed
 619 in the estimations based on bovines and equids because mean $\delta^{13}\text{C}$ diet values differed relatively little.

Site	Sample	Level	Species	MAT (°C)		Summer (°C)		Winter (°C)		Seasonality (°C)	MAP (mm)	
				Estimated	Relative	Estimated	Relative	Estimated	Relative		Estimated	Relative
Axlor	AXL59	III	<i>Bos/Bison</i> sp.	9.4	-2.8	17.6	-0.3	-3.9	-11.0	21.5	204	-843
	AXL60	III	<i>Bos/Bison</i> sp.	10.8	-1.4	22.7	4.7	4.8	-2.3	17.9	300	-747
	AXL65	III	<i>Bos/Bison</i> sp.	9.7	-2.5	22.7	4.8	-2.5	-9.6	25.2	204	-843
	AXL66	III	<i>Bos/Bison</i> sp.	12.6	0.4	22.8	4.8	-3.2	-10.3	26.0	204	-843
	AXL70	IV	<i>Bos/Bison</i> sp.	11.1	-1.1	21.9	3.9	-8.0	-15.1	29.9	227	-820
	AXL77	VI	<i>Bos/Bison</i> sp.	9.1	-3.1	20.4	2.5	-10.9	-17.9	31.3	300	-747
	AXL86	VI	<i>Bos/Bison</i> sp.	11.1	-1.1	25.9	8.0	3.1	-4.0	22.8	326	-721
El Castillo	CAS141	21A	<i>Bos/Bison</i> sp.	11.7	-1.7	24.2	5.6	-0.8	-9.9	25.1	546	-486
	CAS142	21A	<i>Bison priscus</i>	12.6	-0.9	19.6	1.0	3.1	-5.9	16.5	536	-496
	CAS143	21A	<i>Equus</i> sp.	5.7	-7.8	20.7	2.1	-5.6	-14.7	26.3	645	-387
	CAS60	20E	<i>Equus</i> sp.					1.6	-7.5		510	-522
	CAS61	20E	<i>Equus</i> sp.	9.7	-3.8	25.9	7.3	-4.1	-13.2	30.1	561	-471
	CAS139	20E	<i>Bos/Bison</i> sp.	11.2	-2.3	18.8	0.2	1.8	-7.3	17.0	622	-410
	CAS140	20E	<i>Bos/Bison</i> sp.	11.3	-2.1						602	-430
	CAS135	18C	<i>Bos/Bison</i> sp.			17.0	-1.6				551	-481
	CAS136	18C	<i>Bos/Bison</i> sp.	10.6	-2.9						699	-333
	CAS137	18C	<i>Bos/Bison</i> sp.					0.0	-9.1		376	-656
	CAS138	18C	<i>Bos/Bison</i> sp.	11.8	-1.7	18.3	-0.3	3.1	-6.0	15.3	612	-420
	CAS132	18B	<i>Bos/Bison</i> sp.	9.8	-3.6	26.3	7.6	-1.2	-10.3	27.5	548	-484
	CAS133	18B	<i>Bos/Bison</i> sp.					-0.1	-9.2		477	-555
	CAS134	18B	<i>Bos/Bison</i> sp.					0.8	-8.3		784	-248
	CAS58	18B	<i>Equus</i> sp.	4.6	-8.8	13.5	-5.1	-11.2	-20.3	24.7	460	-572
		CAS59	18B	<i>Equus</i> sp.	13.0	-0.5						440
Labeko Koba	LAB38	IX inf	<i>Equus</i> sp.	5.2	-7.4	14.5	-4.1	-1.8	-9.1	16.2	521	-526
	LAB36	IV	<i>Equus</i> sp.	7.0	-5.6	16.3	-2.3	-2.4	-9.7	18.7	448	-599
	LAB42	V	<i>Equus</i> sp.	7.6	-5.0				-7.3		501	-546
	LAB69	V	<i>Bos primigenius</i>	6.3	-6.3	17.3	-1.2	-4.9	-12.2	22.2	248	-799
	LAB20	VI	<i>Equus</i> sp.	9.1	-3.5	15.7	-2.9	-0.9	-8.2	16.6	517	-530
	LAB53	VII	<i>Bos primigenius</i>	11.3	-1.3	27.3	8.7	-2.4	-9.7	29.7	278	-769
	LAB55	VII	<i>Bos primigenius</i>	11.4	-1.2	26.3	7.8	1.9	-5.4	24.4	397	-650
	LAB62	VII	<i>Bos/Bison</i> sp.	7.2	-5.4	20.6	2.1	-2.9	-10.2	23.5	295	-752
Canyers	CAN01	I	<i>Equus</i> sp.	9.8	-5.4	16.3	-5.9	1.7	-7.5	14.6	232	-410
	CAN02	I	<i>Equus ferus</i>	11.9	-3.3						284	-358
	CAN03	I	<i>Equus ferus</i>	10.4	-4.7	18.6	-3.6	-0.5	-9.7	19.1	316	-326
	CAN04	I	<i>Bos primigenius</i>	17.2	2.1	27.5	5.3				247	-395
	CAN05	I	<i>Bos primigenius</i>	11.3	-3.9	17.5	-4.7	1.8	-7.4	15.7	211	-431
Aitzbitarte III int	AIT10	V	<i>Bos/Bison</i> sp.	13.0	-0.4	19.7	0.7	-2.9	-11.4	22.6	235	-1127
Otero	OTE11	IV	<i>Equus</i> sp.	8.8	-4.9	19.7	0.9	-10.4	-19.8	30.1	456	-699
	OTE12	IV	<i>Equus</i> sp.	12.6	-1.0	23.8	5.0	-3.1	-12.5	26.8	400	-755

620

Site	Sample	Level	Species	MAT (°C)		Summer (°C)		Winter (°C)		MAP (mm)	
				Estimated	Relative	Estimated	Relative	Estimated	Relative	Estimated	Relative
Axlor	AXL59	III	<i>Bos/Bison</i> sp.	10.5	-1.7	15.4	-2.6	0.9	-6.2	204	-843
Axlor	AXL60	III	<i>Bos/Bison</i> sp.	12.0	-0.2	20.4	2.5	10.8	3.7	300	-747
Axlor	AXL65	III	<i>Bos/Bison</i> sp.	10.8	-1.4	20.5	2.5	2.5	-4.6	204	-843
Axlor	AXL66	III	<i>Bos/Bison</i> sp.	14.0	1.8	20.5	2.5	1.7	-5.4	204	-843
Axlor	AXL70	IV	<i>Bos/Bison</i> sp.	12.4	0.2	19.6	1.6	-3.8	-10.9	227	-820
Axlor	AXL77	VI	<i>Bos/Bison</i> sp.	10.1	-2.1	18.2	0.2	-7.0	-14.1	300	-747
Axlor	AXL86	VI	<i>Bos/Bison</i> sp.	12.3	0.2	23.7	5.7	8.9	1.8	326	-721
El Castillo	CAS141	21A	<i>Bos/Bison</i> sp.	13.1	-0.4	22.0	3.3	4.4	-4.7	546	-486
El Castillo	CAS142	21A	<i>Bison priscus</i>	14.0	0.5	17.3	-1.3	8.9	-0.2	536	-496
El Castillo	CAS143	21A	<i>Equus</i> sp.	10.8	-2.7	20.1	1.5	5.0	-4.1	645	-387
El Castillo	CAS60	20E	<i>Equus</i> sp.					11.3	2.3	510	-522
El Castillo	CAS61	20E	<i>Equus</i> sp.	14.2	0.7	24.2	5.6	6.3	-2.8	561	-471
El Castillo	CAS139	20E	<i>Bos/Bison</i> sp.	12.5	-1.0	16.5	-2.1	7.3	-1.8	622	-410
El Castillo	CAS140	20E	<i>Bos/Bison</i> sp.	12.6	-0.9					602	-430
El Castillo	CAS135	18C	<i>Bos/Bison</i> sp.			14.8	-3.8			551	-481
El Castillo	CAS136	18C	<i>Bos/Bison</i> sp.	11.8	-1.6					699	-333
El Castillo	CAS137	18C	<i>Bos/Bison</i> sp.					5.4	-3.7	376	-656
El Castillo	CAS138	18C	<i>Bos/Bison</i> sp.	13.1	-0.4			8.8	-0.3	612	-420
El Castillo	CAS102	10B	<i>Bos/Bison</i> sp.	11.0	-2.5	24.0	-5.4	4.0	-5.1	540	-404
El Castillo	CAS133	18B	<i>Bos/Bison</i> sp.					5.2	-3.9	477	-555
El Castillo	CAS134	18B	<i>Bos/Bison</i> sp.					6.2	-2.9	784	-248
El Castillo	CAS58	18B	<i>Equus</i> sp.	9.9	-3.6	14.5	-4.1	0.1	-9.0	460	-572
El Castillo	CAS59	18B	<i>Equus</i> sp.	17.0	3.6					440	-592
Labeko Koba	LAB38	IXinf	<i>Equus</i> sp.	10.3	-2.3	15.3	-3.3	8.4	1.1	521	-526
Labeko Koba	LAB36	IV	<i>Equus</i> sp.	11.9	-0.7	16.7	-1.9	7.8	0.5	448	-599
Labeko Koba	LAB42	V	<i>Equus</i> sp.	13.1	0.5					501	-546
Labeko Koba	LAB69	V	<i>Bos primigenius</i>	7.0	-5.6	15.1	-3.5	-0.2	-7.6	248	-799
Labeko Koba	LAB20	VI	<i>Equus</i> sp.	13.7	1.1	16.2	-2.3	9.1	1.8	517	-530
Labeko Koba	LAB53	VII	<i>Bos primigenius</i>	12.5	-0.1	25.0	6.4	2.6	-4.7	278	-769
Labeko Koba	LAB55	VII	<i>Bos primigenius</i>	12.7	0.1	24.0	5.5	7.5	0.2	397	-650
Labeko Koba	LAB62	VII	<i>Bos/Bison</i> sp.	8.1	-4.5	18.3	-0.2	2.1	-5.3	295	-752
Canyars	CAN01	I	<i>Equus</i> sp.	14.3	-0.9	16.7	-5.5	11.4	2.2	232	-410
Canyars	CAN02	I	<i>Equus ferus</i>							284	-358
Canyars	CAN03	I	<i>Equus ferus</i>	14.8	-0.3	18.5	-3.7	9.5	0.3	316	-326
Canyars	CAN04	I	<i>Bos primigenius</i>			25.2	3.0			247	-395
Canyars	CAN05	I	<i>Bos primigenius</i>	12.5	-2.6	15.2	-7.0	7.3	-1.8	211	-431
Aitzbitarte III	ATI10	V	<i>Bos/Bison</i> sp.	14.5	1.1	17.5	-1.5	2.1	-6.5	235	-1127
Otero	OTE11	IV	<i>Equus</i> sp.	13.4	-0.3	19.4	0.6	0.8	-8.6	456	-699
Otero	OTE12	IV	<i>Equus</i> sp.	16.7	3.0	22.5	3.7	7.2	-2.2	400	-755

621

622 **Table 4.** Summary of paleoclimatic estimations, based on $\delta^{18}\text{O}$ for temperatures (Mean Annual Temperatures, MAT; summer; winter) and in $\delta^{13}\text{C}$ for precipitation (Mean Annual Precipitations, MAP). Only teeth with validated seasonal curves are included in the summer and winter temperature estimations were obtained from teeth with clear seasonal profiles after modelling, teeth peaks and trough while MAT was averaged between summer and winter before modelling profiles. For in cases some of profiles with an unclear seasonal shapes, MATs were deduced from the original average of all points of the teeth profiles with an unclear seasonal shape, MAT was deduced from the original average of all teeth points without a seasonal profile (values marked in red italics). Mean Details on teeth selection are presented in Appendix B, error associated to temperature estimations is 5.1 ± 0.6 (see details in Appendix B). Seasonality is calculated as the temperature difference between summer and winter.

630 5. Discussion

631 5.1 Diet and ecological niches: carbon ratios

632 Carbon isotopic ratios are valuable indicators for discerning past animal diets based on the ecosystems or parts of the ecosystem where the animals most frequently foraged. They are also, partially influenced by the physiology of the animal. Considering species trends in the studied sites, bovines have generally higher mean $\delta^{13}\text{C}_{\text{carb}}$ values (from -12.4‰ to -8.9‰ to -12.4‰ to -8.9‰) than horses (from -12.6‰ to -11.3‰ to -11.3‰ to -12.6‰), whereas the red deer fall within the horses' range (from -13‰ to -11.3‰ to -13‰ to -11.3‰). In Canyars, in the Mediterranean northeastern site of Canyars area, bovines also show higher mean $\delta^{13}\text{C}_{\text{carb}}$ values (-9‰ to -9.3‰) compared to horses (-10.7‰ to -10.7‰). These differentiated isotopic ranges for equids and bovines can be potentially linked to feeding behaviour, but still, these species are expected to present different basal $\delta^{13}\text{C}_{\text{carb}}$ driven not only by their feeding behavior but also by their feeding behaviour and distinct physiological characteristics considering their physiology and diet. Bovines, being ruminants, have been suggested in previous studies to exhibit higher $\delta^{13}\text{C}_{\text{carb}}$ values due to increased methane

643 production (Cerling and Harris, 1999; Tejada-Lara et al., 2018). Therefore, transforming $\delta^{13}\text{C}_{\text{carb}}$ to $\delta^{13}\text{C}_{\text{diet}}$
644 values [using species-specific equations](#) is crucial to mitigate the species-specific impact, particularly when
645 comparing ruminants and non-ruminants. Bovines report $\delta^{13}\text{C}_{\text{diet}}$ values between [-27.5‰](#) [-23.5‰](#) and [-](#)
646 [23.5‰](#) [-27.5‰](#) and horses between [-26‰](#) [-25‰](#) and [-26‰](#) [-25‰](#). These carbon compositions are typical of
647 animals feeding on C3 plants (commonly accepted range between -34‰ and -23‰), as can be expected
648 from high-latitude ecosystems during the Pleistocene (Bocherens, 2003; Cerling and Harris, 1999; Drucker,
649 2022).

650 Environmental factors such as light exposure, water stress, temperature fluctuations, salinity, and
651 atmospheric CO_2 changes can influence variations in $\delta^{13}\text{C}$ values in a diet primarily based on C3 plants
652 (Bocherens, 2003; Kohn, 2010). Typically, $\delta^{13}\text{C}_{\text{diet}}$ values below -27‰ ($\delta^{13}\text{C}_{\text{carb}} = -13‰$) are associated with
653 animals feeding on C3 vegetation found in closed forested environments, whereas $\delta^{13}\text{C}_{\text{diet}}$ values between
654 -27‰ and -23‰ are linked to C3 open landscapes, which could include grasslands and steppe areas
655 (Bocherens, 2003). The relatively high $\delta^{13}\text{C}_{\text{diet}}$ observed here points to animals predominantly feeding in
656 open environments. The canopy effect, characterised by a depletion in ^{13}C isotopes due to dense tree cover,
657 seems unlikely among the analysed samples since none of the individuals reported $\delta^{13}\text{C}_{\text{diet}}$ below the
658 [common-standard](#) cut-off of -27‰ (Drucker et al., 2008; Kohn, 2010; van der Merwe, 1991). Therefore, in
659 general terms, open mosaic landscapes, ranging from light forests to meadows and grasslands, can be
660 inferred for northwestern Iberia. Given the generally higher $\delta^{13}\text{C}_{\text{diet}}$ values reported by bovines, it is likely
661 that they were foraging in more open environments than horses and can be considered predominantly
662 grazers. Particularly, bovines from El Castillo exhibit distinct feeding behavior compared to other Vasco-
663 Cantabrian sites, as evidenced by their lower $\delta^{13}\text{C}_{\text{diet}}$ values, indicating a potential preference for browsing
664 and feeding in closer environments, possibly in lightly forested areas. Both extinct aurochs (*Bos primigenius*)
665 and steppe bison (*Bison priscus*) are usually classified as grass-dominant mix-feeders during the
666 Pleistocene, although it should be noted that modern European bison (*Bison bonasus*) could include
667 browsing in their diet (Rivals et al., 2022). For aurochs, a browse-dominated mixed feeding behaviour is also
668 frequently described.

669 The $\delta^{13}\text{C}_{\text{diet}}$ range in equids [also](#) indicates feeding in open environments [as well](#), suggesting a general
670 [mixed](#)-feeding pattern for the Vasco-Cantabrian region. However, individuals from [the northeastern](#)
671 [Mediterranean-Iberia area](#) are likely grazing in more open environments, as evidenced by their notably
672 higher $\delta^{13}\text{C}_{\text{diet}}$ values compared to the Vasco-Cantabrian region (+1-2‰). [It is important to evaluate if other](#)
673 [factors are contributing to lower \$\delta^{13}\text{C}_{\text{diet}}\$ values in horses](#) [Evaluating if other factors contribute to lower \$\delta^{13}\text{C}_{\text{diet}}\$](#)
674 [values in horses is critical](#). In the case of equid [samples](#) from the Vasco-Cantabrian region, it should be
675 considered that they have been pretreated with a combination of NaClO and acetic acid, which could
676 potentially affect the isotopic values. Samples after organic removal pretreatment can potentially show either
677 higher or lower $\delta^{13}\text{C}$ values and higher $\delta^{18}\text{O}$ values based on previous experiments (Pellegrini and Snoeck,
678 2016; Snoeck and Pellegrini, 2015), with $\delta^{13}\text{C}$ values generally varying below 0.3‰. Based on the
679 observation that horses in the Vasco-Cantabrian region present lower $\delta^{13}\text{C}_{\text{carb}}$ values compared to bovines
680 but similar mean $\delta^{18}\text{O}_{\text{carb}}$ value ranges, the influence of the pre-treatment on our samples is deemed to be
681 limited.

682 Furthermore, the high variability in $\delta^{18}\text{O}_{\text{carb}}$ values at El Castillo and Labeko Koba does not correlate with a
683 significant variation in $\delta^{13}\text{C}_{\text{carb}}$ values. Based on dental wear and stable isotopes analysis, Middle and Late
684 Pleistocene horses (*Equus ferus*) were primarily grazers, although some rare cases have been reported as
685 mixed feeders or browsers, such as at Igue des Rameaux [ament of and](#) Schöningen (Kuitens et al., 2015;
686 Rivals et al., 2009, 2015; Uzunidis, 2020). Horse populations from northern and eastern Europe were found
687 to be browsers or mixed feeders, while those from the Mediterranean region tend to be grazers (Rivals et
688 al., 2022).

Formatted: Superscript

Formatted: Subscript

Formatted: Subscript

689 Finally, the few cervids included in this study exhibit $\delta^{13}\text{C}_{\text{diet}}$ values that frequently overlap with ~~those of~~
690 horses, indicating a mixed feeding behaviour that varies from more closed environments in El Castillo to
691 more open habitats in El Otero. During the Pleistocene, the red deer (*Cervus elaphus*) exhibit a flexible,
692 mixed-feeding ~~behavior~~behaviour, consuming leaves, shrubs, forbs, grass, and sedges, similar to their
693 present-day counterparts (Merceron et al., 2021; Rivals et al., 2022). Today, ~~†~~This species inhabits diverse
694 habitats ranging from steppes to closed temperate forests.

695 5.2 Seasonality, mobility and water acquisition: oxygen ratios and intratooth profiles

696 Average values of $\delta^{18}\text{O}_{\text{carb}}$ in Vasco-Cantabrian individuals extend between ~~-7.2‰-3.3‰~~ and ~~-3.3‰-7.2‰~~
697 (Table 3). Even if no clear species patterns in $\delta^{18}\text{O}_{\text{carb}}$ are observed, in general, bovines present slightly
698 lower $\delta^{18}\text{O}_{\text{carb}}$ values from ~~-7.2‰-4.8‰~~ to ~~4.8‰-7.2‰~~ than other species; horses have a large-significant
699 variation from ~~-6.6‰-3.3‰~~ to ~~-3.3‰-6.6‰~~ and red deer from ~~-6.8‰ to -4.4‰~~ to ~~-6.8‰~~. In Canyars, both
700 species have relatively high $\delta^{18}\text{O}_{\text{carb}}$ values that fall inside the variation range observed in the Vasco-
701 Cantabrian region, between ~~-5.5‰ and -3.6‰~~ and ~~-5.5‰~~ in bovines and between ~~-4.8‰-4.4‰~~ and ~~-4.4‰-~~
702 ~~4.8‰~~ in horses. Each species shows different $\delta^{18}\text{O}_{\text{carb}}$ intratooth ranges, with bovines between 1‰ and 3‰,
703 ~~equids-horses~~ mostly around 1.5‰, and ~~cervids-red deer~~ from 1‰ to 6‰ presenting the higher ranges; ~~from~~
704 ~~4‰ to 6‰~~ (Table 3; Appendix CD). After applying inverse modelling to correct the dampening effect (Passey
705 et al., 2005b) (Passey et al., 2005), the majority of teeth increase the $\delta^{18}\text{O}_{\text{carb}}$ intratooth range, between 3‰
706 and 8‰ for bovines and 2‰ and 7‰ for horses (Appendix EB). Most bovines from Axlor and Labeko Koba
707 and ~~equids-horses~~ from El Castillo and El Otero exhibit well-defined sinusoidal profiles in their $\delta^{18}\text{O}_{\text{carb}}$ and
708 large intratooth individual ranges values, related to the predominant consumption of water sources that
709 reflects seasonal indicating potential seasonal fluctuations between $\delta^{18}\text{O}$ values of environmental summer
710 and winter meteoric waters, A, although not all samples consistently follow this pattern consistently, e-
711 Certain specific intratooth profiles, particularly those from bovines in El Castillo and Canyars, exhibit sharp
712 profiles with narrow ranges (<1.5‰). This phenomenon was previously reported in the region in preliminary
713 studies conducted at the sites of El Castillo (Jones et al., 2019) and in the Magdalenian levels of El Mirón
714 cave (Geiling, 2020).

715 Non-sinusoidal profiles observed in the data can be attributed to various factors, including issues-related-to
716 sample techniques and preservation sample techniques and preservation issues and the inherent variability
717 in the original isotopic signal. Factors related to sampling and methods can be connected to 1) the sampling
718 process (e.g. too deep or too distant sampling grooves); 2) the imprecision of the mass spectrometer
719 measurements; 3) uncontrolled effects of samples pretreatments; 4) diagenetic alterations affecting the
720 carbonate fraction. However, it must be noted that technical reasons, whether related to sampling or
721 pretreatment, do not appear to impact the obtained results significantly. First, this study reproduces the
722 same intratooth sampling methods that previously yielded reliable results in similar research (e.g., Pederzani
723 et al., 2023, 2021a). Second, non-significant alterations in intratooth profiles of pretreated horse samples
724 (El Castillo, Labeko Koba, Otero) are noticed in comparison to untreated bovid samples (Appendix DE).
725 Some bovid samples are equally showing these non-sinusoidal profiles show these non-sinusoidal profiles
726 equally. In sites where both species are analysed, no correlation is observed between $\delta^{18}\text{O}_{\text{carb}}$ and $\delta^{13}\text{C}_{\text{carb}}$.
727 In tooth enamel, diagenetic alterations are generally less pronounced than in bone due to its larger-higher
728 mineral content. However, carbonates within tooth enamel can be more susceptible to diagenesis and
729 recrystallisation compared to the phosphate fraction, which contains a larger-more extensive reservoir of
730 oxygen and stronger oxygen bonds (Zazzo et al., 2004; Chenery et al., 2012; Bryant et al., 1996). The
731 carbonate content in our samples, ranging from 3.9% to 8.9%, is similar to the proportion found in modern
732 tooth enamel, suggesting no immediate indication of diagenetic alteration. Diagenesis can also be evaluated
733 by comparing the isotopic values of the carbonate and phosphate fractions in a sample, as there is a
734 predictable difference between them. However, phosphate fraction measurements were still unavailable in

735 our study, except inat the site of Axlor (Pederzani et al., 2023) where good preservation was attested.
736 Additionally, in the case of diagenetic alteration, we would expect specimens from the same archaeological
737 levels to be affected similarly, which is not the case.

738 Based on these arguments, it is suggested that the non-sinusoidal $\delta^{18}\text{O}_{\text{carb}}$ signal observed in some
739 individuals may not be attributed to poor preservation; instead, it is likely attributed to the preservation
740 of reflects the original isotopic signature from water input, which appears to be non-seasonal. Several factors
741 can explain why some teeth do not reflect a clearn evident seasonal fluctuation, which could be related to
742 animals' mobility of the isotopic composition of the water sources, and seasonal buffering within those water
743 sources (Pederzani and Britton, 2019). The main factors considered in our study are 1) the high mobility of
744 the animals analysed among ecosystems with different isotopic baselines due to large migrations; 2) the
745 inland-coastal or short altitudinal movements through the region, which lead to the acquisition of water from
746 sources with different isotopic signal; and 3) the acquisition of water from sources with no clear seasonal
747 signal, such as large bodies of water, rivers, groundwaters, or meltwaters. Furthermore, variability between
748 species and within the same species, even within populations living in the same habitat, is also possible.
749 This can be attributed to multiple factors, from minor differences in foraging and drinking behaviorbehaviour
750 to slight metabolic and physiological variations, including body size, metabolic rate, breathing rate, moisture
751 content of food, and faeces, among others (Hoppe et al., 2004; Kohn, 1996; Magozzi et al., 2019).

752 Analyses of nitrogen and sulphur stable isotopes on ungulate bone collagen from Axlor, El Castillo and
753 Labeko Koba (Jones et al., 2018, 2019; Pederzani et al., 2023) have already revealed large variation ranges
754 linked to the existence of several microenvironments just in a few kilometres within the Vasco-Cantabria
755 region. Long migrations and long hunting distances cannot solely explain these diversified-diverse values;
756 because of the range of species involved and their likely small-scale movements. In our study, the minimal
757 $\delta^{13}\text{C}_{\text{carb}}$ intratooth variation within individuals ($<1\text{‰}$) indicates limited seasonal changes in their feeding
758 behaviorbehaviour that influenced the carbon isotopic composition (Appendix D). Therefore, considering
759 the diverse topography of the Vasco-Cantabrian, characterized by steep diverse orography with
760 perpendicular valleys that connecting the Cantabrian Cordillera with the Atlantic Ocean through rivers over
761 short distances (30-50 km), the availability in the past of a wide range of water sources in small areas seems
762 highly likely. Certain drinking behaviorbehaviours can influence $\delta^{18}\text{O}$, as animals may acquire water from
763 various sources, with small streams better reflecting seasonal isotopic oscillations than large lakes or
764 evaporating ponds (see synthesis in Pederzani and Britton, 2019). Systematic consumption of highly
765 buffered water sources can significantly attenuate the final recorded signal. Furthermore, rivers in the region
766 frequently contain meltwater from snow during the winter-spring months, and water springs are also
767 common.

768

769 5.3 Regional trends and ecological niches

770 This study provides valuable insights despite the limited sample size at each archaeological level. It
771 establishes a baseline of isotopic values for northern Iberia, allowing for the evaluation of regional trends.
772 In the northwest, in the Vasco-Cantabrian region, the $\delta^{13}\text{C}_{\text{carb}}$ values obtained oscillated between -13‰ -
773 8.9‰ and -13‰ -8.9‰ and between -7.2‰ -3.3‰ and -3.3‰ -7.2‰ in the case of $\delta^{18}\text{O}_{\text{carb}}$ values. These
774 values are within the range expected, considering previous regional studies in ungulates (Carvalho et al.,
775 2022; Jones et al., 2019; Lécuyer et al., 2021; Pederzani et al., 2023). Although oxygen variability trends
776 are less precise, the main factor distinguishing the observed changes over time is the variation of carbon
777 isotopic composition among species and regions. The combination of mean $\delta^{13}\text{C}_{\text{diet}}$ and $\delta^{18}\text{O}_{\text{mw}}$ values (Fig.
778 4; 5) accentuates disparities in ecological niche overlap between horses and bovines, whereas cervids and
779 horses frequently exhibit shared ecological niches. The dissimilarities between bovines and horses could

Formatted: Subscript

Field Code Changed

780 be attributed to shifts in feeding ~~behavior~~behaviour, which may be accompanied by ecological and
781 environmental changes, either independently or in parallel.

782 Upon evaluating the entire dataset by sites ~~Comparing the entire dataset and across all sites~~, the consistently
783 lower $\delta^{13}\text{C}_{\text{diet}}$ values in horses compared to bovids throughout time suggest both animals inhabited open
784 landscapes, with bovines exhibiting a grazer preference while horses show a mix-feeding diet. Only in the
785 Middle-to-Upper Paleolithic transition 18B and 18C levels of El Castillo, an exception is observed with lower
786 $\delta^{13}\text{C}_{\text{diet}}$ values in bovines, linked to a higher browser input due to a higher habitat in closer environments,
787 such as open forests, similar to those inhabited by the horses. This generates a niche overlapping between
788 horses and bovines, most likely reflecting stable conditions that could support both species in similar
789 ecosystems. Contrarily, in the Châtelperronian and early Aurignacian levels from Labeko Koba, a clear
790 differentiation between horses and bovines is observed, mainly in $\delta^{13}\text{C}_{\text{diet}}$ values, highlighting the occupation
791 of different ~~landscapes-parts of the landscape~~ by both species. This ~~niche fractionation-spatially-driven niche~~
792 ~~separation~~ between species could result from resource competition derived from an unstable climatic period,
793 where species needed to specialise to adapt to the changing conditions. Notable changes are also observed
794 in the $\delta^{18}\text{O}_{\text{carb}}$ values from Labeko Koba compared to the older El Castillo and Axlor sites, with bovines
795 exhibiting a higher fluctuation range and the lowest values in the region. These trends are consistent with
796 values observed on bone collagen from previous studies in the ~~studiedse~~ sites. During the Middle-to-Upper
797 Paleolithic transition in the region, by comparing horses and red deer, a decrease in mean $\delta^{13}\text{C}$ (from ~~-21.9‰~~
798 to ~~-20.4‰~~) and $\delta^{15}\text{N}$ values (from ~~2.56‰~~ to ~~6.2-5.5‰~~) in bone collagen was observed in contrast to stable red
799 deer mean $\delta^{13}\text{C}$ (Fernández-García et al., 2023; Jones et al., 2018, 2019). This decrease was ~~already~~
800 ~~previously~~ interpreted as niche fractionation, derived from an opening landscape, that drove equids into low-
801 quality pastures compared to cervids. Pollen evidence in the region suggests a prevalence of steppe
802 vegetation and low tree cover for the Châtelperronian and Aurignacian (Iriarte-Chiapusso, 2000).

803 In the same period, ~~Canyars in the northeastern at the Mediterranean sitearea-of, Canyars~~, higher mean
804 $\delta^{13}\text{C}_{\text{diet}}$ are observed in both species (between $-23.6‰$ and $-24.4‰$), indicating a preference for more open
805 landscapes by bovines and equids. The indication of open areas could be linked to the arid climatic
806 conditions associated with the Heinrich Event 4, which coincides with the formation of the ~~archaeological~~
807 ~~studied level-at Canyars~~. This predominance of open areas coincides with the presence of typical steppe
808 herbivore species, such as *Equus hydruntinus* and *Coelodonta antiquitatis*, the microfauna and pollen taxa,
809 and ~~the data offered by the~~ use-wear analysis on ungulate remains identified at the site (Daura et al., 2013;
810 López-García et al., 2022; Rivals et al., 2017).

811 Aridity is a plausible explanation for the higher niche partitioning observed in Labeko Koba and the higher
812 $\delta^{13}\text{C}_{\text{diet}}$ values found in ~~Canyars for both species in-during the Aurignacian-levels~~. The $\delta^{13}\text{C}_{\text{diet}}$ results of
813 bovines from Aitzbitarte III ~~interior~~ during the Gravettian are consistent with the trend observed in Labeko
814 Koba, ~~and where~~ previous studies have already suggested this time to be notably arid and cold (~~Arrizabalaga~~
815 ~~et al., 2010~~). Finally, in the Magdalenian level of El Otero, higher $\delta^{13}\text{C}_{\text{diet}}$ values resemble those observed in
816 Canyars. However, this time, carbon values are related to niche partitioning between horses and red deer.
817 In contrast, higher $\delta^{18}\text{O}_{\text{mw}}$ values might indicate warmer conditions but are still associated with open
818 landscapes in the Vasco-Cantabrian area.

819 5.4 Late Pleistocene climatic evolution in Northern Iberia

820 Carbon and oxygen isotopes were used to estimate quantitative parameters related to past temperatures
821 and precipitation. In the case of oxygen isotopic compositions, an evaluation of environmental water
822 composition can be addressed before approaching temperature estimations. When transformed to $\delta^{18}\text{O}_{\text{mw}}$
823 using species-adapted correlations ~~and correcting bias in sea water $\delta^{18}\text{O}_{\text{mw}}$~~ , the summer $\delta^{18}\text{O}_{\text{mw}}$ values
824 obtained from the modelled teeth range from ~~-84.9-4‰~~ to ~~-42.2-4.9‰~~, while the winter values range from -

Formatted: Subscript

Formatted: Subscript

Formatted: Subscript

Formatted: Subscript

Formatted: Subscript

Field Code Changed

825 ~~17.0-16.4~~2‰ to ~~-8.94-2~~-10.6‰. These values ~~agree can be tentatively compared~~ with the current trends
826 ~~observed in~~ $\delta^{18}\text{O}_{\text{mw}}$ range of values recorded by the IAEA station (IAEA/ WMO, 2022) in Santander (from -
827 3.5‰ in summer to -6.6‰ in winter) and in Barcelona (from -2.2‰ in summer to -6.3‰ in winter) and the
828 OIPC (Bowen, 2022) estimations for studied locations (from -1‰ to -9‰) (Appendix B). As observed in the
829 present, Canyars exhibit higher mean annual $\delta^{18}\text{O}_{\text{mw}}$ values of around -8.25-5‰, which are close is lower to
830 than the current $\delta^{18}\text{O}_{\text{mw}}$ estimated for this location (-5.4‰) but higher than Labeko Koba mean annual $\delta^{18}\text{O}_{\text{mw}}$
831 (-9.5‰). This raises the question of whether suggests that the baseline $\delta^{18}\text{O}_{\text{mw}}$ differences between
832 Canyars and the other sites can be primarily attributed to the Mediterranean influence rather than the
833 Atlantic, assuming equivalent air circulation patterns and moisture sources in the past as experienced in the
834 past as in the present (Araguas-Araguas and Diaz Teijeiro, 2005; García-Alix et al., 2021; Moreno et al.,
835 2021) and considering IAEA stations. However, it's important to note that these comparisons must be
836 approached thoughtfully, considering that moisture fluxes and precipitation trends may have varied
837 significantly during the Pleistocene and the Holocene (Dansgaard, 1964; Shackleton, 1987).

838 Considering this work's climatic reconstruction, As indicated by the climate reconstructed here, temperatures
839 are were generally colder and precipitation levels were are notably lower in the Late Pleistocene period in
840 this region than, and precipitation levels were notably lower in the Late Pleistocene period in this region than
841 they are nowadays (Table 4; Appendix B). From 80,000 to 50.57-46 ka, 000 cal BP, in the Mousterian levels
842 of the Axlor site, temperatures were generally slightly colder than today, but there is no clear trend observed
843 throughout the sequence, but with older levels showing showed higher differences between summer and
844 winter temperatures. Rainfall estimations in these levels exhibit an unusual arid pattern, possibly affected
845 by bovines mainly predominantly feeding in open areas at that time. Indeed, even if the species' impact has
846 been corrected through $\delta^{13}\text{C}_{\text{diet}}$ estimation (Tejada-Lara et al., 2018), this aligns study observed that with
847 the impact the influence of basal feeding behavior behaviour on rainfall estimations, as previously advised
848 by Lécuyer et al. (2021) should be considered. In this case, it is not possible to isolate the effect of diet from
849 environmental interference, but previous studies have highlighted stable climatic conditions for at the site
850 (Pederzani et al., 2023). Climatic reconstruction, relying on a compilation of lake sediments from northern
851 Iberia (Moreno et al., 2012) suggests that from late MIS4 to 60 ka cal BP, cold but relatively humid conditions
852 predominated, with drier conditions emerging later. Additionally, stalagmites from the Ejulve cave in the
853 Iberian range indicate a dry climate until 65.5 ka BP, preceding HE6, followed by more humid conditions
854 afterwards (Pérez-Mejías et al., 2019).

855
856 During the late Middle to Upper Paleolithic transition and early Aurignacian occupations, the observed a shift
857 in the niche configuration of species is observed, suggests potential indicating climatic perturbations. There
858 is a decreasing trend in temperatures from the Transitional Aurignacian levels in El Castillo (18C and 18B;
859 ca. 47-46 ka, 000 cal BP) to the Châtelperronian (Xinf; 45.2-1 ka, 100 cal BP) and Early Aurignacian (VII-V;
860 from 40.74-136.4 to 36.37-88,570 ka cal BP) levels in Labeko Koba. Lower mean annual and winter
861 temperatures are particularly notable at El Castillo and, while Labeko Koba, Labeko Koba levels exhibits
862 high seasonal amplitude, especially in at level VII. Additionally, there is a slight decrease in rainfall and
863 increased fluctuations from the Transitional Aurignacian levels from El Castillo (18B-18C) to the
864 Aurignacian levels in Labeko Koba (VII-V). Previous studies in the northern Iberian region underlined an
865 environmental and ecological shift after GS13/HE5, from 48,000 to 44 ka, 000 cal BP, based on a progressive
866 trend to colder temperatures, aridity increase, and open environmental conditions, matching with the late
867 Neanderthal occupations, followed by a population hiatus before the arrival of Anatomically Modern Humans
868 (Fernández-García et al., 2023; Vidal-Cordasco et al., 2022). This episode coincides with the region's
869 maximum extension of the glaciers maximum extent of glaciers in this region, as recorded in Lake Enol and
870 Vega Comeya and thean associated a significant decrease in plant biomass and herbivore abundance

871 around 44 to 38 ka BP (Ballesteros et al., 2020; Jiménez-Sánchez et al., 2013; Ruiz-Fernández et al., 2022).
 872 Moreover, previous isotopic analyses in the region pointed to some ecological alterations considering
 873 perturbations observed in the $\delta^{13}\text{C}$ and $\delta^{15}\text{N}$ of bone collagen (Jones et al., 2018, 2019). This tendency of
 874 increased aridity aligns with observations made in regional lake sediments from northern Iberia between 60
 875 and 23.5 ka cal BP, marked by abrupt climate changes associated with HE (Moreno et al., 2012). Supporting
 876 this, the marine core MD04-2845 in the northern margin of Iberia reveals a decline in the Atlantic forest and
 877 an expansion of steppe and cold grasses from 47 to 40 ka BP (Fourcade et al., 2022).

878 When comparing the environmental reconstruction of the Aurignacian period ~~in-between~~ the Vasco-
 879 Cantabrian ~~region~~ (levels V-IV from Labeko Koba) and the Mediterranean-northeastern region (Layer I from
 880 Canyars), which are synchronous to HE4 (39,000 ka BP), ~~thise~~ study reveals notably lower rainfall levels for
 881 the ~~northeastern site~~ latter Mediterranean. ~~This is, consistent with implied by due to the feeding~~
 882 ~~behavior/behaviour described for observed in animals mainly feeding, mainly~~ in open areas. ~~But~~ However,
 883 ~~these~~ drier conditions ~~align~~ with the unique specific climatic ~~expectations~~ conditions expected for this
 884 period and support previous findings suggesting-revealing aridity and the predominance of open landscapes
 885 (Daura et al., 2013; Rivals et al., 2017). The temperature data indicates that ~~at~~ Canyars, colder conditions
 886 were experienced, ~~colder conditions~~, especially during the winter season, compared to the present.
 887 However, in comparison to Labeko Koba, Canyars experienced warmer conditions. As explained earlier, the
 888 Mediterranean basin had consistently higher temperatures, even during colder periods. ~~In line with this,~~
 889 ~~previous studies conducted at the site have also highlighted the~~ This is consistent with the persistence of
 890 Mediterranean open forests in the surroundings, as indicated by other studies (López-García et al., 2013;
 891 Rivals et al., 2017). Continuous natural records are lacking in the northeastern Iberian margin. However, the
 892 inland stalagmite record from Eijulve Cave (Pérez-Mejías et al., 2019) and the sedimentary lacustrine
 893 sequence of Cañizar de Villarquemado (González-Sampérez et al., 2020) have identified the most arid
 894 intervals during HE5 and HE4. These periods were characterized by steppe vegetation expansions, followed
 895 by deciduous woodland expansion. To the south, the Padul sequence agrees with cold and dry conditions
 896 alternating with forest recovery (Camuera et al., 2019), as documented in the Alborean Sea (Martrat et al.,
 897 2004).

898 Finally, the sites Aitzbitarte III interior (27,967,692 ka cal BP) and El Otero (179,303 ka cal BP) provided
 899 valuable climatic insights into the Vasco-Cantabrian region during the Upper Paleolithic, specifically during
 900 the Gravettian and Magdalenian ~~periods~~, respectively. Considering previous research in the region, the
 901 climatic trend reported for the Aurignacian, characterised by colder and more arid conditions, was expected
 902 to continue or even intensify during the Gravettian ~~period~~ (Fernández-García et al., 2023; Garcia-
 903 Ibaibarriaga et al., 2019b; Lécuyer et al., 2021). Both sites ~~exhibit indicate~~ lower precipitation ~~levels~~
 904 ~~compared to the present~~ than presently found in these area, indicating significant aridity, supported by
 905 ~~the~~ with ungulates animals predominantly feeding in open landscapes predominantly today in this area,
 906 indicating significant aridity, with ungulates feeding predominantly in open landscapes. Finally, However,
 907 ~~El~~ Otero's higher mean annual temperatures ~~recorded in the Magdalenian horses~~ respect to other sites
 908 within the Vasco-Cantabrian, are consistent with a climatic amelioration following the Last Glacial Maximum
 909 (Jones et al., 2021). MIS 2 is marked by the most extreme glacial conditions, as indicated by NGRIP and
 910 marine cores in Iberian margins (Martrat et al., 2004; Sánchez Goñi et al., 2002). However, other regional
 911 proxies, such as lake sediment and the stalagmite sequence in Pindal Cave (Moreno et al., 2010), suggest
 912 a complex and highly variable climate during MIS 2. These proxies identify the coldest and most arid period
 913 within MIS 2 as the interval from 18 to 14 ka cal BP, rather than the global Last Glacial Maximum (23 to 19
 914 ka cal BP).

915 5. Conclusions

Formatted: Subscript

916 This study provides a ~~comprehensive-detailed~~ analysis of the temporal evolution of the environment and
917 climatic conditions in northern Iberia, spanning from the ~~late~~ Middle Paleolithic to the late Upper Paleolithic,
918 this is from the GS21 to the GS2, ranging from ~~ca.~~ 80 ka BP,000 to 17975 ka cal,000 cal-BP. In the Vasco-
919 Cantabrian region, the results reveal a heterogeneous ~~open mosaic~~ landscape ~~characterised by an open~~
920 ~~mosaic~~, ranging from light forest to meadows and grasslands. This landscape reconstruction is primarily
921 ~~influenced-inferred~~ by the feeding locations of the studied animals and, consequently, related to the
922 ecosystems where hominins captured them. Despite shifts in niche configuration observed between equids
923 and bovines, both species typically foraging ~~in~~ open areas, with bovines showing a higher preference for
924 grazing. Only in El Castillo, during the late Mousterian and the Transitional Aurignacian levels, bovines show
925 unusually low $\delta^{13}\text{C}_{\text{diet}}$ related to higher browsing and overlapping with horse isotopic niche. This might
926 indicate a slightly closed mosaic landscape that could sustain both species. In contrast, only horses from
927 Canyars exhibit a preference for grazing ~~behavior~~behaviour.

928 Stable climatic conditions are described for Mousterian ~~in~~ Axlor and El Castillo levels from 80,000 to 50,000
929 ka cal BP. However, some elements indicate ~~some~~ environmental perturbations initiated during the
930 Transitional Aurignacian levels ~~from of~~ El Castillo, around 48486-453 ka,000 BP and after HE5/GS13. After
931 GS12 (44,200-43,3 ka00 BP), horses and bovines are potentially occupying different ecological niches
932 during the Châtelperronian and early Aurignacian levels ~~from of~~ Labeko Koba, pointing to a species'
933 environmental specialisation, which can be a consequence of competition for food resources during an
934 unstable ecological period. The climatic estimations indicate a temperature shift during this period, with a
935 slight decrease in temperatures and evidence of fluctuations in rainfall ~~from the Transitional Aurignacian~~
936 ~~levels of El Castillo to the early Aurignacian levels of Labeko Koba~~. Previous environmental studies on the
937 region have underlined ecological stress and ~~aridity increase~~increasing aridity from around 42,58,000 ka cal
938 BP, ~~which could sustain this biological impoverishment which may relate to a w~~broader ecosystem decline.
939 When comparing the environmental conditions during the Aurignacian period in the ~~Mediterranean-northeast~~
940 (Canyars) and the ~~Vasco-Cantabrian region~~northwest (Labeko Koba), the ~~Mediterranean-are first~~a
941 had higher baseline temperatures but also experienced higher aridity. Animals continued to feed on open
942 landscapes during the Gravettian and Magdalenian levels in the Vasco-Cantabrian region, represented by
943 Aitzbitarte III ~~interior~~ and El Otero ~~sites~~. However, there is evidence of a temperature recovery after the LGM
944 at the El Otero ~~site~~.

945 ~~For the first time, a regional approach is obtained by measuring $\delta^{13}\text{C}$ and $\delta^{18}\text{O}$ in enamel carbonates from~~
946 ~~ungulates teeth for the late Middle and Upper Paleolithic in northern Iberia. Stable isotope composition of~~
947 ~~oxygen and carbon from ungulate teeth has provided valuable insights into the diet and foraging areas of~~
948 ~~bovines, equids, and cervids. These results, The results presented here, derived from this the first~~ extensive
949 sampling in the Vasco-Cantabrian, establish the basis of ~~future~~ stable isotopic studies on ~~teeth faunal tooth~~
950 enamel ~~in this region Iberia, which were slightly explored in the region~~. Despite the uncertainties inherent in
951 this work, ~~derived from using the carbonate enamel fraction for paleoclimatic estimations, both $\delta^{18}\text{O}$ and~~
952 ~~$\delta^{13}\text{C}$ contributed to the regional climatic characterisation, including the estimation of temperatures and~~
953 ~~precipitations, as well as the seasonality range between summer and winter. The potential influence of~~
954 ~~pretreatment effects and uncontrolled diagenetic alterations on the enamel carbonate fraction has been~~
955 ~~assessed. However, further investigation complementary diagenetical test, using new techniques like~~
956 ~~$\delta^{18}\text{O}_{\text{phos}}$ phosphate analysis and FTIR analyses are needed-advised in further works in the region,~~ to gain
957 more insights into sample preservation. Ongoing sulphur, hydrogen and strontium studies will provide
958 additional information on the ~~animal~~-mobility patterns ~~of animals that were hunted by Late Pleistocene~~
959 ~~consumed for~~ hominins and, therefore, ~~will help better understandus better understand the landscape~~
960 ~~exploitation-ecological and environmental context of occupied by the through this transition between late~~
961 Neanderthal and ~~early~~ modern humans ~~groupshabitations in this region and their landscape use in this~~

962 [particular region](#). ~~Finally, a A~~ more comprehensive characterisation of the baseline oxygen values ~~in the~~
963 ~~region~~ would also enhance the environmental interpretation of the existing data.

964 **Appendices**

965 Appendices A, C, ~~D~~ and ~~ED~~ are presented after bibliography. Raw data is ~~found~~ [presented](#) in Appendix B,
966 ~~At~~ available at https://github.com/ERC-Subsilience/Ungulate_enamel-carbonate

Field Code Changed

967 **Code availability**

968 R code used to perform plots, [temperature and error calculations](#), [Bayesian models code and results](#) and
969 [inverse](#) models in this manuscript can be accessed at GitHub ([https://github.com/ERC-](https://github.com/ERC-Subsilience/Ungulate_enamel-carbonate)
970 [Subsilience/Ungulate_enamel-carbonate](#)).

Field Code Changed

971 **Data availability**

972 The available datasets used for this article are provided in the supplementary materials (Appendix A-~~ED~~).

973 **Author contribution**

974 A.B.M.-A. got the funding and designed the research. A.B.M.-A and M.F.-G. get the permissions for sampling
975 in the regional museums. M.F.-G., K.B, and S.P. defined the analysis strategy. M.F.-G. analysed the data
976 and wrote the manuscript with critical inputs from A.B.M.-A., K.B, and S.P. J.M.G., L.A., M.F.-G., and A.C.
977 M.F.-G., L.A., J.M.G., and A.C. achieved the teeth sampling and lab sample preparation. J.D. and M.S. are
978 responsible for the excavations in Canyars and contribute to the discussion. All the authors revised and
979 commented on the manuscript.

980 **Competing interests**

981 The contact author has declared that none of the authors has any competing interests.

982 **Acknowledgements**

983 We acknowledge the Museo de Arqueología y Prehistoria de Cantabria (MUPAC), the Consejería de
984 Educación, Cultura y Deporte del Gobierno de Cantabria, the Museo de Arqueología de Bizkaia (Arkeologi
985 Museoa) and the Centro de Colecciones Patrimoniales de la Diputación Foral de Gipuzkoa (Gordailua) –
986 Provincial Government of Guipuzkoa's Heritage Collection Centre for the access to the archaeological
987 collections. We do appreciate the work achieved by H. Reade during the initial sampling, pretreatment and
988 analyses of samples undertaken at the University of Cantabria and Cambridge. [We want to thank the two](#)
989 [anonymous referees for their valuable comments, which significantly improved the quality of the paper.](#)

990 **Financial support**

991 Funding for Vasco-Cantabria research was obtained from the Spanish Ministry of Science and Innovation
992 (PID2021-125818NB-I00, HAR2017-84997-P and HAR2012-33956), ~~and~~ the European Research Council
993 under the European Union's Horizon 2020 Research and Innovation Programme (grant agreement number
994 818299; SUBSILIENCE project) [and Proyecto Puente by Consejería de Educación, Cultura y Deporte del](#)
995 [Gobierno de Cantabria](#). Research for Canyars was funded by the Spanish Ministry of Science and
996 Innovation (PID2020-113960GB-I00), Departament de Cultura de la Generalitat de Catalunya
997 (CLT/2022/ARQ001SOLC/128) and AGAUR (SGR2021-00337). [M.F.-G. is supported by the APOSTD](#)
998 [postdoctoral fellowship \(CIAPOS/2022/081/AEI/10.13039/501100011033\), funded by the Generalitat](#)
999 [Valenciana and the European Social Fund](#). S.P. was supported by a German Academy of Sciences
1000 Leopoldina postdoctoral fellowship (LPDS 2021-13) during this project. M.S. benefited from financial support

1001 from a Ramon y Cajal postdoctoral grant (RYC2021-032999-I)- funded by the Spanish Ministry of Science
1002 and Innovation and the European Union-NextGenerationEU.

1003 **References**

1004 Allué, E., Martínez-Moreno, J., Roy, M., Benito-Calvo, A., and Mora, R.: Montane pine forests in NE Iberia during MIS 3 and MIS 2.
1005 A study based on new anthracological evidence from Cova Gran (Santa Linya, Iberian Pre-Pyrenees), Rev. Palaeobot.
1006 Palynol., 258, 62–72, <https://doi.org/10.1016/j.revpalbo.2018.06.012>, 2018.

1007 Altuna, J. and Maríquezkurrena, K.: Estrategias de caza en el Paleolítico superior de la Región Cantábrica., *Sagvntvm, Extra* 21, 219–
1008 225, 2020.

1009 Altuna, J., Maríquezkurrena, K., de la Peña, P., and Ríos-Garaizar, J.: Ocupaciones Humanas En La Cueva de Aitzbitarte III (Rentería,
1010 País Vasco) Sector Entrada: 33.000-18.000 BP, Serv. Cent. Publicaciones del Gob. Vasco; EKOB, 11–21, 2011.

1011 Altuna, J., Maríquezkurrena, K., de la Peña, P., and Ríos-Garaizar, J.: Los niveles gravetienses de la cueva de Aitzbitarte III
1012 (Gipuzkoa). Industrias y faunas asociada. in: *Pensando El Gravetiense: Nuevos Datos Para La Región Cantábrica En
1013 Su Contexto Peninsular Y Pirenaico. Monografías Del Museo Nacional Y Centro de Investigación de Altamira*, 23, 184–
1014 204, 2013.

1015 Altuna, J., Maríquezkurrena, K., Ríos-Garaizar, J., and San Emeterio, A.: Ocupaciones Humanas en Aitzbitarte III (País Vasco) 26.000
1016 -13.000 BP (zona profunda de la cueva), Servicio Central de Publicaciones del Gobierno Vasco, 348 pp., 2017.

1017 Álvarez-Lao, D. J., Rivals, F., Sánchez-Hernández, C., Blasco, R., and Rosell, J.: Ungulates from Teixoneres Cave (Moia,
1018 Barcelona, Spain): Presence of cold-adapted elements in NE Iberia during the MIS 3, *Palaeogeogr. Palaeoclimatol.
1019 Palaeoecol.*, 466, 287–302, <https://doi.org/10.1016/j.palaeo.2016.11.040>, 2017.

1020 Ambrose, S. H. and Norr, L.: Experimental Evidence for the Relationship of the Carbon Isotope Ratios of Whole Diet and Dietary
1021 Protein to Those of Bone Collagen and Carbonate. in: *Prehistoric Human Bone*, Springer Berlin Heidelberg, Berlin,
1022 Heidelberg, 1–37, https://doi.org/10.1007/978-3-662-02894-0_1, 1993.

1023 Araquas-Araquas, L. J. and Díaz Teijeiro, M. F.: Isotope composition of precipitation and water vapour in the Iberian Peninsula. First
1024 results of the Spanish Network of Isotopes in Precipitation. in: *Isotopic Composition of Precipitation in the Mediterranean
1025 Basin in Relation to Air Circulation Patterns and Climate*, IAEA-TECDOC-1453, Vienna, 173–190, 2005.

1026 Arrizabalaga, Á. and Altuna, J.: Labeko Koba (País Vasco), Hienas y Humanos en los Albores del Paleolítico Superior, *Sociedad
1027 de Ciencias Naturales Aranzadi, San Sebastián-Donostia*, 395 pp., 2000.

1028 Arrizabalaga, Á. and Ríos-Garaizar, J.: The Early Aurignacian in the Basque Country, *Quat. Int.*, 207, 25–36, 2009.

1029 Arrizabalaga, Á., Iriarte-Chiapusso, M. J., and Villaluenga, A.: Labeko Koba y Lezetxiki (País Vasco). Dos yacimientos, una
1030 problemática común, *Zo. Arqueol.*, 13, 322–334, 2010.

1031 Balasse, M., Ambrose, S. H., Smith, A. B., and Price, T. D.: The Seasonal Mobility Model for Prehistoric Herders in the South-
1032 western Cape of South Africa Assessed by Isotopic Analysis of Sheep Tooth Enamel, *J. Archaeol. Sci.*, 29, 917–932,
1033 <https://doi.org/10.1006/jasc.2001.0787>, 2002.

1034 Ballesteros, D., Álvarez-Vena, A., Monod-Del Daqo, M., Rodríguez-Rodríguez, L., Sanjurjo-Sánchez, J., Álvarez-Lao, D., Pérez-
1035 Mejías, C., Valenzuela, P., DeFelipe, I., Laplana, C., Cheng, H., and Jiménez-Sánchez, M.: Paleoenvironmental evolution of
1036 Picos de Europa (Spain) during marine isotopic stages 5c to 3 combining glacial reconstruction, cave sedimentology
1037 and paleontological findings, *Quat. Sci. Rev.*, 248, 106581, <https://doi.org/10.1016/j.quascirev.2020.106581>, 2020.

1038 Barandiarán, J. M.: Excavaciones en Axlor. 1967- 1974. in: *Obras Completas*, Tomo XVII, edited by: Barandiarán, J. M., 341–359,
1039 1980.

1040 Bendrey, R., Vella, D., Zazzo, A., Balasse, M., and Lepetz, S.: Exponentially decreasing tooth growth rate in horse teeth: implications
1041 for isotopic analyses, *Archaeometry*, 57, 1104–1124, <https://doi.org/10.1111/arc.12151>, 2015.

1042 Bernaldo de Quirós, F. and Maillo-Fernández, J. M.: Middle to Upper Palaeolithic at Cantabrian Spain, in: *A sourcebook of
1043 Palaeolithic transitions: methods, theories and interpretations*, edited by: Camps, M. and Chauhan, P. R., Springer, New
1044 York, 341–359, 2009.

1045 Blumenthal, S. A., Cerling, T. E., Chritz, K. L., Bromage, T. G., Kozdon, R., and Valley, J. W.: Stable isotope time-series in
1046 mammalian teeth: In situ $\delta^{18}O$ from the innermost enamel layer, *Geochim. Cosmochim. Acta.*, 124, 223–236,
1047 <https://doi.org/10.1016/j.gca.2013.09.032>, 2014.

1048 Blumenthal, S. A., Cerling, T. E., Smiley, T. M., Badgley, C. E., and Plummer, T. W.: Isotopic records of climate seasonality in equid
1049 teeth, *Geochim. Cosmochim. Acta.*, 260, 329–348, <https://doi.org/10.1016/j.gca.2019.06.037>, 2019.

1050 Bocherens, H.: Isotopic biogeochemistry and the paleoecology of the mammoth steppe fauna, *Deinsea*, 91, 57–76, 2003.

1051 Brand, W. A., Coplen, T. B., Vogl, J., Rosner, M., and Prohaska, T.: Assessment of international reference materials for isotope-
1052 ratio analysis (IUPAC Technical Report), *Pure Appl. Chem.*, 86, 425–467, <https://doi.org/10.1515/pac-2013-1023>, 2014.

1053 Britton, K., Pederzani, S., Kindler, L., Roebroeks, W., Gaudzinski-Windheuser, S., Richards, M. P., and Tütken, T.: Oxygen isotope
1054 analysis of Equus teeth evidences early Eemian and early Weichselian palaeotemperatures at the Middle Palaeolithic
1055 site of Neumark-Nord 2, Saxony-Anhalt, Germany, *Quat. Sci. Rev.*, 226, 106029,
1056 <https://doi.org/10.1016/j.quascirev.2019.106029>, 2019.

1057 Bryant, J. D., Luz, B., and Froelich, P. N.: Oxygen isotopic composition of fossil horse tooth phosphate as a record of continental
1058 paleoclimate, *Palaeogeogr. Palaeoclimatol. Palaeoecol.*, 107, 303–316, [https://doi.org/10.1016/0031-0182\(94\)90102-3](https://doi.org/10.1016/0031-0182(94)90102-3),
1059 1994.

1060 Bryant, J. D., Koch, P. L., Froelich, P. N., Showers, W. J., and Genna, B. J.: Oxygen isotope partitioning between phosphate and
1061 carbonate in mammalian apatite, *Geochim. Cosmochim. Acta.*, 60, 5145–5148, [https://doi.org/10.1016/S0016-7037\(96\)00308-0](https://doi.org/10.1016/S0016-7037(96)00308-0), 1996.

1062 Cabrera, V., Maillo, J. M., Lloret, M., and Bernaldo de Quirós, F.: La transition vers le Paléolithique supérieur dans la grotte du
1063 Castillo (Cantabrie, Espagne): La couche 18, *Anthropologie*, 105, 505–532, [https://doi.org/10.1016/S0003-5521\(01\)180050-9](https://doi.org/10.1016/S0003-5521(01)180050-9), 2001.

Commented [MF1]: FALTAN LAS DEL APENDICE DE YACIMIENTOS

1066 Cabrera Valdés, V.: El Yacimiento de la cueva de «El Castillo» (Puente Viesgo, Santander), *Bibliothec.*, CSIC, 485 pp., 1984.

1067 Camuera, J., Jiménez-Moreno, G., Ramos-Román, M. J., García-Alix, A., Toney, J. L., Anderson, R. S., Jiménez-Espejo, F., Bright,
1068 J., Webster, C., Yanes, Y., and Carrión, J. S.: Vegetation and climate changes during the last two glacial-interglacial
1069 cycles in the western Mediterranean: A new long pollen record from Padul (southern Iberian Peninsula), *Quat. Sci. Rev.*,
1070 205, 86–105, <https://doi.org/10.1016/j.quascirev.2018.12.013>, 2019.

1071 Carvalho, M., Jones, E. L., Ellis, M. G., Cascalheira, J., Bicho, N., Meiggs, D., Benedetti, M., Friedl, L., and Haws, J.: Neanderthal
1072 palaeoecology in the late Middle Palaeolithic of western Iberia: a stable isotope analysis of ungulate teeth from Lapa do
1073 Picareiro (Portugal), *J. Quat. Sci.*, 37, 300–319, <https://doi.org/10.1002/jqs.3363>, 2022.

1074 Cascalheira, J., Alcaraz-Castaño, M., Alcolea-González, J., de Andrés-Herrero, M., Arizabalaga, A., Aura Tortosa, J. E., García-
1075 Ibaibarriaga, N., and Iriarte-Chiapusso, M.-J.: Paleoenvironments and human adaptations during the Last Glacial
1076 Maximum in the Iberian Peninsula: A review, *Quat. Int.*, 581–582, 28–51, <https://doi.org/10.1016/j.quaint.2020.08.005>,
1077 2021.

1078 Cerling, T. E. and Harris, J. M.: Carbon isotope fractionation between diet and bioapatite in ungulate mammals and implications for
1079 ecological and paleoecological studies, *Oecologia*, 120, 347–363, <https://doi.org/10.1007/s004420050868>, 1999.

1080 Chappell, J. and Shackleton, N. J.: Oxygen isotopes and sea level, *Nature*, 324, 137–140, <https://doi.org/10.1038/324137a0>, 1986.

1081 Chesson, L. A., Beaslev, M. M., Bartelink, E. J., Jans, M. M. E., and Berg, G. E.: Using bone bioapatite yield for quality control in
1082 stable isotope analysis applications, *J. Archaeol. Sci. Reports*, 35, 102749, <https://doi.org/10.1016/j.jasrep.2020.102749>,
1083 2021.

1084 Chillón, B. S., Alberdi, M. T., Leone, G., Bonadonna, F. P., Stenni, B., and Longinelli, A.: Oxygen isotopic composition of fossil equid
1085 tooth and bone phosphate: an archive of difficult interpretation, *Palaeogeogr. Palaeoclimatol. Palaeoecol.*, 107, 317–328,
1086 [https://doi.org/10.1016/0031-0182\(94\)90103-1](https://doi.org/10.1016/0031-0182(94)90103-1), 1994.

1087 Coplen, T. B.: Guidelines and recommended terms for expression of stable-isotope-ratio and gas-ratio measurement results, *Rapid
1088 Commun. Mass Spectrom.*, 25, 2538–2560, <https://doi.org/10.1002/rcm.5129>, 2011.

1089 Coplen, T. B., Kendall, C., and Hopple, J.: Comparison of stable isotope reference samples, *Nature*, 302, 236–238,
1090 <https://doi.org/10.1038/302236a0>, 1983.

1091 D'Angela, D. and Longinelli, A.: Oxygen isotopes in living mammal's bone phosphate: Further results, *Chem. Geol.*, 86, 75–82,
1092 1990.

1093 D'Errico, F. and Sánchez Goñi, M. F.: Neandertal extinction and the millennial scale climatic variability of OIS 3, *Quat. Sci. Rev.*,
1094 22, 769–788, [https://doi.org/10.1016/S0277-3791\(03\)00009-X](https://doi.org/10.1016/S0277-3791(03)00009-X), 2003.

1095 Dansgaard, W.: Stable isotopes in precipitation, *Tellus*, XVI, 436–468, 1964.

1096 Daura, J. and Sanz, M.: Informe de la troballa del jaciment arqueològic "Terrasses dels Canyars" (Castelldefels-Gavà). Notificació
1097 de la descoberta i propostes d'actuació. Grup de Recerca del Quaternari, SERP, UB, 2006.

1098 Daura, J., Sanz, M., García, N., Allué, E., Vaquero, M., Fierro, E., Carrión, J. S., López-García, J. M., Blain, H. a., Sánchez-Marco,
1099 a., Valls, C., Albert, R. M., Fornós, J. J., Julià, R., Fullola, J. M., and Zilhão, J.: Terrasses de la Riera dels Canyars (Gavà,
1100 Barcelona): The landscape of Heinrich Stadial 4 north of the "Ebro frontier" and implications for modern human dispersal
1101 into Iberia, *Quat. Sci. Rev.*, 60, 26–48, <https://doi.org/10.1016/j.quascirev.2012.10.042>, 2013.

1102 Delgado Huertas, A., lacumin, P., Stenni, B., Sánchez Chillón, B., and Longinelli, A.: Oxygen isotope variations of phosphate in
1103 mammalian bone and tooth enamel, *Geochim. Cosmochim. Acta*, 59, 4299–4305, [https://doi.org/10.1016/0016-7037\(95\)00286-9](https://doi.org/10.1016/0016-7037(95)00286-9), 1995.

1104 Demuro, M., Arnold, L. J., González-Urquijo, J., Lazuen, T., and Frochoso, M.: Chronological constraint of Neanderthal cultural and
1105 environmental changes in southwestern Europe: MIS 5–MIS 3 dating of the Axlor site (Biscay, Spain), *J. Quat. Sci.*, 38,
1106 891–920, <https://doi.org/10.1002/jqs.3527>, 2023.

1107 Doyon, L., Faure, T., Sanz, M., Daura, J., Cassard, L., and D'Errico, F.: A 39,600-year-old leather punch board from Canyars, Gavà,
1108 Spain, *Sci. Adv.*, 9, <https://doi.org/10.1126/sciadv.adg0834>, 2023.

1109 Drucker, D. G.: The Isotopic Ecology of the Mammoth Steppe, *Annu. Rev. Earth Planet. Sci.*, 50, 395–418,
1110 <https://doi.org/10.1146/annurev-earth-100821-081832>, 2022.

1111 Drucker, D. G., Bridault, A., Hobson, K. A., Szuma, E., and Bocherens, H.: Can carbon-13 in large herbivores reflect the canopy
1112 effect in temperate and boreal ecosystems? Evidence from modern and ancient ungulates, *Palaeogeogr. Palaeoclimatol.*
1113 *Palaeoecol.*, 266, 69–82, <https://doi.org/10.1016/j.palaeo.2008.03.020>, 2008.

1114 Eggleston, S., Schmitt, J., Bereiter, B., Schneider, R., and Fischer, H.: Evolution of the stable carbon isotope composition of
1115 atmospheric CO₂ over the last glacial cycle, *Paleoceanogr. Paleoclimatology*, 31, 434–452,
1116 <https://doi.org/10.1002/2015PA002874>, 2016.

1117 Fagoaga, A.: Aproximación paleoclimática y paisajística durante el MIS3 a partir del estudio de los micromamíferos del yacimiento
1118 de El Salt (Alcoi, Alicante), Universidad de Burgos, 34 pp., 2014.

1119 Fernández-García, M., Royer, A., López-García, J. M., Bennásar, M., Goedert, J., Fourel, F., Julien, M.-A., Bañuls-Cardona, S.,
1120 Rodríguez-Hidalgo, A., Vallverdú, J., and Lécuyer, C.: Unravelling the oxygen isotope signal ($\delta^{18}O$) of rodent teeth from
1121 northeastern Iberia, and implications for past climate reconstructions, *Quat. Sci. Rev.*, 218, 107–121,
1122 <https://doi.org/10.1016/j.quascirev.2019.04.035>, 2019.

1123 Fernández-García, M., López-García, J. M., Royer, A., Lécuyer, C., Allué, E., Burjachs, F., Chacón, M. G., Saladié, P., Vallverdú,
1124 J., and Carbonell, E.: Combined palaeoecological methods using small-mammal assemblages to decipher environmental
1125 context of a long-term Neanderthal settlement in northeastern Iberia, *Quat. Sci. Rev.*, 228, 106072,
1126 <https://doi.org/10.1016/j.quascirev.2019.106072>, 2020.

1127 Fernández-García, M., Vidal-Cordasco, M., Jones, J. R., and Marin-Arroyo, A. B.: Reassessing palaeoenvironmental conditions
1128 during the Middle to Upper Palaeolithic transition in the Cantabrian region (Southwestern Europe), *Quat. Sci. Rev.*, 301,
1129 107928, <https://doi.org/10.1016/j.quascirev.2022.107928>, 2023.

1130 Fick, S. E. and Hijmans, R. J.: WorldClim 2: new 1-km spatial resolution climate surfaces for global land areas, *Int. J. Climatol.*, 37,
1131 4302–4315, <https://doi.org/10.1002/joc.5086>, 2017.

1133 Finlayson, C. and Carrión, J. S.: Rapid ecological turnover and its impact on Neanderthal and other human populations, *Trends*
1134 *Ecol. Evol.*, 22, 213–222, <https://doi.org/10.1016/j.tree.2007.02.001>, 2007.

1135 Fourcade, T., Sánchez Goñi, M. F., Lahaye, C., Rossignol, L., and Philippe, A.: Environmental changes in SW France during the
1136 Middle to Upper Paleolithic transition from the pollen analysis of an eastern North Atlantic deep-sea core, *Quat. Res.*, 1–
1137 18, <https://doi.org/10.1017/qua.2022.21>, 2022.

1138 France, C. A. M., Sugiyama, N., and Aguayo, E.: Establishing a preservation index for bone, dentin, and enamel biapatite mineral
1139 using ATR-FTIR, *J. Archaeol. Sci. Reports*, 33, 102551, <https://doi.org/10.1016/j.jasrep.2020.102551>, 2020.

1140 Freeman, L. G.: *Mousterian Developments in Cantabrian Spain*, University of Chicago, 1964.

1141 García-Alix, A., Camuera, J., Ramos-Román, M. J., Toney, J. L., Sachse, D., Schefuß, E., Jiménez-Moreno, G., Jiménez-Espejo,
1142 F. J., López-Avilés, A., Anderson, R. S., and Yanes, Y.: Paleohydrological dynamics in the Western Mediterranean during
1143 the last glacial cycle, *Glob. Planet. Change*, 202, 103527, <https://doi.org/10.1016/j.gloplacha.2021.103527>, 2021.

1144 García-Ibaibarriaga, N., Suárez-Bilbao, A., Iriarte-Chiapusso, M. J., Arrizabalaga, A., and Murelaqa, X.: Palaeoenvironmental
1145 dynamics in the Cantabrian Region during Greenland stadial 2 approached through pollen and micromammal records:
1146 State of the art, *Quat. Int.*, 506, 14–24, <https://doi.org/10.1016/j.quaint.2018.12.004>, 2019a.

1147 García-Ibaibarriaga, N., Suárez-Bilbao, A., Iriarte-Chiapusso, M. J., Arrizabalaga, A., and Murelaqa, X.: Palaeoenvironmental
1148 dynamics in the Cantabrian Region during Greenland stadial 2 approached through pollen and micromammal records:
1149 State of the art, *Quat. Int.*, 506, 14–24, <https://doi.org/10.1016/j.quaint.2018.12.004>, 2019b.

1150 Garralda, M.-D.: Los Neandertales en la Península Ibérica: The Neandertals from the Iberian Peninsula, *Munibe* 57, 289–314, 2005.

1151 Garralda, M.-D., Maíllo-Fernández, J.-M., Maureille, B., Neira, A., and de Quirós, F. B.: > 42 ka human teeth from El Castillo
1152 Cave (Cantabria, Spain) Mid-Upper Paleolithic transition, *Archaeol. Anthropol. Sci.*, 14, 126,
1153 <https://doi.org/10.1007/s12520-022-01587-2>, 2022.

1154 Geiling, J. M.: Human Ecodynamics in the Late Upper Pleistocene of Northern Spain: An Archeozoological Study of Ungulate
1155 Remains from the Lower Magdalenian and other Periods in El Mirón Cave (Cantabria), *Universidad de Cantabria*, 734
1156 pp., 2020.

1157 Gómez-Olivencia, A., Arceredillo, D., Álvarez-Lao, D. J., Garate, D., San Pedro, Z., Castañón, P., and Ríos-Garaizar, J.: New
1158 evidence for the presence of reindeer (*Rangifer tarandus*) on the Iberian Peninsula in the Pleistocene: an
1159 archaeopalaeontological and chronological reassessment, *Boreas*, 43, 286–308, <https://doi.org/10.1111/bor.12037>,
1160 2014.

1161 Gómez-Olivencia, A., Sala, N., Núñez-Lahuerta, C., Sanchis, A., Arlegi, M., and Ríos-Garaizar, J.: First data of Neanderthal bird and
1162 carnivore exploitation in the Cantabrian Region (Axlor, Barandiaran excavations: Dima, Biscay, Northern Iberian
1163 Peninsula), *Sci. Rep.*, 8, 10551, <https://doi.org/10.1038/s41598-018-28377-y>, 2018.

1164 González-Sampériz, P., Gil-Romera, G., García-Prieto, E., Aranbarri, J., Moreno, A., Morellón, M., Sevilla-Callejo, M., Leunda, M.,
1165 Santos, L., Franco-Múgica, F., Andrade, A., Carrión, J. S., and Valero-Garcés, B. L.: Strong continentality and effective
1166 moisture drove unforeseen vegetation dynamics since the last interglacial at inland Mediterranean areas: The
1167 Villarquemedo sequence in NE Iberia, *Quat. Sci. Rev.*, 242, <https://doi.org/10.1016/j.quascirev.2020.106425>, 2020.

1168 González-Urquijo, J.: Abrigo de Axlor (Dima), *Arkeoikuska. Investigac.*, 90–93, 2001.

1169 González-Urquijo, J., Ibáñez Estévez, J. J., Ríos-Garaizar, J., Bourguignon, L., Castañón, P., and Tarrío Vinagre, A.: Excavaciones
1170 recientes en Axlor. Movilidad y planificación de actividades en grupos de neandertales, in: *Actas de La Reunión*
1171 *Científica: Neandertales Cantábricos. Estado de La Cuestión. Monografías Del Museo Nacional Y Centro de*
1172 *Investigación de Altamira*, 20, edited by: Montes Barquin, R. and Lasheras, J. A., Ministerio de Cultura, 527–539, 2005.

1173 González Echegaray, J. G.: *Cueva del Otero. Excavaciones Arqueol. en España*, 53, 1966.

1174 Hoppe, K. A.: Correlation between the oxygen isotope ratio of North American bison teeth and local waters: Implication for
1175 paleoclimatic reconstructions, *Earth Planet. Sci. Lett.*, 244, 408–417, <https://doi.org/10.1016/j.epsl.2006.01.062>, 2006.

1176 Hoppe, K. A., Stover, S. M., Pascoe, J. R., and Amundson, R.: Tooth enamel biomineralization in extant horses: implications for
1177 isotopic microsampling, *Palaeogeogr. Palaeoclimatol. Palaeoecol.*, 206, 355–365,
1178 <https://doi.org/10.1016/j.palaeo.2004.01.012>, 2004.

1179 Iacumin, P., Bocherens, H., Mariotti, A., and Longinelli, A.: Oxygen isotope analyses of co-existing carbonate and phosphate in
1180 biogenic apatite: a way to monitor diagenetic alteration of bone phosphate?, *Earth Planet. Sci. Lett.*, 142, 1–6,
1181 [https://doi.org/10.1016/0012-821X\(96\)00093-3](https://doi.org/10.1016/0012-821X(96)00093-3), 1996.

1182 Iriarte-Chiapusso, M. J.: El entorno vegetal del yacimiento paleolítico de Labeko Koba (Arrasate, País Vasco): análisis polínico,
1183 *Labeko Koba (País Vasco). Hienas y humanos en los albores del Paleolítico Super.*, Munibe, 89–106, 2000.

1184 Jiménez-Sánchez, M., Rodríguez-Rodríguez, L., García-Ruiz, J. M., Domínguez-Cuesta, M. J., Farias, P., Valero-Garcés, B.,
1185 Moreno, A., Rico, M., and Valcárcel, M.: A review of glacial geomorphology and chronology in northern Spain: Timing
1186 and regional variability during the last glacial cycle, *Geomorphology*, 196, 50–64,
1187 <https://doi.org/10.1016/j.geomorph.2012.06.009>, 2013.

1188 Jimenez, I. J., Sanz, M., Daura, J., De Gaspar, I., and García, N.: Ontogenetic dental patterns in Pleistocene hyenas (*Crocota*
1189 *crocuta* Erxleben, 1777) and their palaeobiological implications, *Int. J. Osteoarchaeol.*, 29, 808–821,
1190 <https://doi.org/10.1002/oa.2796>, 2019.

1191 Jones, J. R., Richards, M. P., Straus, L. G., Reade, H., Altuna, J., Mariezkurrena, K., and Marín-Arroyo, A. B.: Changing
1192 environments during the Middle-Upper Palaeolithic transition in the eastern Cantabrian Region (Spain): direct evidence
1193 from stable isotope studies on ungulate bones, *Sci. Rep.*, 8, 14842, <https://doi.org/10.1038/s41598-018-32493-0>, 2018.

1194 Jones, J. R., Richards, M. P., Reade, H., Bernaldo de Quirós, F., and Marín-Arroyo, A. B.: Multi-isotope investigations of ungulate
1195 bones and teeth from El Castillo and Covalejos caves (Cantabria, Spain): Implications for paleoenvironment
1196 reconstructions across the Middle-Upper Palaeolithic transition, *J. Archaeol. Sci. Reports*, 23, 1029–1042,
1197 <https://doi.org/10.1016/j.jasrep.2018.04.014>, 2019.

1198 Jones, J. R., Marín-Arroyo, A. B., Corchón Rodríguez, M. S., and Richards, M. P.: After the Last Glacial Maximum in the refugium
1199 of northern Iberia: Environmental shifts, demographic pressure and changing economic strategies at Las Caldas Cave

1200 (Asturias, Spain). *Quat. Sci. Rev.* 262, 106931. <https://doi.org/10.1016/j.quascirev.2021.106931>, 2021.

1201 Klein, K., Weniger, G.-C., Ludwig, P., Stepanek, C., Zhang, X., Wegener, C., and Shao, Y.: Assessing climatic impact on transition
1202 from Neanderthal to anatomically modern human population on Iberian Peninsula: a macroscopic perspective. *Sci. Bull.*,
1203 68, 1176–1186. <https://doi.org/10.1016/j.scib.2023.04.025>, 2023.

1204 Kohn, M. J.: Predicting animal $\delta^{18}O$: Accounting for diet and physiological adaptation. *Geochim. Cosmochim. Acta.* 60, 4811–4829,
1205 [https://doi.org/10.1016/S0016-7037\(96\)00240-2](https://doi.org/10.1016/S0016-7037(96)00240-2), 1996.

1206 Kohn, M. J.: Comment: Tooth Enamel Mineralization in Ungulates: Implications for Recovering a Primary Isotopic Time-Series, by
1207 B. H. Passey and T. E. Cerling (2002). *Geochim. Cosmochim. Acta.* 68, 403–405. [https://doi.org/10.1016/S0016-7037\(03\)00443-5](https://doi.org/10.1016/S0016-7037(03)00443-5), 2004.

1208 Kohn, M. J.: Carbon isotope compositions of terrestrial C3 plants as indicators of (paleo)ecology and (paleo)climate. *Proc. Natl.*
1209 *Acad. Sci.*, 107, 19691–19695. <https://doi.org/10.1073/pnas.1004933107>, 2010.

1210 Lécuyer, C., Hillaire-Marcel, C., Burke, A., Julien, M.-A., and Hélie, J.-F.: Temperature and precipitation regime in LGM human
1211 refugia of southwestern Europe inferred from $\delta^{13}C$ and $\delta^{18}O$ of large mammal remains. *Quat. Sci. Rev.* 255, 106796,
1212 <https://doi.org/10.1016/j.quascirev.2021.106796>, 2021.

1213 Leuenberger, M., Siegenthaler, U., and Langway, C.: Carbon isotope composition of atmospheric CO2 during the last ice age from
1214 an Antarctic ice core. *Nature*, 357, 488–490. <https://doi.org/10.1038/357488a0>, 1992.

1215 Libberda, J. J., Thompson, J. W., Rink, W. J., Bernaldo de Quirós, F., Jayaraman, R., Selvaratnam, K., Chancellor-Maddison, K.,
1216 and Volterra, V.: ESR dating of tooth enamel in Mousterian layer 20, El Castillo, Spain. *Geochronology*, n/a-n/a,
1217 <https://doi.org/10.1002/gea.20320>, 2010.

1218 López-García, J. M., Blain, H.-A., Bennàsar, M., Sanz, M., and Daura, J.: Heinrich event 4 characterized by terrestrial proxies in
1219 southwestern Europe. *Clim. Past* 9, 1053–1064. <https://doi.org/10.5194/cp-9-1053-2013>, 2013.

1220 López-García, J. M., Blain, H.-A., Bennàsar, M., Alcover, J. A., Bañuls-Cardona, S., Fernández-García, M., Fontanals, M., Martín,
1221 P., Morales, J. I., Muñoz, L., Pedro, M., and Vergés, J. M.: Climate and landscape during Heinrich Event 3 in south-
1222 western Europe: The small-vertebrate association from Galls Carboners cave (Mont-ral, Tarragona, north-eastern Iberia).
1223 *J. Quat. Sci.* 29, 130–140, 2014a.

1224 López-García, J. M., Blain, H.-A., Bennàsar, M., and Fernández-García, M.: Environmental and climatic context of Neanderthal
1225 occupation in southwestern Europe during MIS3 inferred from the small-vertebrate assemblages. *Quat. Int.*, 326–327,
1226 319–328. <https://doi.org/10.1016/j.quaint.2013.09.010>, 2014b.

1227 López-García, J. M., Blain, H. A., Fagoaga, A., Bandera, C. S., Sanz, M., and Daura, J.: Environment and climate during the
1228 Neanderthal-AMH presence in the Garraf Massif mountain range (northeastern Iberia) from the late Middle Pleistocene
1229 to Late Pleistocene inferred from small-vertebrate assemblages. *Quat. Sci. Rev.*, 288,
1230 <https://doi.org/10.1016/j.quascirev.2022.107595>, 2022.

1231 Luret, M., Burke, A., Bernaldo de Quirós, F., and Besse, M.: El Castillo cave (Cantabria, Spain): Archeozoological comparison
1232 between the Mousterian occupation level (unit 20) and the “Aurignacien de transition de type El Castillo” (unit 18). *J.*
1233 *Archaeol. Sci. Reports*, 31, 102339. <https://doi.org/10.1016/j.jasrep.2020.102339>, 2020.

1234 Luz, B., Kolodny, Y., and Horowitz, M.: Fractionation of oxygen isotopes between mammalian. *Geochim. Cosmochim. Acta.* 48,
1235 1689–1693, 1984.

1236 Magozzi, S., Vander Zanden, H. B., Wunder, M. B., and Bowen, G. J.: Mechanistic model predicts tissue–environment relationships
1237 and trophic shifts in animal hydrogen and oxygen isotope ratios. *Oecologia*, 191, 777–789,
1238 <https://doi.org/10.1007/s00442-019-04532-8>, 2019.

1239 Marin-Arroyo, A. B. and Sanz-Royo, A.: What Neanderthals and AMH ate: reassessment of the subsistence across the Middle–
1240 Upper Palaeolithic transition in the Vasco-Cantabrian region of SW Europe. *J. Quat. Sci.*, 37, 320–334,
1241 <https://doi.org/10.1002/jqs.3291>, 2022.

1242 Marin-Arroyo, A. B., Rios-Garaizar, J., Straus, L. G., Jones, J. R., de la Rasilla, M., González Morales, M. R., Richards, M., Altuna,
1243 J., Mariézkurrena, K., and Ocio, D.: Chronological reassessment of the Middle to Upper Paleolithic transition and Early
1244 Upper Paleolithic cultures in Cantabrian Spain. *PLoS One*, 13, 1–20. <https://doi.org/10.1371/journal.pone.0194708>, 2018.

1245 Maroto, J., Vaquero, M., Arrizabalaga, A., Baena, J., Baquedano, E., Jordà, J., Julià, R., Montes, R., Van Der Plicht, J., Rasines,
1246 P., and Wood, R.: Current issues in late Middle Palaeolithic chronology: New assessments from Northern Iberia. *Quat.*
1247 *Int.* 247, 15–25. <https://doi.org/10.1016/j.quaint.2011.07.007>, 2012.

1248 Martín-Perea, D. M., Mallo-Fernández, J., Marin, J., Arroyo, X., and Asiain, R.: A step back to move forward: a geological re-
1249 evaluation of the El Castillo Cave Middle Palaeolithic lithostratigraphic units (Cantabria, northern Iberia). *J. Quat. Sci.*,
1250 38, 221–234. <https://doi.org/10.1002/jqs.3473>, 2023.

1251 Martrat, B., Grimalt, J. O., Lopez-Martinez, C., Cacho, I., Sierro, F. J., Flores, J. A., Zahn, R., Canals, M., Curtis, J. H., and Hodell,
1252 D. A.: Abrupt Temperature Changes in the Western Mediterranean over the Past 250,000 Years. *Science* (80-.), 306,
1253 1762–1765. <https://doi.org/10.1126/science.1101706>, 2004.

1254 Merceron, G., Berlioz, E., Vohhof, H., Green, D., Garel, M., and Tütken, T.: Tooth tales told by dental diet proxies: An alpine
1255 community of sympatric ruminants as a model to decipher the ecology of fossil fauna. *Palaeogeogr. Palaeoclimatol.*
1256 *Palaeoecol.* 562, 110077. <https://doi.org/10.1016/j.palaeo.2020.110077>, 2021.

1257 van der Merwe, N. J.: Light Stable Isotopes and the Reconstruction of Prehistoric Diets. *Proc. Br. Acad.*, 77, 247–264, 1991.

1258 Moreno, A., Stoll, H., Jiménez-Sánchez, M., Cacho, I., Valero-Garcés, B., Ito, E., and Edwards, R. L.: A speleothem record of glacial
1259 (25–11.6 kyr BP) rapid climatic changes from northern Iberian Peninsula. *Glob. Planet. Change*, 71, 218–231,
1260 <https://doi.org/10.1016/j.gloplacha.2009.10.002>, 2010.

1261 Moreno, A., González-Sampériz, P., Morellón, M., Valero-Garcés, B. L., and Fletcher, W. J.: Northern Iberian abrupt climate change
1262 dynamics during the last glacial cycle: A view from lacustrine sediments. *Quat. Sci. Rev.*, 36, 139–153,
1263 <https://doi.org/10.1016/j.quascirev.2010.06.031>, 2012.

1264 Moreno, A., Iglesias, M., Azorin-Molina, C., Pérez-Mejías, C., Bartolomé, M., Sancho, C., Stoll, H., Cacho, I., Frigola, J., Osácar,
1265 C., Muñoz, A., Delgado-Hurtas, A., Bladé, I., and Vimeux, F.: Measurement report: Spatial variability of northern Iberian

1267 rainfall stable isotope values – investigating atmospheric controls on daily and monthly timescales, *Atmos. Chem. Phys.*,
1268 21, 10159–10177, <https://doi.org/10.5194/acp-21-10159-2021>, 2021.

1269 Naughton, F., Sánchez-Gofí, M. F., Desprat, S., Turon, J.-L., and Duprat, J.: Present-day and past (last 25 000 years) marine pollen
1270 signal off western Iberia, *Mar. Micropaleontol.*, 62, 91–114, <https://doi.org/10.1016/j.marmicro.2006.07.006>, 2007.

1271 North Greenland Ice Core Project members: High-resolution record of Northern Hemisphere climate extending into the last
1272 interglacial period, *Nature*, 431, 147–151, <https://doi.org/10.1038/nature02805>, 2004.

1273 Ochando, J., Amorós, G., Carrión, J. S., Fernández, S., Munuera, M., Camuera, J., Jiménez-Moreno, G., González-Sampériz, P.,
1274 Burjachs, F., Marín-Arroyo, A. B., Roksandic, M., and Finlayson, C.: Iberian Neanderthals in forests and savannahs, *J.*
1275 *Quat. Sci.*, 1–28, <https://doi.org/10.1002/jqs.3339>, 2021.

1276 Passey, B. H. and Cerling, T. E.: Tooth enamel mineralization in ungulates: implications for recovering a primary isotopic time-
1277 series, *Geochim. Cosmochim. Acta*, 66, 3225–3234, [https://doi.org/10.1016/S0016-7037\(02\)00933-X](https://doi.org/10.1016/S0016-7037(02)00933-X), 2002.

1278 Passey, B. H., Robinson, T. F., Ayliffe, L. K., Cerling, T. E., Sponheimer, M., Dearing, M. D., Roeder, B. L., and Ehleringer, J. R.:
1279 Carbon isotope fractionation between diet, breath CO₂, and bioapatite in different mammals, *J. Archaeol. Sci.*, 32, 1459–
1280 1470, <https://doi.org/10.1016/j.jas.2005.03.015>, 2005a.

1281 Passey, B. H., Cerling, T. E., Schuster, G. T., Robinson, T. F., Roeder, B. L., and Krueger, S. K.: Inverse methods for estimating
1282 primary input signals from time-averaged isotope profiles, *Geochim. Cosmochim. Acta*, 69, 4101–4116,
1283 <https://doi.org/10.1016/j.gca.2004.12.002>, 2005b.

1284 Pederzani, S. and Britton, K.: Oxygen isotopes in bioarchaeology: Principles and applications, challenges and opportunities, *Earth-*
1285 *Science Rev.*, 188, 77–107, <https://doi.org/10.1016/j.earscirev.2018.11.005>, 2019.

1286 Pederzani, S., Aldeias, V., Dibble, H. L., Goldberg, P., Hublin, J. J., Madelaine, S., McPherron, S. P., Sandgathe, D., Steele, T. E.,
1287 Turg, A., and Britton, K.: Reconstructing Late Pleistocene paleoclimate at the scale of human behavior: an example from
1288 the Neanderthal occupation of La Ferrassie (France), *Sci. Rep.*, 11, 1–10, <https://doi.org/10.1038/s41598-020-80777-1>,
1289 2021a.

1290 Pederzani, S., Britton, K., Aldeias, V., Bourgon, N., Fewlass, H., Lauer, T., McPherron, S. P., Rezek, Z., Sirakov, N., Smith, G. M.,
1291 Spasov, R., Tran, N. H., Tsanova, T., and Hublin, J. J.: Subarctic climate for the earliest Homo sapiens in Europe, *Sci.*
1292 *Adv.*, 7, 1–11, <https://doi.org/10.1126/sciadv.abi4642>, 2021b.

1293 Pederzani, S., Britton, K., Jones, J. R., Aguado Pérez, L., Geiling, J. M., and Marín-Arroyo, A. B.: Late Pleistocene Neanderthal
1294 exploitation of stable and mosaic ecosystems in northern Iberia shown by multi-isotope evidence, *Quat. Res.*, 1–25,
1295 <https://doi.org/10.1017/qua.2023.32>, 2023a.

1296 Pederzani, S., Britton, K., Jones, J. R., Aguado Pérez, L., Geiling, J. M., and Marín-Arroyo, A. B.: Late Pleistocene Neanderthal
1297 exploitation of stable and mosaic ecosystems in northern Iberia shown by multi-isotope evidence, *Quat. Res.*, 1–25,
1298 <https://doi.org/10.1017/qua.2023.32>, 2023b.

1299 Pellegrini, M. and Snoeck, C.: Comparing bioapatite carbonate pre-treatments for isotopic measurements: Part 2 — Impact on
1300 carbon and oxygen isotope compositions, *Chem. Geol.*, 420, 88–96, <https://doi.org/10.1016/j.chemgeo.2015.10.038>,
1301 2016.

1302 Pellegrini, M., Lee-Thorp, J. A., and Donahue, R. E.: Exploring the variation of the $\delta^{18}O_p$ and $\delta^{18}O_c$ relationship in enamel
1303 increments, *Palaeogeogr. Palaeoclimatol. Palaeoecol.*, 310, 71–83, <https://doi.org/10.1016/j.palaeo.2011.02.023>, 2011.

1304 Pérez-Mejías, C., Moreno, A., Sancho, C., Martín-García, R., Spötl, C., Cacho, I., Cheng, H., and Edwards, R. L.: Orbital-to-
1305 millennial scale climate variability during Marine Isotope Stages 5 to 3 in northeast Iberia, *Quat. Sci. Rev.*, 224,
1306 <https://doi.org/10.1016/j.quascirev.2019.105946>, 2019.

1307 Posth, C., Yu, H., Ghalichi, A., Rougier, H., Crevecoeur, I., Huang, Y., Ringbauer, H., Rohlfach, A. B., Nägele, K., Villalba-Mouco,
1308 V., Radzevičiute, R., Ferraz, T., Stoessel, A., Tukhbatova, R., Drucker, D. G., Lari, M., Modi, A., Vai, S., Saue, T.,
1309 Scheib, C. L., Catalano, G., Pagani, L., Talamo, S., Fewlass, H., Klaric, L., Morala, A., Rué, M., Madelaine, S., Crépin,
1310 L., Caverne, J.-B., Bogaëge, E., Ricci, S., Boschin, F., Bayle, P., Maureille, B., Le Brun-Ricalens, F., Bordes, J.-G., Oxilia,
1311 G., Bortolini, E., Bignon-Lau, O., Debout, G., Orliac, M., Zazzo, A., Sparacello, V., Starnini, E., Sineo, L., van der Plicht,
1312 J., Pecqueur, L., Merceron, G., Garcia, G., Leuvery, J.-M., Garcia, C. B., Gómez-Olivencia, A., Poltowicz-Bobak, M.,
1313 Bobak, D., Le Luyer, M., Storm, P., Hoffmann, C., Kabaciński, J., Filimonova, T., Shnaider, S., Berezina, N., González-
1314 Rabanal, B., González Morales, M. R., Marín-Arroyo, A. B., López, B., Alonso-Llamazares, C., Ronchitelli, A., Polet, C.,
1315 Jadin, I., Cauwe, N., Soler, J., Coromina, N., Ruff, I., Cottiaux, R., Clark, G., Straus, L. G., Julien, M.-A., Renhart, S.,
1316 Talaa, D., Benazzi, S., Romandini, M., Amkreutz, L., Bocherens, H., Wülsing, C., Villotte, S., de Pablo, J. F.-L., Gómez-
1317 Puche, M., Esquembre-Bebia, M. A., Bodu, P., Smits, L., Souffi, B., Jankauskas, R., Kozakaitė, J., Cupillard, C., Benthien,
1318 H., Wehrberger, K., Schmitz, R. W., Feine, S. C., et al.: Palaeogenomics of Upper Palaeolithic to Neolithic European
1319 hunter-gatherers, *Nature*, 615, 117–126, <https://doi.org/10.1038/s41586-023-05726-0>, 2023.

1320 Pryor, A. J. E., Stevens, R. E., Connell, T. C. O., and Lister, J. R.: Quantification and propagation of errors when converting
1321 vertebrate biomineral oxygen isotope data to temperature for palaeoclimate reconstruction, *Palaeogeogr. Palaeoclimatol.*
1322 *Palaeoecol.*, 412, 99–107, <https://doi.org/10.1016/j.palaeo.2014.07.003>, 2014.

1323 Ramsey, C. B.: Bayesian Analysis of Radiocarbon Dates, *Radiocarbon*, 51, 337–360, <https://doi.org/10.1017/S0033822200033865>,
1324 2009.

1325 Rasmussen, S. O., Bigler, M., Blockley, S. P., Blunier, T., Bucharadt, S. L., Clausen, H. B., Cvijanovic, I., Dahl-Jensen, D., Johnsen,
1326 S. J., Fischer, H., Gkinis, V., Guillevic, M., Hoek, W. Z., Lowe, J. J., Pedro, J. B., Popp, T., Seierstad, I. K., Steffensen,
1327 J. P., Svensson, A. M., Vallelonga, P., Vinther, B. M., Walker, M. J. C., Wheatley, J. J., and Winstrup, M.: A stratigraphic
1328 framework for abrupt climatic changes during the Last Glacial period based on three synchronized Greenland ice-core
1329 records: Refining and extending the INTIMATE event stratigraphy, *Quat. Sci. Rev.*, 106, 14–28,
1330 <https://doi.org/10.1016/j.quascirev.2014.09.007>, 2014.

1331 Reimer, P. J., Austin, W. E. N., Bard, E., Bayliss, A., Blackwell, P. G., Bronk Ramsey, C., Butzin, M., Cheng, H., Edwards, R. L.,
1332 Friedrich, M., Grootes, P. M., Guilderson, T. P., Haidas, I., Heaton, T. J., Hogg, A. G., Hughen, K. A., Kromer, B., Manning,
1333 S. W., Muscheler, R., Palmer, J. G., Pearson, C., van der Plicht, J., Reimer, R. W., Richards, D. A., Scott, E. M., Southon,

1334 J. R., Turney, C. S. M., Wacker, L., Adolphi, F., Büntgen, U., Capano, M., Fahrni, S. M., Fogtmann-Schulz, A., Friedrich,
1335 R., Köhler, P., Kudsk, S., Miyake, F., Olsen, J., Reinig, F., Sakamoto, M., Sookdeo, A., and Talamo, S.: The IntCal20
1336 Northern Hemisphere Radiocarbon Age Calibration Curve (0–55 cal kBP), *Radiocarbon*, 62, 725–757,
1337 <https://doi.org/10.1017/RDC.2020.41>, 2020.

1338 Rey, K., Amiot, R., Lécuyer, C., Koufos, G. D., Martineau, F., Fourel, F., Kostopoulos, D. S., and Merceron, G.: Late Miocene climatic
1339 and environmental variations in northern Greece inferred from stable isotope compositions (6180–613C) of equid teeth
1340 apatite, *Palaeogeogr. Palaeoclimatol. Palaeoecol.*, 388, 48–57, <https://doi.org/10.1016/j.palaeo.2013.07.021>, 2013.

1341 Rink, W. J., Schwarcz, H. P., Lee, H. K., Cabrera Valdés, V., Bernaldo de Quirós, F., and Hoyos, M.: ESR dating of Mousterian
1342 levels at El Castillo Cave, Cantabria, Spain, *J. Archaeol. Sci.*, 24, 593–600, <https://doi.org/10.1006/jasc.1996.0143>, 1997.

1343 Rios-Garaizar, J.: *Industria lítica y sociedad en la Transición del Paleolítico Medio al Superior en torno al Golfo de Bizkaia*, PUBLICan
1344 - Ediciones de la Universidad de Cantabria, 432 pp., 2012.

1345 Rios-Garaizar, J.: A new chronological and technological synthesis for Late Middle Paleolithic of the Eastern Cantabrian Region,
1346 *Quat. Int.*, 433, 50–63, <https://doi.org/10.1016/j.quaint.2016.02.020>, 2017.

1347 Rios-Garaizar, J., Arrizabalaga, A., and Villaluenga, A.: Haltes de chasse du Châtelperronien de la Péninsule Ibérique : Labeko
1348 Koba et Ekain (Pays Basque Péinsulaire), *Anthropologie*, 116, 532–549, <https://doi.org/10.1016/j.anthro.2012.10.001>,
1349 2012.

1350 Rios-Garaizar, J., de la Peña, P., and Maillou-Fernández, J. M.: El final del Auriñaciense y el comienzo del Gravetiense en la región
1351 cantábrica: una visión tecno-tipológica, in: *Pensando El Gravetiense: Nuevos Datos Para La Región Cantábrica En Su*
1352 *Contexto Peninsular Y Pirenaico*, Monografías Del Museo Nacional Y Centro de Investigación de Altamira, 23, edited by:
1353 de las Heras, C., Lasheras, J. A., Arrizabalaga, A., and de la Rasilla, M., Ministerio de Educación, Cultura, Madrid, 369–
1354 382, 2013.

1355 Rios-Garaizar, J., Iriarte, E., Arnold, L. J., Sánchez-Romero, L., Marín-Arroyo, A. B., San Emeterio, A., Gómez-Olivencia, A., Pérez-
1356 Garrido, C., Demuro, M., Campaña, I., Bourquignon, L., Benito-Calvo, A., Iriarte, M. J., Aranburu, A., Arranz-Otaegi, A.,
1357 Garate, D., Silva-Gago, M., Lahaye, C., and Ortega, I.: The intrusive nature of the Châtelperronian in the Iberian
1358 Peninsula, *PLoS One*, 17, e0265219, 2022.

1359 Rivals, F., Uzunidis, A., Sanz, M., and Daura, J.: Faunal dietary response to the Heinrich Event 4 in southwestern Europe,
1360 *Palaeogeogr. Palaeoclim. Palaeoecol.*, 473, 123–130, <https://doi.org/10.1016/j.palaeo.2017.02.033>, 2017.

1361 Rivals, F., Bocherens, H., Camarós, E., and Rosell, J.: Diet and ecological interactions in the Middle and Late Pleistocene, in:
1362 *Updating Neanderthals. Understanding Behavioural Complexity in the Late Middle Palaeolithic*, 39–54, 2022.

1363 Roucoux, K. H., Shackleton, N. J., Abreu, L. De, Schönfeld, J., and Tzedakis, P. C.: Combined marine proxy and pollen analyses
1364 reveal rapid Iberian vegetation response to North Atlantic millennial-scale climate oscillations, 56, 128–132,
1365 <https://doi.org/10.1006/qres.2001.2218>, 2001.

1366 Rozanski, K., Araguás-Araguás, L., and Gonfiantini, R.: Relation Between Long-Term Trends of Oxygen-18 Isotope Composition of
1367 Precipitation and Climate, *Science (80-)*, 258, 981–985, 1992.

1368 Rufi, I., Solés, A., Soler, J., and Soler, N.: A mammoth (*Mammuthus primigenius* Blumenbach 1799, Proboscidea) calf tooth from
1369 the Mousterian of Arbreda Cave (Serinyà, NE Iberian Peninsula), *Estud. Geològics*, 74, e079,
1370 <https://doi.org/10.3989/eegeol.43130.478>, 2018.

1371 Ruiz-Fernández, J., García-Hernández, C., and Gallinar Cañedo, D.: The glaciers of the Picos de Europa, in: *Iberia, Land of*
1372 *Glaciers*, Elsevier, 237–263, <https://doi.org/10.1016/B978-0-12-821941-6.00012-8>, 2022.

1373 Sánchez-Goñi, M. F., Eynaud, F., Turon, J.-L., and Shackleton, N. J.: High resolution palynological record off the Iberian margin:
1374 direct land-sea correlation for the Last Interglacial complex, *Earth Planet. Sci. Lett.*, 171, 123–137, 1999.

1375 Sánchez-Goñi, M. F., Landais, A., Cacho, I., Duprat, J., and Rossignol, L.: Contrasting intrainterstadial climatic evolution between
1376 high and middle North Atlantic latitudes: A close-up of Greenland Interstadials 8 and 12, *Geochemistry, Geophys.*
1377 *Geosystems*, 10, 1–16, <https://doi.org/10.1029/2008GC002369>, 2009.

1378 Sánchez Goñi, M., Cacho, I., Turon, J., Guiot, J., Sierro, F., Peyrouquet, J., Grimalt, J., and Shackleton, N.: Synchronicity between
1379 marine and terrestrial responses to millennial scale climatic variability during the last glacial period in the Mediterranean
1380 region, *Clim. Dyn.*, 19, 95–105, <https://doi.org/10.1007/s00382-001-0212-x>, 2002.

1381 Sánchez Goñi, M. F.: Regional impacts of climate change and its relevance to human evolution, *Evol. Hum. Sci.*, 2, e55,
1382 <https://doi.org/10.1017/ehs.2020.56>, 2020.

1383 Sanz-Royo, A., Sanz, M., and Daura, J.: Upper Pleistocene equids from Terrasses de la Riera dels Canyars (NE Iberian Peninsula):
1384 The presence of *Equus ferus* and *Equus hydruntinus* based on dental criteria and their implications for palaeontological
1385 identification and palaeoenvironmental reconstr., *Quat. Int.*, 566–567, 78–90,
1386 <https://doi.org/10.1016/j.quaint.2020.06.026>, 2020.

1387 Sanz-Royo, A., Terlato, G., and Marín-Arroyo, A. B.: Taphonomic data from the transitional Aurignacian of El Castillo cave (Spain)
1388 reveals the role of carnivores at the Aurignacian Delta level, *Quat. Sci. Adv.*, 13, 100147,
1389 <https://doi.org/10.1016/j.qsa.2023.100147>, 2024.

1390 Schmitt, J., Schneider, R., Elsig, J., Leuenberger, D., Lourantou, A., Chappellaz, J., Köhler, P., Joos, F., Stocker, T. F., Leuenberger,
1391 M., and Fischer, H.: Carbon Isotope Constraints on the Deglacial CO₂ Rise from Ice Cores, *Science (80-)*, 336, 711–
1392 714, <https://doi.org/10.1126/science.1217161>, 2012.

1393 Schrag, D. P., Adkins, J. F., McIntyre, K., Alexander, J. L., Hodell, A., Charles, C. D., and McManus, J. F.: The oxygen isotopic
1394 composition of seawater during the Last Glacial Maximum, *Quat. Sci. Rev.*, 21, 331–342, 2002.

1395 Sepulchre, P., Ramstein, G., Kageyama, M., Vanhaeren, M., Krinner, G., Sánchez-Goñi, M. F., and d'Errico, F.: H4 abrupt event
1396 and late Neanderthal presence in Iberia, *Earth Planet. Sci. Lett.*, 258, 283–292,
1397 <https://doi.org/10.1016/j.epsl.2007.03.041>, 2007.

1398 Shackleton, N. J.: Oxygen isotopes, ice volume and sea level, *Quat. Sci. Rev.*, 6, 183–190, [https://doi.org/10.1016/0277-3791\(87\)90003-5](https://doi.org/10.1016/0277-3791(87)90003-5), 1987.

1399 Skrzypek, G., Wiśniowski, A., and Grierson, P. F.: How cold was it for Neanderthals moving to Central Europe during warm phases

Formatted: Spanish (Spain)

Formatted: Spanish (Spain)

1401 of the last glaciation? *Quat. Sci. Rev.*, 30, 481–487. <https://doi.org/10.1016/j.quascirev.2010.12.018>, 2011.

1402 Skrzypek, G., Sadler, R., and Wi, A.: Reassessment of recommendations for processing mammal phosphate $\delta^{18}O$ data for
1403 paleotemperature reconstruction, *Palaeogeogr. Palaeoclimatol. Palaeoecol.*, 446, 162–167,
1404 <https://doi.org/10.1016/j.palaeo.2016.01.032>, 2016.

1405 Snoeck, C. and Pellegrini, M.: Comparing bioapatite carbonate pre-treatments for isotopic measurements: Part 1—Impact on
1406 structure and chemical composition, *Chem. Geol.*, 417, 394–403. <https://doi.org/10.1016/j.chemgeo.2015.10.004>, 2015.

1407 Staubwasser, M., Drägusin, V., Onac, B. P., Assonov, S., Ersek, V., Hoffmann, D. L., and Veres, D.: Impact of climate change on
1408 the transition of Neanderthals to modern humans in Europe, *Proc. Natl. Acad. Sci.*, 115, 9116–9121,
1409 <https://doi.org/10.1073/pnas.1808647115>, 2018.

1410 Tejada-Lara, J. V., MacFadden, B. J., Bermudez, L., Rojas, G., Salas-Gismondí, R., and Flynn, J. J.: Body mass predicts isotope
1411 enrichment in herbivorous mammals, *Proc. R. Soc. B Biol. Sci.*, 285, 20181020, <https://doi.org/10.1098/rspb.2018.1020>,
1412 2018.

1413 Timmermann, A.: Quantifying the potential causes of Neanderthal extinction: Abrupt climate change versus competition and
1414 interbreeding, *Quat. Sci. Rev.*, 238, 106331, <https://doi.org/10.1016/j.quascirev.2020.106331>, 2020.

1415 Traylor, R. B. and Kohn, M. J.: Tooth enamel maturation reequilibrates oxygen isotope compositions and supports simple sampling
1416 methods, *Geochim. Cosmochim. Acta*, 198, 32–47, <https://doi.org/10.1016/j.gca.2016.10.023>, 2017.

1417 Tütken, T., Furrer, H., and Vennemann, T. W.: Stable isotope compositions of mammoth teeth from Niederweningen, Switzerland:
1418 Implications for the Late Pleistocene climate, environment, and diet, *Quat. Int.*, 164–165, 139–150,
1419 <https://doi.org/10.1016/j.quaint.2006.09.004>, 2007.

1420 Vidal-Cordasco, M., Ocio, D., Hickler, T., and Marín-Arroyo, A. B.: Ecosystem productivity affected the spatiotemporal
1421 disappearance of Neanderthals in Iberia, *Nat. Ecol. Evol.*, 6, 1644–1657, <https://doi.org/10.1038/s41559-022-01861-5>,
1422 2022.

1423 Vidal-Cordasco, M., Terlato, G., Ocio, D., and Marín-Arroyo, A. B.: Neanderthal coexistence with *Homo sapiens* in Europe was
1424 affected by herbivore carrying capacity, *Sci. Adv.*, 9, <https://doi.org/10.1126/sciadv.adi4099>, 2023.

1425 Villaluenga, A., Arrizabalaga, A., and Ríos-Garaizar, J.: Multidisciplinary approach to two Châtelperronian series: lower IX layer of
1426 Labeko Koba and X Level of Ekain (Basque country, Spain), *J. Taphon.*, 10, 525–548, 2012.

1427 Wood, R., Bernaldo de Quirós, F., Maillo-Fernández, J. M., Tejero, J. M., Neira, A., and Higham, T.: El Castillo (Cantabria, northern
1428 Iberia) and the Transitional Aurignacian: Using radiocarbon dating to assess site taphonomy, *Quat. Int.*, 474, 56–70,
1429 <https://doi.org/10.1016/j.quaint.2016.03.005>, 2018.

1430 Wood, R. E., Arrizabalaga, A., Camps, M., Fallon, S., Iriarte-Chiapusso, M. J., Jones, R., Maroto, J., De la Rasilla, M., Santamaría,
1431 D., Soler, J., Soler, N., Villaluenga, A., and Higham, T. F. G.: The chronology of the earliest Upper Palaeolithic in northern
1432 Iberia: New insights from L'Arbreda, Labeko Koba and La Viña, *J. Hum. Evol.*, 69, 91–109,
1433 <https://doi.org/10.1016/j.jhevol.2013.12.017>, 2014.

1434 Yravedra, J. and Gómez-Castanedo, A.: Estudio zooarqueológico y tafonómico del yacimiento del Otero (Secadura, Voto,
1435 Cantabria), *Espac. Tiempo y Forma. Ser. I, Nueva época. Prehist. y Arqueol.*, 3, 21–38, 2010.

1436 Zazzo, A., Bendrey, R., Vella, D., Moloney, A. P., Monahan, F. J., and Schmidt, O.: A refined sampling strategy for intra-tooth stable
1437 isotope analysis of mammalian enamel, *Geochim. Cosmochim. Acta*, 84, 1–13,
1438 <https://doi.org/10.1016/j.gca.2012.01.012>, 2012.

1439 Zilhao, J. and D'Errico, F.: The chronology of the Aurignacian and Transitional technocomplexes. Where do we stand?, in: *The
1440 chronology of the Aurignacian and of the transitional technocomplexes. Dating, stratigraphies, cultural implications*,
1441 *Proceedings of Symposium 61 of the XIVth Congress of the UISPP*, 313–349, 2003.

1442

1443 Allué, E., Martínez-Moreno, J., Roy, M., Benito-Calvo, A., and Mora, R.: Montane pine forests in NE Iberia during MIS-3 and MIS-2.
1444 A study based on new anthracological evidence from Cova Gran (Santa Linya, Iberian Pre-Pyrenees), *Rev. Palaeobot.
1445 Palynol.*, 258, 62–72, <https://doi.org/10.1016/j.revpalbo.2018.06.012>, 2018.

1446 Álvarez-Lao, D. J., Rivals, F., Sánchez-Hernández, C., Blasco, R., and Rosell, J.: Ungulates from Teixoneres Cave (Moia,
1447 Barcelona, Spain): Presence of cold-adapted elements in NE Iberia during the MIS 3, *Palaeogeogr. Palaeoclimatol.
1448 Palaeoecol.*, 466, 287–302, <https://doi.org/10.1016/j.palaeo.2016.11.040>, 2017.

1449 Balasse, M., Ambrose, S. H., Smith, A. B., and Price, T. D.: The Seasonal-Mobility-Model for Prehistoric Herders in the South-
1450 western Cape of South Africa Assessed by Isotopic Analysis of Sheep Tooth Enamel, *J. Archaeol. Sci.*, 29, 917–932,
1451 <https://doi.org/10.1006/jasc.2001.0787>, 2002.

1452 Bendrey, R., Vella, D., Zazzo, A., Balasse, M., and Lepetz, S.: Exponentially decreasing tooth growth rate in horse teeth: implications
1453 for isotopic analyses, *Archaeometry*, 57, 1104–1124, <https://doi.org/10.1111/arem.12451>, 2015.

1454 Blumenthal, S. A., Cerling, T. E., Chritz, K. L., Bromage, T. G., Kozdon, R., and Valley, J. W.: Stable isotope time series in
1455 mammalian teeth: In situ $\delta^{18}O$ from the innermost enamel layer, *Geochim. Cosmochim. Acta*, 124, 223–236,
1456 <https://doi.org/10.1016/j.gca.2013.09.032>, 2014.

1457 Blumenthal, S. A., Cerling, T. E., Smiley, T. M., Badgley, C. E., and Plummer, T. W.: Isotopic records of climate seasonality in equid
1458 teeth, *Geochim. Cosmochim. Acta*, 260, 329–348, <https://doi.org/10.1016/j.gca.2019.06.037>, 2019.

1459 Bocherens, H.: Isotopic biogeochemistry and the paleoecology of the mammoth steppe fauna, *Deinsea*, 91, 57–76, 2003.

1460 Brand, W. A., Coplen, T. B., Vogl, J., Rosner, M., and Prohaska, T.: Assessment of international reference materials for isotope-
1461 ratio analysis (IUPAC Technical Report), *Pure Appl. Chem.*, 86, 425–467, <https://doi.org/10.1515/pac-2013-1023>, 2014.

1462 Britton, K., Pederzani, S., Kinder, L., Roebroeks, W., Gaudzinski-Windheuser, S., Richards, M. P., and Tütken, T.: Oxygen isotope
1463 analysis of Equus teeth evidences early Eemian and early Weichselian palaeotemperatures at the Middle Palaeolithic
1464 site of Neumark Nord 2, Saxony-Anhalt, Germany, *Quat. Sci. Rev.*, 226, 106029,
1465 <https://doi.org/10.1016/j.quascirev.2019.106029>, 2019.

1466 Bryant, J. D., Luz, B., and Froelich, P. N.: Oxygen isotopic composition of fossil horse tooth phosphate as a record of continental
1467 paleoclimate, *Palaeogeogr. Palaeoclimatol. Palaeoecol.*, 107, 303–316, [https://doi.org/10.1016/0031-0182\(94\)90102-3](https://doi.org/10.1016/0031-0182(94)90102-3),

1468 1994.

1469 Bryant, J. D., Koch, P. L., Froelich, P. N., Showers, W. J., and Genna, B. J.: Oxygen isotope partitioning between phosphate and
1470 carbonate in mammalian apatite, *Geochim. Cosmochim. Acta*, 60, 5145–5148, [https://doi.org/10.1016/S0016-](https://doi.org/10.1016/S0016-7037(96)00308-0)
1471 [7037\(96\)00308-0](https://doi.org/10.1016/S0016-7037(96)00308-0), 1996.

1472 Carvalho, M., Jones, E. L., Ellis, M. G., Cascalheira, J., Bicho, N., Meiggs, D., Benedetti, M., Friedl, L., and Haws, J.: Neanderthal
1473 palaeoecology in the late Middle Palaeolithic of western Iberia: a stable isotope analysis of ungulate teeth from Lapa do
1474 Picareiro (Portugal), *J. Quat. Sci.*, 37, 300–319, <https://doi.org/10.1002/jqs.3363>, 2022.

1475 Cascalheira, J., Alcaraz-Castaño, M., Alcolea-González, J., de Andrés Herrero, M., Arrizabalaga, A., Aura Tortosa, J. E., García-
1476 Ibaibarriga, N., and Iriarte-Chiapusso, M. J.: Paleoenvironments and human adaptations during the Last Glacial
1477 Maximum in the Iberian Peninsula: A review, *Quat. Int.*, 581–582, 28–51, <https://doi.org/10.1016/j.quaint.2020.08.005>,
1478 2021.

1479 Cerling, T. E. and Harris, J. M.: Carbon isotope fractionation between diet and bioapatite in ungulate mammals and implications for
1480 ecological and paleoecological studies, *Oecologia*, 120, 347–363, <https://doi.org/10.1007/s004420050868>, 1999.

1481 Chillón, B. S., Alberdi, M. T., Leone, G., Bonadonna, F. P., Stenni, B., and Longinelli, A.: Oxygen isotopic composition of fossil equid
1482 tooth and bone phosphate: an archive of difficult interpretation, *Palaeogeogr. Palaeoclimatol. Palaeoecol.*, 107, 317–328,
1483 [https://doi.org/10.1016/0031-0182\(94\)90403-1](https://doi.org/10.1016/0031-0182(94)90403-1), 1994.

1484 Coplen, T. B.: Guidelines and recommended terms for expression of stable isotope ratio and gas ratio measurement results, *Rapid*
1485 *Commun. Mass Spectrom.*, 25, 2538–2560, <https://doi.org/10.1002/rcm.5129>, 2011.

1486 Coplen, T. B., Kendall, C., and Hoppe, J.: Comparison of stable isotope reference samples, *Nature*, 302, 236–238,
1487 <https://doi.org/10.1038/302236a0>, 1983.

1488 D'Angela, D. and Longinelli, A.: Oxygen isotopes in living mammal's bone phosphate: Further results, *Chem. Geol.*, 86, 75–82,
1489 1990.

1490 Dansgaard, W.: Stable isotopes in precipitation, *Tellus*, XVI, 436–468, 1964.

1491 Daura, J., Sanz, M., García, N., Allué, E., Vaquero, M., Fierro, E., Carrión, J. S., López-García, J. M., Blain, H. a., Sánchez-Marcos,
1492 a., Valls, C., Albert, R. M., Fornós, J. J., Julià, R., Fullola, J. M., and Zilhão, J.: Terrasses de la Riera dels Canyars (Gavà,
1493 Barcelona): The landscape of Heinrich Stadial 4 north of the “Ebro frontier”, and implications for modern human dispersal
1494 into Iberia, *Quat. Sci. Rev.*, 60, 26–48, <https://doi.org/10.1016/j.quascirev.2012.10.042>, 2013.

1495 Delgado Huertas, A., Iacumin, P., Stenni, B., Sánchez-Chillón, B., and Longinelli, A.: Oxygen isotope variations of phosphate in
1496 mammalian bone and tooth enamel, *Geochim. Cosmochim. Acta*, 59, 4299–4305, [https://doi.org/10.1016/0016-](https://doi.org/10.1016/0016-7037(95)00286-9)
1497 [7037\(95\)00286-9](https://doi.org/10.1016/0016-7037(95)00286-9), 1995.

1498 Drucker, D. G.: The Isotopic Ecology of the Mammoth Steppe, *Annu. Rev. Earth Planet. Sci.*, 50, 395–418,
1499 <https://doi.org/10.1146/annurev-earth-100821-081832>, 2022.

1500 Drucker, D. G., Bridault, A., Hobson, K. A., Szuma, E., and Bocherens, H.: Can carbon-13 in large herbivores reflect the canopy
1501 effect in temperate and boreal ecosystems? Evidence from modern and ancient ungulates, *Palaeogeogr. Palaeoclimatol.*
1502 *Palaeoecol.*, 266, 69–82, <https://doi.org/10.1016/j.palaeo.2008.03.020>, 2008.

1503 Fagoaga, A.: Aproximación paleoclimática y paisajística durante el MIS3 a partir del estudio de los micromamíferos del yacimiento
1504 de El Salt (Alicante), *Universidad de Burgos*, 34 pp., 2014.

1505 Fernández-García, M., Royer, A., López-García, J. M., Bennàsar, M., Goedert, J., Fourel, F., Julien, M.-A., Bañuls-Cardona, S.,
1506 Rodríguez-Hidalgo, A., Vallverdú, J., and Lécuyer, C.: Unravelling the oxygen isotope signal ($\delta^{18}O$) of rodent teeth from
1507 northeastern Iberia, and implications for past climate reconstructions, *Quat. Sci. Rev.*, 218, 107–121,
1508 <https://doi.org/10.1016/j.quascirev.2019.04.035>, 2019.

1509 Fernández-García, M., López-García, J. M., Royer, A., Lécuyer, C., Allué, E., Burjachs, F., Chacón, M. G., Saladié, P., Vallverdú,
1510 J., and Carbonell, E.: Combined palaeoecological methods using small-mammal assemblages to decipher environmental
1511 context of a long-term Neanderthal settlement in northeastern Iberia, *Quat. Sci. Rev.*, 228, 106072,
1512 <https://doi.org/10.1016/j.quascirev.2019.106072>, 2020.

1513 Fernández-García, M., Vidal-Cordasco, M., Jones, J. R., and Marin-Arroyo, A. B.: Reassessing palaeoenvironmental conditions
1514 during the Middle to Upper Palaeolithic transition in the Cantabrian region (Southwestern Europe), *Quat. Sci. Rev.*, 301,
1515 107928, <https://doi.org/10.1016/j.quascirev.2022.107928>, 2023.

1516 Fick, S. E. and Hijmans, R. J.: WorldClim 2: new 1-km spatial resolution climate surfaces for global land areas, *Int. J. Climatol.*, 37,
1517 4302–4315, <https://doi.org/10.1002/joc.5086>, 2017.

1518 García-Ibaibarriga, N., Suárez-Bilbao, A., Iriarte-Chiapusso, M. J., Arrizabalaga, A., and Murelaga, X.: Palaeoenvironmental
1519 dynamics in the Cantabrian Region during Greenland stadial 2 approached through pollen and micromammal records:
1520 State of the art, *Quat. Int.*, 506, 14–24, <https://doi.org/10.1016/j.quaint.2018.12.004>, 2019a.

1521 García-Ibaibarriga, N., Suárez-Bilbao, A., Iriarte-Chiapusso, M. J., Arrizabalaga, A., and Murelaga, X.: Palaeoenvironmental
1522 dynamics in the Cantabrian Region during Greenland stadial 2 approached through pollen and micromammal records:
1523 State of the art, *Quat. Int.*, 506, 14–24, <https://doi.org/10.1016/j.quaint.2018.12.004>, 2019b.

1524 Geiling, J. M.: Human Ecodynamics in the Late Upper Pleistocene of Northern Spain: An Archaeozoological Study of Ungulate
1525 Remains from the Lower Magdalenian and other Periods in El Mirón Cave (Cantabria), *Universidad de Cantabria*, 734
1526 pp., 2020.

1527 Hoppe, K. A.: Correlation between the oxygen isotope ratio of North American bison teeth and local waters: Implication for
1528 paleoclimatic reconstructions, *Earth Planet. Sci. Lett.*, 244, 408–417, <https://doi.org/10.1016/j.epsl.2006.01.062>, 2006.

1529 Hoppe, K. A., Stover, S. M., Pascoe, J. R., and Amundson, R.: Tooth enamel biomineralisation in extant horses: implications for
1530 isotopic microsampling, *Palaeogeogr. Palaeoclimatol. Palaeoecol.*, 206, 355–366,
1531 <https://doi.org/10.1016/j.palaeo.2004.01.012>, 2004.

1532 Iacumin, P., Bocherens, H., Mariotti, A., and Longinelli, A.: Oxygen isotope analyses of co-existing carbonate and phosphate in
1533 biogenic apatite: a way to monitor diagenetic alteration of bone phosphate?, *Earth Planet. Sci. Lett.*, 142, 1–6,
1534 [https://doi.org/10.1016/0012-821X\(96\)00093-3](https://doi.org/10.1016/0012-821X(96)00093-3), 1996.

1535 Iriarte-Chiapusso, M. J.: El entorno vegetal del yacimiento paleolítico de Labeko Koba (Arrasate, País Vasco): análisis polínico,
1536 Labeko Koba (País Vasco). Hienas y humanos en los albores del Paleolítico Super., Munibe, 89–106, 2000.

1537 Jiménez-Sánchez, M., Rodríguez-Rodríguez, L., García-Ruiz, J. M., Domínguez-Cuesta, M. J., Fariás, P., Valero-Garcés, B.,
1538 Moreno, A., Rico, M., and Valcárcel, M.: A review of glacial geomorphology and chronology in northern Spain: Timing
1539 and regional variability during the last glacial cycle, *Geomorphology*, 196, 50–64,
1540 <https://doi.org/10.1016/j.geomorph.2012.06.009>, 2013.

1541 Jones, J. R., Richards, M. P., Straus, L. G., Reade, H., Altuna, J., Mariozkurrena, K., and Marin-Arroyo, A. B.: Changing
1542 environments during the Middle Upper Palaeolithic transition in the eastern Cantabrian Region (Spain): direct evidence
1543 from stable isotope studies on ungulate bones, *Sci. Rep.*, 8, 14842, <https://doi.org/10.1038/s41598-018-32493-0>, 2018.

1544 Jones, J. R., Richards, M. P., Reade, H., Bernaldo de Quirós, F., and Marin-Arroyo, A. B.: Multi isotope investigations of ungulate
1545 bones and teeth from El Castillo and Covalejos caves (Cantabria, Spain): Implications for paleoenvironment
1546 reconstructions across the Middle-Upper Palaeolithic transition, *J. Archaeol. Sci. Reports*, 23, 1029–1042,
1547 <https://doi.org/10.1016/j.jasrep.2018.04.014>, 2019.

1548 Jones, J. R., Marin-Arroyo, A. B., Corchón Rodríguez, M. S., and Richards, M. P.: After the Last Glacial Maximum in the refugium
1549 of northern Iberia: Environmental shifts, demographic pressure and changing economic strategies at Las Galdas Cave
1550 (Asturias, Spain), *Quat. Sci. Rev.*, 262, 106931, <https://doi.org/10.1016/j.quascirev.2021.106931>, 2021.

1551 Kohn, M. J.: Comment: Tooth Enamel Mineralization in Ungulates: Implications for Recovering a Primary Isotopic Time Series, by
1552 B. H. Passey and T. E. Cerling (2002), *Geochim. Cosmochim. Acta*, 68, 403–405, [https://doi.org/10.1016/S0016-7037\(03\)00443-5](https://doi.org/10.1016/S0016-7037(03)00443-5), 2004.

1553 Kohn, M. J.: Carbon isotope compositions of terrestrial C3 plants as indicators of (paleo)ecology and (paleo)climate, *Proc. Natl.
1554 Acad. Sci.*, 107, 19694–19695, <https://doi.org/10.1073/pnas.1004933107>, 2010.

1555 Lécuyer, C., Hillaire-Marcel, C., Burke, A., Julien, M. A., and Hôlie, J.-F.: Temperature and precipitation regime in LGM human
1556 refugia of southwestern Europe inferred from $\delta^{13}C$ and $\delta^{18}O$ of large mammal remains, *Quat. Sci. Rev.*, 255, 106796,
1557 <https://doi.org/10.1016/j.quascirev.2021.106796>, 2021.

1558 Leuenberger, M., Siegenthaler, U., and Langway, C.: Carbon isotope composition of atmospheric CO2 during the last ice age from
1559 an Antarctic ice core, *Nature*, 357, 488–490, <https://doi.org/10.1038/357488a0>, 1992.

1560 López-García, J. M., Blain, H. A., Bennásar, M., Sanz, M., and Daura, J.: Heinrich event 4 characterised by terrestrial proxies in
1561 southwestern Europe, *Clim. Past*, 9, 1053–1064, <https://doi.org/10.5194/cp-9-1053-2013>, 2013.

1562 López-García, J. M., Blain, H. A., Bennásar, M., and Fernández-García, M.: Environmental and climatic context of Neanderthal
1563 occupation in southwestern Europe during MIS3 inferred from the small vertebrate assemblages, *Quat. Int.*, 326–327,
1564 319–328, <https://doi.org/10.1016/j.quaint.2013.09.010>, 2014.

1565 López-García, J. M., Blain, H. A., Fagoaga, A., Bandera, C. S., Sanz, M., and Daura, J.: Environment and climate during the
1566 Neanderthal-AMH presence in the Garraf Massif mountain range (northeastern Iberia) from the late Middle Pleistocene
1567 to Late Pleistocene inferred from small vertebrate assemblages, *Quat. Sci. Rev.*, 288,
1568 <https://doi.org/10.1016/j.quascirev.2022.107595>, 2022.

1569 Marin-Arroyo, A. B. and Sanz-Royo, A.: What Neanderthals and AMH ate: reassessment of the subsistence across the Middle-
1570 Upper Palaeolithic transition in the Vasco-Cantabrian region of SW Europe, *J. Quat. Sci.*, 37, 320–334,
1571 <https://doi.org/10.1002/jqs.3291>, 2022.

1572 Merceron, G., Berlioz, E., Vonhof, H., Green, D., Garel, M., and Tütken, T.: Tooth tales told by dental diet proxies: An alpine
1573 community of sympatric ruminants as a model to decipher the ecology of fossil fauna, *Palaeogeogr. Palaeoclimatol.
1574 Palaeoecol.*, 562, 110077, <https://doi.org/10.1016/j.palaeo.2020.110077>, 2021.

1575 van der Merwe, N. J.: Light Stable Isotopes and the Reconstruction of Prehistoric Diets, *Proc. Br. Acad.*, 77, 247–264, 1991.

1576 North Greenland Ice Core Project members: High resolution record of Northern Hemisphere climate extending into the last
1577 interglacial period, *Nature*, 431, 147–151, <https://doi.org/10.1038/nature02805>, 2004.

1578 Ochando, J., Amorós, G., Carrión, J. S., Fernández, S., Munuera, M., Camuera, J., Jiménez-Moreno, G., González-Sampériz, P.,
1579 Burgsch, F., Marin-Arroyo, A. B., Roksandic, M., and Finlayson, C.: Iberian Neanderthals in forests and savannahs, *J.
1580 Quat. Sci.*, 1–28, <https://doi.org/10.1002/jqs.3339>, 2021.

1581 Passey, B. H. and Cerling, T. E.: Tooth enamel mineralisation in ungulates: implications for recovering a primary isotopic time
1582 series, *Geochim. Cosmochim. Acta*, 66, 3225–3234, [https://doi.org/10.1016/S0016-7037\(02\)00933-X](https://doi.org/10.1016/S0016-7037(02)00933-X), 2002.

1583 Passey, B. H., Robinson, T. F., Ayliffe, L. K., Cerling, T. E., Sponheimer, M., Dearing, M. D., Roeder, B. L., and Ehleringer, J. R.:
1584 Carbon isotope fractionation between diet, breath CO2 and bioapatite in different mammals, *J. Archaeol. Sci.*, 32, 1459–
1585 1470, <https://doi.org/10.1016/j.jas.2005.03.015>, 2005.

1586 Pederzani, S. and Britton, K.: Oxygen isotopes in bioarchaeology: Principles and applications, challenges and opportunities, *Earth
1587 Science Rev.*, 188, 77–107, <https://doi.org/10.1016/j.earscirev.2018.11.005>, 2019.

1588 Pederzani, S., Aldeias, V., Dibble, H. L., Goldberg, P., Hublin, J. J., Madelaine, S., McPherron, S. P., Sandgathe, D., Steele, T. E.,
1589 Turq, A., and Britton, K.: Reconstructing Late Pleistocene paleoclimate at the scale of human behavior: an example from
1590 the Neanderthal occupation of La Ferrassie (France), *Sci. Rep.*, 11, 1–10, <https://doi.org/10.1038/s41598-020-80777-1>,
1591 2021a.

1592 Pederzani, S., Britton, K., Aldeias, V., Bourgon, N., Fewlass, H., Lauer, T., McPherron, S. P., Rezek, Z., Sirakov, N., Smith, G. M.,
1593 Spasov, R., Tran, N. H., Tsanova, T., and Hublin, J. J.: Subarctic climate for the earliest Homo sapiens in Europe, *Sci.
1594 Adv.*, 7, 1–11, <https://doi.org/10.1126/sciadv.abi4642>, 2021b.

1595 Pederzani, S., Britton, K., Jones, J. R., Agudo Pérez, L., Geiling, J. M., and Marin-Arroyo, A. B.: Late Pleistocene Neanderthal
1596 exploitation of stable and mosaic ecosystems in northern Iberia shown by multi-isotope evidence, *Quat. Res.*, 1–25,
1597 <https://doi.org/10.1017/qua.2023.32>, 2023.

1598 Pellegriani, M. and Snoeck, C.: Comparing bioapatite carbonate pre-treatments for isotopic measurements: Part 2 — Impact on
1599 carbon and oxygen isotope compositions, *Chem. Geol.*, 420, 88–96, <https://doi.org/10.1016/j.chemgeo.2015.10.038>,
1600 2016.

1601

1602 Pellegrini, M., Lee-Thorp, J. A., and Donahue, R. E.: Exploring the variation of the $\delta^{18}O_p$ and $\delta^{18}O_c$ relationship in enamel
1603 increments, *Palaeogeogr. Palaeoclimatol. Palaeoecol.*, 310, 71–83, <https://doi.org/10.1016/j.palaeo.2011.02.023>, 2011.

1604 Posth, C., Yu, H., Ghalichi, A., Rougier, H., Crevecoeur, I., Huang, Y., Ringbauer, H., Rohrlach, A. B., Nägele, K., Villalba-Mouco,
1605 V., Radzeviciute, R., Ferraz, T., Stoessel, A., Tukhbatova, R., Drucker, D. G., Lari, M., Modi, A., Vai, S., Saupe, T.,
1606 Scheib, C. L., Catalano, G., Pagani, L., Talamo, S., Fewlass, H., Klaric, L., Morala, A., Rué, M., Madelaine, S., Crépin,
1607 L., Caverne, J. B., Bocaege, E., Ricci, S., Boschini, F., Bayle, P., Maureille, B., Le Brun-Ricalens, F., Bordes, J. G., Oxilia,
1608 G., Bortolini, E., Bignon-Lau, O., Debout, G., Orliac, M., Zazzo, A., Sparacello, V., Starnini, E., Sineo, L., van der Plicht,
1609 J., Pequeur, L., Merceron, G., Garcia, G., Leuvey, J. M., Garcia, C. B., Gómez-Olivencia, A., Poltowicz-Bobak, M.,
1610 Bobak, D., Le Luyer, M., Storm, P., Hoffmann, C., Kabaciński, J., Filimonova, T., Shneider, S., Berezina, N., González-
1611 Rabanal, B., González-Morales, M. R., Marín-Arroyo, A. B., López, B., Alonso-Llamazares, C., Ronchitelli, A., Polet, C.,
1612 Jadin, I., Cauwe, N., Soler, J., Coromina, N., Ruff, I., Cottiaux, R., Clark, G., Straus, L. G., Julien, M. A., Renhart, S.,
1613 Talaa, D., Benazzi, S., Romandini, M., Amkreutz, L., Bocherens, H., Wilfling, C., Villotte, S., de Pablo, J. F. L., Gómez-
1614 Pucho, M., Esquembre-Bobia, M. A., Bodu, P., Smits, L., Souffi, B., Jankauskas, R., Kozakaitė, J., Cupillard, C., Benthien,
1615 H., Wehrberger, K., Schmitz, R. W., Feine, S. C., et al.: Palaeogenomics of Upper Palaeolithic to Neolithic European
1616 hunter-gatherers, *Nature*, 615, 117–126, <https://doi.org/10.1038/s41586-023-05726-0>, 2023.

1617 Pryor, A. J. E., Stevens, R. E., Connell, T. C. O., and Lister, J. R.: Quantification and propagation of errors when converting
1618 vertebrate biomineral oxygen isotope data to temperature for palaeoclimate reconstruction, *Palaeogeogr. Palaeoclimatol.*
1619 *Palaeoecol.*, 412, 99–107, <https://doi.org/10.1016/j.palaeo.2014.07.003>, 2014.

1620 Rasmussen, S. O., Bigler, M., Blockley, S. P., Blunier, T., Buchardt, S. L., Clausen, H. B., Cvijanovic, I., Dahl-Jensen, D., Johnsen,
1621 S. J., Fischer, H., Gkinis, V., Guillevic, M., Hoek, W. Z., Lowe, J. J., Pedro, J. B., Popp, T., Seierstad, I. K., Steffensen,
1622 J. P., Svensson, A. M., Vallelonga, P., Vinther, B. M., Walker, M. J. C., Wheatley, J. J., and Winstrup, M.: A stratigraphic
1623 framework for abrupt climatic changes during the Last Glacial period based on three synchronised Greenland ice-core
1624 records: Refining and extending the INTIMATE event stratigraphy, *Quat. Sci. Rev.*, 106, 14–28,
1625 <https://doi.org/10.1016/j.quascirev.2014.09.007>, 2014.

1626 Rey, K., Amiot, R., Lécuyer, C., Koufos, G. D., Martineau, F., Feurel, F., Kostopoulos, D. S., and Merceron, G.: Late-Miocene climatic
1627 and environmental variations in northern Greece inferred from stable isotope compositions ($\delta^{18}O$, $\delta^{13}C$) of equid teeth
1628 apatite, *Palaeogeogr. Palaeoclimatol. Palaeoecol.*, 388, 48–57, <https://doi.org/10.1016/j.palaeo.2013.07.021>, 2013.

1629 Rivals, F., Uzunidis, A., Sanz, M., and Daura, J.: Faunal dietary response to the Heinrich Event 4 in southwestern Europe,
1630 *Palaeogeogr. Palaeoclimatol. Palaeoecol.*, 473, 123–130, <https://doi.org/10.1016/j.palaeo.2017.02.033>, 2017.

1631 Rivals, F., Bocherens, H., Camarós, E., and Rosell, J.: Diet and ecological interactions in the Middle and Late Pleistocene, in:
1632 *Updating Neanderthals: Understanding Behavioural Complexity in the Late-Middle Palaeolithic*, 39–54, 2022.

1633 Rozanski, K., Araguás-Araguás, L., and Confiantini, R.: Relation Between Long-Term Trends of Oxygen-18 Isotope Composition of
1634 Precipitation and Climate, *Science (80-)*, 258, 981–985, 1992.

1635 Ruff, I., Solés, A., Soler, J., and Soler, N.: Un diente de cría de mamut (*Mammuthus primigenius* Blumenbach 1799, Proboscidea)
1636 procedente del Musteriense de la Cueva de la Arbrera (Serinyà, NE de la Península Ibérica), *Estud. Geològics*, 74,
1637 e079, <https://doi.org/10.3989/egool.43130.478>, 2018.

1638 Ruiz-Fernández, J., García-Hernández, C., and Gallinar Cañedo, D.: The glaciers of the Picos de Europa, in: *Iberia, Land of*
1639 *Glaciers*, Elsevier, 237–263, <https://doi.org/10.1016/B978-0-12-821941-6.00012-8>, 2022.

1640 Schmitt, J., Schneider, R., Elsig, J., Leuenberger, D., Lourantou, A., Chappellaz, J., Köhler, P., Joes, F., Stocker, T. F., Leuenberger,
1641 M., and Fischer, H.: Carbon Isotope Constraints on the Deglacial CO₂ Rise from Ice Cores, *Science (80-)*, 336, 711–
1642 714, <https://doi.org/10.1126/science.1217161>, 2012.

1643 Skrzypek, G., Sadler, R., and Wi, A.: Reassessment of recommendations for processing mammal phosphate $\delta^{18}O$ data for
1644 paleotemperature reconstruction, *Palaeogeogr. Palaeoclimatol. Palaeoecol.*, 446, 162–167,
1645 <https://doi.org/10.1016/j.palaeo.2016.01.032>, 2016.

1646 Snoeck, C. and Pellegrini, M.: Comparing bioapatite carbonate pre-treatments for isotopic measurements: Part 1 – Impact on
1647 structure and chemical composition, *Chem. Geol.*, 417, 394–403, <https://doi.org/10.1016/j.chemgeo.2015.10.004>, 2015.

1648 Tejada-Lara, J. V., MacFadden, B. J., Bermudez, L., Rojas, G., Salas-Gismondi, R., and Flynn, J. J.: Body mass predicts isotope
1649 enrichment in herbivorous mammals, *Proc. R. Soc. B Biol. Sci.*, 285, 20181020, <https://doi.org/10.1098/rspb.2018.1020>,
1650 2018.

1651 Traylor, R. B. and Kohn, M. J.: Tooth enamel maturation reequilibrates oxygen isotope compositions and supports simple sampling
1652 methods, *Geochim. Cosmochim. Acta*, 198, 32–47, <https://doi.org/10.1016/j.gca.2016.10.023>, 2017.

1653 Vidal-Cordasco, M., Ocio, D., Hickler, T., and Marín-Arroyo, A. B.: Ecosystem productivity affected the spatiotemporal
1654 disappearance of Neanderthals in Iberia, *Nat. Ecol. Evol.*, 6, 1644–1657, <https://doi.org/10.1038/s41559-022-01861-5>,
1655 2022.

1656 Zazzo, A., Bendrey, R., Vella, D., Moloney, A. P., Monahan, F. J., and Schmidt, O.: A refined sampling strategy for intra-tooth stable
1657 isotope analysis of mammalian enamel, *Geochim. Cosmochim. Acta*, 84, 1–13,
1658 <https://doi.org/10.1016/j.gca.2012.01.012>, 2012.

1659

1660 **Appendix A. Sites description**

1661

1662 **A1. Vasco-Cantabrian sites**

1663 **Axlor (Dima, Vizcaya, País Vasco)**

1664 Axlor is a rock-shelter located in Dima (43.2706; -1.8905), with a continuous Middle Paleolithic sequence
1665 from the MIS5 to the MIS3 (DeMuro et al., 2023; Pederzani et al., 2023; Marín-Arroyo et al., 2018). It is
1666 placed on the southwestern slope of the Dima ~~valley~~Valley, with an elevation of approximately 320 m above
1667 sea level (a.s.l.), at 33 km straight from the present-day coastline, next to one of the lowest mountain passes
1668 linking the Cantabrian basins and the Alavese Plateau. The site was discovered in 1932 and initial
1669 excavations were performed by Barandiarán (1967-1974). J. M. Barandiarán undertook the excavations
1670 between 1967 and 1974, identifying eight Mousterian levels (I-VIII) (Barandiarán, 1980).

1671 From 2000 to 2008, new excavations by González-Urquijo, Ibáñez-Estévez and Rios-Garaizar were
1672 achieved and, since 2019, these are ongoing by González-Urquijo and Lazuén. Due to the lack of
1673 chronology during Barandiarán excavations, among other aspects, work was focused on obtaining a detailed
1674 stratigraphy on the new excavation areas to correlate it with Barandiarán's levels (González-Urquijo &
1675 Ibáñez-Estévez, 2021; González Urquijo et al., 2005). The new stratigraphic sequence is roughly equivalent
1676 to the previous one, but with additional levels, not previously identified or excavated by Barandiarán. Some
1677 of these levels were deposited before Level VIII (Gómez-Olivencia et al., 2018; 2020). The Middle Paleolithic
1678 sequence extends from layers VIII to III (or from N to B-C). Levallois production is predominant in the lower
1679 levels (VI to VIII), while Quina Mousterian technocomplex does in the upper ones (from III to V) (Rios-
1680 Garaizar, 2012, 2017). ~~New~~Recent chronological data by radiocarbon (Pederzani et al., 2023; Marín-Arroyo
1681 et al., 2018) and OSL (Demuro et al., 2023) methods confirm that a sequence Axlor levels VI, VIII, and VIII
1682 probably accumulated during MIS5d-a (109–82 ka), while levels D to B probably were formed during the
1683 period encompassing the start of MIS 4 (71–57 ka) through to the beginning or middle of MIS 3 (57–29 ka)
1684 (Demuro et al., 2023) and upper Level III to -46,200 ±3,000 BP, which calibrates between 45,510-350 cal
1685 BP and ~~the end of~~beyond the calibration curve at > 55,000 cal BP (see Pederzani et al., 2023: Fig. 1).

1686 The archaeozoological study indicates an anthropic origin of the faunal assemblage with scarce carnivore
1687 activity documented (Altuna, 1989; Castaños, 2005; Gómez-Olivencia et al., 2018). In lower layers, the most
1688 abundant taxa are *Cervus elaphus* (VIII) and *Capra pyrenaica* (VII), while in upper layers III-V, *Cervus*
1689 *elaphus* is substituted by *Bos primigenius*/*Bison priscus* and *Equus sp.* The material included in this work
1690 comes from the faunal collection of the Barandiarán excavation currently curated at the Bizkaia Museum of
1691 Archaeology (Bilbao), where teeth were sampled and the stable isotope analyses on enamel phosphate
1692 were included in Pederzani et al. (2023).

1693

1694 **El Castillo (Puente Viesgo, Cantabria)**

1695 El Castillo is cave is located in Puente Viesgo (43.2924; -3.9656), with an elevation of approximately 195m
1696 a.s.l., at 17 km straight from the present-day coastline. The cave belongs to the karstic system that was
1697 formed in the Monte Castillo, which dominates the Pas ~~valley~~Valley. The site was discovered in 1903 by H.
1698 Alcalde del Río. H. Obermaier carried out the first excavation seasons between 1910 and 1914, when many
1699 of the archaeological remains were recovered, mainly from the ~~hall of the cave~~cave hall. These interventions
1700 were done under the supervision of the "Institut de Paléontologie Humaine" (IPH) and of Prince Albert I of
1701 Monaco. From 1980 to 2011, V. Cabrera and F. Bernaldo de Quirós underwent new excavations focusing
1702 on the cave entrance, on the Middle to Upper Paleolithic transitional levels, mainly 16, 18 and 20 (Cabrera-
1703 Valdes, 1984). The site has yielded an important stratigraphic sequence, composed by 26 sedimentological

1704 units (1-26) related to different anthropic occupational units, often separated by archaeologically sterile units:
1705 Eneolithic (2), Azilian (4), Magdalenian (6 and 8), Solutrean (10), Aurignacian (12, 14, 16 and 18),
1706 Mousterian (20, 21 and 22) and Acheulean (24) (Cabrera-Valdés, 1984).

1707 Unit 21 is mostly sterile (Cabrera Valdés, 1984; Martín-Perea et al., 2023) and ~~it was dated by ESR~~
1708 ~~dated it~~, yielding a mean date of 69,000 ± 9,200 years BP (Rink et al., 1997). However, Martín-Perea et al.
1709 (2023) suggested some dating uncertainty ~~arising from the interpretation of interpreting~~ the initial
1710 stratigraphic nomenclature. They suggest that the ESR dates provided for level 21 by Rink et al. (1997) were
1711 erroneously attributed to this unit and it might correspond to 20E, indicating that below that subunit, the
1712 chronology is older than 70,000 years BP (Martín-Perea et al., 2023). The Mousterian Unit 20 cave is divided
1713 into several subunits (Martín-Perea et al., 2023). In Unit 20, a cave roof collapse took place, transforming
1714 the cave system into an open rock shelter. This unit contains abundant archaeological and paleontological
1715 remains. Lithic industry ~~consistent-consists in-of~~ sidescrapers, denticulates, notches and cleavers, the
1716 majority on quartzite and presents both unifacial, bifacial discoid debitage and Levallois debitage. Unit 20E
1717 was attributed to Quina Mousterian by Sánchez-Fernández and Bernaldo De Quiros (2009) and contains a
1718 Neanderthal tooth ~~remain~~ (Garralda, 2005). Considering the geochronological uncertainties for dates on
1719 20E related ~~with to~~ Rink et al. (1997), we have decided to ~~solely-rely solely~~ on ESR date of 47,000 ± 9400
1720 BP provided by Liberda et al. (2010) for this level. Unit 20C presents clear evidence of the Mousterian lithic
1721 industry and radiocarbon dates of 48,700±3,400 uncal BP (OxA-22204) and 49,400±3,700 uncal BP (OxA-
1722 22205) (Wood et al., 2018) and mean ESR date of 42,700 ±9900 BP (Liberda et al., 2010). Level 19 is
1723 archaeologically sterile and separates Unit 20 from Unit 18 (Wood et al., 2018).

1724 Unit 18 is divided into ~~three parts~~: 18A (archaeologically sterile), 18B, and 18C. Levels 18B and 18C were
1725 classified as Transitional Aurignacian, representing a gradual transformation from the Mousterian to the
1726 Aurignacian, which is unique to El Castillo cave (Cabrera et al., 2001; Maïllo and Bernaldo de Quiros, 2010;
1727 Wood et al., 2018). ~~The dates and the cultural attribution of these levels~~ ~~se levels:~~ ~~dates and cultural~~
1728 ~~attribution~~ have been the subject of much debate (e.g. Zilhao and D'Errico, 2003; Wood et al., 2018).
1729 According to Wood et al. (2018), the last dates of these levels range between 42,000±1,500 uncal BP (OxA-
1730 22203) and 46,000±2,400 uncal BP (OxA-21973), which is much earlier than the start of the Aurignacian
1731 period in the Cantabrian region (Marín-Arroyo et al., 2018; Vidal-Cordasco et al., ~~2023~~2022). The lithic
1732 assemblage of Unit 18 appears to be dominated by Discoid/Levallois technology (Bernaldo de Quiros and
1733 Maïllo-Fernández, 2009) but with a high percentage of "Upper Paleolithic" pieces. Additionally, punctual
1734 bone industry, ~~as well as pieces with incisions and engravings, and pieces with incisions and engravings~~
1735 were discovered in Unit 18 (Cabrera-Valdés et al., 2001). Three deciduous tooth crowns attributed to
1736 Neanderthals were found in Unit 18B (Garralda et al., 2022). Above, Unit 17 is sterile but contains scarce
1737 lithic and faunal materials, while Level 16 was attributed to the Proto-Aurignacian, with dates of
1738 38,600±1,000 uncal BP (OxA-22200) (Wood et al., 2018).

1739 According to Luret et al. (2020), there was a shift in hunting practices between the Late Mousterian (unit 20)
1740 and the Transitional Aurignacian (unit 18). During the Late Mousterian, hunting strategies were less
1741 specialized, and the species hunted included red deer, horses, and bovines. However, in Unit 18, a
1742 specialization in red deer hunting is observed. However, the explanation of this shift has been proposed as
1743 a response to a cultural choice or induced by climatic changes. ~~However, recent taphonomic studies by~~
1744 ~~Sanz-Royo et al. (2023) on the old collections of Aurignacian Delta level reveal a more significant role of~~
1745 ~~carnivores than shown by Luret et al. (2020)~~. The material included in this work comes from the faunal
1746 collection recovered during the Cabrera-Valdés and Bernaldo de Quiros excavations curated at Museo de
1747 Prehistoria y Arqueología de Cantabria (MUPAC, Santander).

1748

1749 **Labeko Koba (Arrastre, Guipúzcoa, País Vasco)**

1750 Labeko Koba is a cave located in the Kurtzetxiki Hill (43.0619; -2.4833), at 246 m a.s.l. and 29 km straight
1751 from the present-day Atlantic coast. In 1987 and 1988, due to the construction of the Arrasate ring road, the
1752 site was discovered. The site was discovered due to the construction of the Arrasate ring road, and a savage
1753 excavation was carried out (Arrizabalaga, 2000a). Unfortunately, the site was destroyed after that. The
1754 stratigraphic sequence identified nine different levels. The lower Level IX was attributed to the
1755 Châtelperronian, based on the presence of three Châtelperron points. Although there is a lack of human
1756 remains in few Cantabrian Châtelperronian sites, recent research has suggested that this techno-complex
1757 was produced by Neanderthals (Maroto et al., 2012; Ríos-Garaizar et al., 2022). Level VII marks the
1758 beginning of the Aurignacian sequence, likely Proto-Aurignacian, with a lithic assemblage dominated by
1759 Dufour bladelets (Arrizabalaga, 2000a). Levels VI, V, and IV contain lithic assemblages that suggested an
1760 Early Aurignacian attribution (Arrizabalaga, 2000b; Arrizabalaga et al., 2009). This site is significant because
1761 it is one of the few sites with Châtelperronian assemblages and with both Proto-Aurignacian and Early
1762 Aurignacian separated (Arrizabalaga et al., 2009).

1763 Initial radiocarbon dates were inconsistent with the stratigraphy of the site and much more recent than
1764 expected for the Early Upper Paleolithic (Arrizabalaga, 2000a). This incoherence was determined to be
1765 affected by taphonomic alterations (Wood et al., 2014). Later radiocarbon dates undertaken with an
1766 ultrafiltration pre-treatment provided a new regional framework for the regional Early Upper Paleolithic
1767 (Wood et al., 2014). The Châtelperronian layer IX inf is dated to 38,100±900 uncal BP (OxA-22562) and
1768 37,400±800 uncal BP (OxA-22560). The Proto-Aurignacian levels cover a period from 36,850±800 uncal
1769 BP (OxA-21766) to 35,250±650 uncal BP (OxA-21793). The three Early Aurignacian levels are dated to
1770 35,100±600 uncal BP (OxA-21778) for level VI, ~ 34,000 uncal BP (OxA-21767 and OxA-21779) for level
1771 V, and ~ 33,000 BP (OxA-21768 and OxA-21780) for level IV (Arrizabalaga et al., 2009).

1772 Taphonomic studies indicate an alternation in the use of the cave between carnivores and humans, the latter
1773 ones during short occupation periods (Villaluenda et al., 2012; Ríos-Garaizar et al., 2012; Arrizabalaga et
1774 al., 2010). Labeko Koba is considered to have functioned as a natural trap where carnivores, mainly hyenas,
1775 accessed to animal carcasses. At least in the base of Labeko Koba IX, carnivore activity was higher, and
1776 they would have consumed the same prey as humans (Villaluenda et al., 2012). The presence of humans
1777 is linked to strategic use as a campsite associated with a small assemblage of lithic artifacts. The most
1778 consumed species by Châtelperronian groups were red deer, followed by the consumption of large bovids,
1779 equids, and woolly rhinoceros. During the Aurignacian period, there was some stability in human
1780 occupations, although they still alternated with carnivore occupations (Arrizabalaga et al., 2010). Cold-
1781 adapted fauna such as reindeer and woolly rhinoceros were identified in association with the
1782 Châtelperronian. Reindeer were still present during the Aurignacian levels, as well as the woolly mammoth
1783 and arctic fox and the woolly mammoth and arctic fox were still present during the Aurignacian levels. The
1784 original sampling of the studied teeth studied by this work was performed in the San Sebastian Heritage
1785 Collection headquarters, where the Guipuzcoa archaeological materials were deposited at that time.

1786

1787 Aitzbitarte III interior (Rentería, Guipúzcoa, País Vasco)

1788 Aitzbitarte III is an archaeological site located within a the Landarbaso karstic system comprising of nine
1789 caves in Rentería (43.270; -1.8905). The cave is situated 220 m.a.s.l. and is 10 km away from the present-
1790 day coastline. Initial archaeological interventions were carried out at the end of the 19th century by P.M. de
1791 Soraluze (Altuna, 2011). Recent excavations were initially conducted in the deep zone inside the cave
1792 between 1986 and 1993, where the studied tooth was recovered, and later focused on the cave entrance
1793 between 1994 and 2002, by J. Altuna, K. Mariezkurrena, and J. Ríos-Garaizar (Altuna et al., 2011; 2017).

1794 While the cave's entrance area contains a sequence comprising [possible](#) Mousterian [and](#) [-](#)Evolved
1795 Aurignacian; and Gravettian [layers-levels](#) (Altuna et al., 2011; 2013), the stratigraphy in the inner cave
1796 presents [8-eight](#) levels: level VIII (some tools with Mousterian features), VII (sterile), VIb, VIa and V (Middle
1797 Gravettian technocomplex with abundance of Noailles burins), IV-II (disturbed archaeological levels) and I
1798 (surface) (Altuna et al., 2017). Levels V have dates of 24,910 uncal BP (I-15208) and 23,230 uncal BP (Ua-
1799 2243); whereas level VI extends from 23,830 ± 345 uncal BP (Ua-2628) and 25,380± 430 uncal BP (Ua-
1800 2244) (Altuna, 1992; Altuna et al., 2017), with a possible outlier dated at 21,130 uncal BP (Ua-1917).

1801 The Gravettian occupation in the inner part of the cave was [originally-initially](#) thought to be more recent than
1802 the ones in the cave entrance. However, it was [not-difficult easy](#) to correlate the two excavation areas due
1803 to different sedimentation rates. The [rich-abundant](#) human occupations took place during a singular cold
1804 phase in the Middle Gravettian with a specialized paleoeconomy focused on the hunting of *Bos primigenius*
1805 and *Bison priscus* (85% in level VI and 68% in level V), which is unusual in the Cantabrian region mostly
1806 focused on red deer and ibex. Other ungulates present are *Cervus elaphus* and *Rupicapra rupicapra*, and
1807 to a lesser extent *Capra pyrenaica*, *Capreolus capreolus*, *Rangifer tarandus*, and *Equus ferus* (Altuna et al.,
1808 2017; Altuna & Mariezkurrena, 2020). There is a scarce representation of carnivores. The tooth studied was
1809 sampled at the Gordailua Center for Heritage Collections of the Provincial Council of Gipuzkoa.

1810

1811 **El Otero (Secadura, Voto, Cantabria)**

1812 El Otero cave is located in Secadura (Voto) (43.3565; -3.5360), at 129 m.s.a.l and 12 km [straight](#) from the
1813 present-day coastline. [N](#), near the Matienzo valley in a coastal plain environment covered by meadows and
1814 gentle hills. The discovery was made in 1908 by Lorenzo Sierra. The site was excavated in 1963 by J.
1815 Gonzalez Echeagaray and M.A. García Guinea, in two different sectors (Sala I and Sala II) with an equivalent
1816 stratigraphic sequence (González Echeagaray, 1966). [A total of n](#)Nine levels were identified in Sala I, from
1817 level IX to level I. Levels IX and VIII were [originally-initially](#) related to the "Aurignacian-Mousterian, based on
1818 lithics assemblages with a combination of both technocomplex features. The overlying levels VI-IV were
1819 separated by a speleothem crust (level VII) and were initially related to Aurignacian, due to the presence of
1820 end-scrapers, bone points, blades, or burins on truncation (Freeman, 1964; Rios-Garaizar, 2013). Also,
1821 perforated deer, ibex, and fox teeth were found in levels V and IV. This site lacked chronological dating
1822 methods, until a selection of material from levels VI, V and IV revealed a difference [in](#) chrono-cultural
1823 attribution (Marín-Arroyo et al., 2018). Radiocarbon results yielded younger dates for such a cultural
1824 attribution and showed significant stratigraphic inconsistency. Level VI gave a result of 12,415±55 [uncal BP](#)
1825 (OxA-32585), two dates in Level V are 12,340±55 (OxA-32509) and 10,585±50 [uncal BP](#) (OxA-32510), and
1826 a date in Level IV is 15,990±80 [uncal BP](#) (OxA-32508). All these results fall into the range of the Late Upper
1827 Paleolithic (Magdalenian-Azilian initially identified in levels III-I), eliminating attribution of these levels to the
1828 Aurignacian; despite the presence of apparently characteristic artefacts. [Further assessments of](#)
1829 [archaeological materials will be needed](#).

1830 Red deer dominate the assemblage, except for level IV where horses are more abundant. Wild boar, roe
1831 deer, and ibex are also present, but large bovids are relatively rare (González Echeagaray, 1966). Level IV
1832 is the richest and most anthropogenic level, with evidence of butchering in red deer (captured in winter and
1833 early summer) and chamois (in autumn). The formation of this level involved humans and carnivores, and
1834 although certain data may suggest an anthropogenic predominance, the limited sample analyzed
1835 taphonomically and the pre-selection of preserved pieces do not allow for a definitive conclusion (Yravedra
1836 & Gómez-Castanedo, 2010). The material included in this work is curated at the Museo de Prehistoria y
1837 Arqueología de Cantabria (MUPAC, Santander).

1838

1839 **A2. Mediterranean-Northeastern Iberia sites**

1840 **Terrasses de la Riera dels Canyars (Gavà, Barcelona, Cataluña)**

1841 Terrasses de la Riera dels Canyars (henceforth, Canyars) is an open-air site located near Gavà (Barcelona)
1842 (41.2961;1.9797), at 28 m.s.a.l and 3 km straight from the present-day coastline. The site lies on a fluvial
1843 terrace at the confluence of Riera dels Canyars, a torrential stream between Garraf Massif, Llobregat delta
1844 and Riera de Can Llong (Daura et al., 2013). Archaeo-paleontological remains were discovered during
1845 quarries activities in 2005 and was complete excavated on 2007 by the *Grup de Recerca del Quaternari*
1846 (Daura and Sanz, 2006; Daura et al., 2013). This intervention determined nine lithological units. The
1847 paleontological and archaeological remains come exclusively from one unit, the middle luthitic unit (MLU),
1848 and specifically from layer I. The MLU is composed of coarse sandy clays and gravels, filling a paleochannel
1849 network named lower detrital unit (LDU) (Daura et al., 2013). Five radiocarbon dates were obtained on
1850 charcoals from layer I, which yield statistically consistent ages from 33,800 ±350 uncal BP to 34,900 ±340
1851 uncal BP, which results in mean age of 39,71600 cal BP (from ~~37,405 to 40,890~~ to 38,530 946 cal BP)
1852 (Daura et al., 2013; [this work](#)).

1853 The layer I of the site has yielded a rich faunal assemblage, consisting of over 5,000 remains. Among the
1854 herbivores, the most common species found are *Equus ferus*, *Bos primigenius*, *Equus hydruntinus*, and
1855 *Cervus elaphus* (Daura et al., 2013; Sanz-Royo et al., 2020). *Capra* sp. and *Sus scrofa* are also present,
1856 although in lower frequencies. The carnivores found at the site are also noteworthy, with *Crocuta crocuta*
1857 and *Lynx pardinus* being the most frequent. Presence of cold-adapted fauna associated to stepped
1858 environments is recorded, such as cf. *Mammuthus* sp., *Coelodonta antiquitatis*, and *Equus hydruntinus*.
1859 Small mammal analysis, pollen, and use-wear analysis have provided further evidence that a steppe-
1860 dominated landscape surrounded the Canyars site, supporting a correlation with the Heinrich Event 4, in
1861 coherence with the chronology obtained for the layer (López-García et al. 2013; 2023; Rivals et al., 2017).
1862 However, the presence of woodland is also attested by forest taxa within charcoal and pollen assemblages
1863 (Daura et al., 2013).

1864 Taphonomic study is ongoing. But several evidences point that hyenas have played an important role in the
1865 accumulation of the faunal assemblage (Daura et al., 2013; Jimenez et al. 2019). However, sporadic human
1866 presence is documented by few human modifications found in faunal remains (cutmarks and fire alterations).
1867 Although the paucity of the lithic assemblage in the site, it shows a clear attribution to Upper Palaeolithic
1868 technocomplex, most likely the Early Aurignacian (Daura et al., 2013). Recently, it was documented a
1869 perforated bone fragment, which has been identified as a perforated board for leather production (Doyon et
1870 al., 2023). All teeth included in this work were sampled in *Laboratori de la Guixera* (Ajuntament de
1871 Casteldefels) where the material is stored.

1872
1873 **References Appendix A**

1874 Altuna, J., Mariezkurrena, K., de la Peña, P., Ríos-Garaizar, J. 2011. Ocupaciones Humanas En La Cueva de Aitzbitarte III (Rentería,
1875 País Vasco) Sector Entrada: 33.000-18.000 BP. Servicio Central de Publicaciones del Gobierno Vasco; EKOB: 11-21.
1876 Altuna, J., Mariezkurrena, K., de la Peña, P., Ríos-Garaizar, J. 2013. Los niveles gravetienses de la cueva de Aitzbitarte III
1877 (Gipuzkoa). Industrias y faunas asociadas, in: de las Heras, C., Lasheras, J.A., Arrizabalaga, A., de la Rasilla, M. editors.
1878 Pensando El Gravetiense: Nuevos Datos Para La Región Cantábrica En Su Contexto Peninsular Y Pirenaico.
1879 Monografías Del Museo Nacional Y Centro de Investigación de Altamira, 23. Madrid: Ministerio de Educación, Cultura;
1880 pp.184-204.
1881 Altuna, J. & Mariezkurrena, K. 2020. Estrategias de caza en el Paleolítico superior de la Región Cantábrica. El caso de Aitzbitarte
1882 II (zona profunda de la cueva). *Sagvntvm Extra* 21, Homenaje al Profesor Manuel Pérez Ripoll: 219-225.
1883 Altuna, J., Mariezkurrena, K., Ríos-Garaizar, J., & San Emeterio-Gómez, A. 2017. Ocupaciones Humanas en Aitzbitarte III (País
1884 Vasco) 26.000 – 13.000 BP (zona profunda de la cueva). Servicio Central de Publicaciones del Gobierno Vasco. EKOB;
1885 8: 348pp.

Formatted: English (United Kingdom)

1886 Arrizabalaga, A., 2000a. El yacimiento arqueológico de Labeko Koba (Arrasate, País Vasco). Entorno. Crónica de las
1887 investigaciones. Estratigrafía y estructuras. Cronología absoluta. In: Arrizabalaga, A., Altuna, J. (Eds.), Labeko Koba
1888 (País Vasco). Hienas y Humanos en los Albores del Paleolítico Superior, Munibe (Antropología-Arkeologia) 52. Sociedad
1889 de Ciencias Aranzadi, San Sebastián-Donostia, pp. 15-72.

1890 Arrizabalaga, A., 2000b. Los tecnocomplejos líticos del yacimiento arqueológico de Labeko Koba (Arrasate, País Vasco). In:
1891 Arrizabalaga, A., Altuna, J. (Eds.), Labeko Koba (País Vasco). Hienas y Humanos en los Albores del Paleolítico Superior,
1892 Munibe (Antropología-Arkeologia) 52. Sociedad de Ciencias Aranzadi, San Sebastián-Donostia, pp. 193-343.

1893 Arrizabalaga, A., Iriarte, E., Ríos Garaizar, J., 2009. The Early Aurignacian in the Basque Country. *Quaternary International*, 207:
1894 25-36.

1895 Arrizabalaga, A., Iriarte, M.J. & Villaluenga, A. 2010. Labeko Koba y Lezetxiki (País Vasco). Dos yacimientos, una problemática
1896 común. *Zona Arqueológica*, 13: 322-334.

1897 Barandiarán JM. 1980. Excavaciones en Axlor. 1967-1974. En: Barandiarán, J. M.: Obras Completas. Tomo XVII; pp. 127-384.

1898 Bernaldo de Quirós, F., Maíllo-Fernández, J.-M. 2009. Middle to Upper Palaeolithic at Cantabrian Spain. In: Camps M, Chauhan
1899 PR (eds) A sourcebook of Palaeolithic transitions: methods, theories and interpretations. Springer, New York, pp. 341-
1900 359.

1901 Cabrera-Valdes, V. 1984. El Yacimiento de la cueva de «El Castillo» (Puente Viesgo, Santander). *Bibliotheca Praehistorica Hispana*
1902 22, C.S.I.C., 485 p.

1903 Cabrera-Valdes, V., Maíllo-Fernandez, J.M., Lloret, M., Bernaldo-De Quiros, F. 2001. La transition vers le Paléolithique supérieur
1904 dans la grotte du Castillo (Cantabrie, Espagne) la couche 18. *L'Anthropologie* 105, pp. 505-532.

1905 Daura, J., Sanz, M. (2006). Informe de la troballa del jaciment arqueològic "Terrasses dels Canyars" (Castelldefels-Gavà).
1906 Notificació de la descoberta i propostes d'actuació. Grup de Recerca del Quaternari, SERP, UB. Servei d'Arqueologia i
1907 Paleontologia, Departament de Cultura i Mitjans de Comunicació, Generalitat de Catalunya. Unpublished Archaeological
1908 Report.

1909 Daura, J., Sanz, M., García, N., Allué, E., Vaquero, M., Fierro, E., Carrión, J. S., López-García, J. M., Blain, H. A., Sánchez-Marco,
1910 A., Vallis, C., Albert, R. M., Fornós, J. J., Julià, R., Fullola, J. M., Zilhão, J. 2013. Terrasses de la Riera dels Canyars
1911 (Gavà, Barcelona): The landscape of Heinrich stadial 4 north of the "Ebro frontier" and implications for modern human
1912 dispersal into Iberia. *Quaternary Science Reviews*, 60, 26-48.

1913 Demuro, M., Arnold, L., González-Urquijo, J., Lazuen, T., Frochoso, M. 2023. Chronological constraint of Neanderthal cultural and
1914 environmental changes in southwestern Europe: MIS 5- MIS 3 dating of the Axlor site (Biscay, Spain). *Journal of*
1915 *Quaternary Research*

1916 Doyon, L., Fauro, T., Sanz, M., Daura, J., Cassard, L., D'Errico, F., 2023. A 39,600-year-old leather punch board from Canyars,
1917 Gavà, Spain. *Scientific Advances*, 9, <https://doi.org/10.1126/sciadv.adg0834>

1918 Freeman, L.G. 1964. Mousterian Developments in Cantabrian Spain. Ph.D. thesis. Dept. of Anthropology, University of Chicago,
1919 Chicago.

1920 Garralda, M.D. 2005. Los Neandertales en la Península Ibérica. The Neandertals from the Iberian Peninsula. *Munibe (Antropología-*
1921 *Arkeologia)* 57, Homenaje a Jesús Altuna. pp. 289-314.

1922 Garralda, M.D., Madrigal, T., Zapata, J., & Rosell, J. 2022. Neanderthal deciduous tooth crowns from the Early Upper Paleolithic at
1923 El Castillo Cave (Cantabria, Spain). *Archaeological and Anthropological Sciences*.

1924 Gómez-Olivencia, A., Arceredillo, D., Álvarez-Lao, D.J., Garate, D., San Pedro, Z., Castañes, P., Ríos-Garaizar, J., 2014. New
1925 evidence for the presence of reindeer (*Rangifer tarandus*) on the Iberian Peninsula in the Pleistocene: an
1926 archaeopalaeontological and chronological reassessment. *Boreas* 43, 286-308.

1927 Gómez-Olivencia, A., Sala, N., Nuñez-Lahuerta, C., Sanchis, A., Arlegi, M., Ríos-Garaizar, J., 2018. First data of Neanderthal bird
1928 and carnivore exploitation in the Cantabrian Region (Axlor; Barandiarán excavations; Dima, Biscay, Northern Iberian
1929 Peninsula). *Scientif. Rep.* 8, 10551.

1930 González Echegaray, J.G. 1966. Cueva del Otero. Excavaciones Arqueológicas en España, 53. Madrid: Ministerio de Educación
1931 Nacional Dirección General de Bellas Artes Servicio Nacional de Excavaciones.

1932 González-Urquijo, J.E., Ibáñez-Estévez, J.J. 2001. Abrigo de Axlor (Dima). *Arkeoikuska: Investigación arqueológica* 2001; 2002:
1933 90-93.

1934 González-Urquijo, J.E., Ibáñez-Estévez, J.J., Ríos-Garaizar, J., Bourguignon, L., Castañes Ugarte, P., Tarrío-Vinagre, A. 2005.
1935 Excavaciones recientes en Axlor. Movilidad y planificación de actividades en grupos de neandertales. In: Montes Barquín
1936 R., Lasheras Corruchaga JA, editors. *Actas de La Reunión Científica: Neandertales Cantábricos. Estado de La Cuestión*.
1937 *Monografías Del Museo Nacional Y Centro de Investigación de Altamira No 20*. Madrid: Ministerio de Cultura; 2005, pp.
1938 527-539.

1939 Jimenez, I. J., Sanz, M., Daura, J., Gaspar, I. D., García, N. 2019. Ontogenetic dental patterns in Pleistocene hyenas (*Crocuta*
1940 *crocuta* Erxleben, 1777) and their palaeobiological implications. *International Journal of Osteoarchaeology*, 29, 808-821.

1941 Liberta, J.J., Thompson, J.W., Rink, W.J., Bernaldo de Quirós, F., Jayaraman, R., Selvaretinam, K., Chancellor-Maddison, K.,
1942 Volterra, V., 2010. ESR dating of tooth enamel in Mousterian layer 20, El Castillo, Spain. *Geoarchaeology* n/a-n/a.

1943 López-García, J.M., Blain, H.A., Fagoaga, A., Bandera, C.S., Sanz, M., Daura, J., 2022. Environment and climate during the
1944 Neanderthal-AMH presence in the Garraf Massif mountain range (northeastern Iberia) from the late Middle Pleistocene
1945 to Late Pleistocene inferred from small-vertebrate assemblages. *Quaternary Science Reviews*, 288.

Formatted: English (United Kingdom)

Field Code Changed

Formatted: English (United Kingdom)

1946 López-García, J. M., Blain, H. A., Bennàsar, M., Sanz, M., Daura, J. 2013. Heinrich event 4 characterized by terrestrial proxies in
1947 southwestern Europe. *Climate of the Past*, 9: 1053–1064.

1948 Luret, M., Blasco, R., Arsuaga, J. L., Baquedano, E., Pérez-González, A., Sala, N., & Aranburu, A. 2020. A multi-proxy approach to
1949 the chronology of the earliest Aurignacian at the El Castillo Cave (Spain). *Journal of Archaeological Science: Reports*,
1950 33: 102339.

1951 Maroto, J., Vaquero, M., Arrizabalaga, Á., Baena, J., Baquedano, E., Jordá, J., Julià, R., Montes, R., Van Der Plicht, J., Rasines,
1952 P., Wood, R., 2012. Current issues in late Middle Palaeolithic chronology: New assessments from Northern Iberia.
1953 *Quaternary International*, 247: 15–25.

1954 Marín Arroyo, A.B., Ríos-Garaizar, J., Straus, L.G., Jones, J.R., de la Rasilla, M., González-Morales, M.R., Richards, M., Altuna, J.,
1955 Mariezkurrena, K., Ocio, D., 2018. Chronological reassessment of the Middle to Upper Paleolithic transition and Early
1956 Upper Paleolithic cultures in Cantabrian Spain. *PLoS One* 13: 1–20.

1957 Martín-Perea, D.M., Maíllo-Fernández, J., Marín, J., Arroyo, X., Asiain, R., 2023. A step-back to move forward: a geological re-
1958 evaluation of the El Castillo Cave Middle Palaeolithic lithostratigraphic units (Cantabria, northern Iberia). *Journal of*
1959 *Quaternary Science*, 38: 221–234.

1960 Pederzani, S., Britton, K., Jones, J.R., Agudo-Pérez, L., Geiling, J.M., Marín Arroyo, A.B., 2023. Late Pleistocene Neanderthal
1961 exploitation of stable and mosaic ecosystems in northern Iberia shown by multi-isotope evidence. *Quaternary Research*:
1962 1–25.

1963 Rink, W.J., Schwarcz, H.P., Lee, H.K., Cabrera Valdés, V., Bernaldo de Quirós, F., Hoyos, M. 1997. ESR dating of Mousterian
1964 levels at El Castillo Cave, Cantabria, Spain. *Journal of Archaeological Science*, 24 (7): 593–600.

1965 Ríos-Garaizar J. 2012. *Industria lítica y sociedad en la Transición del Paleolítico Medio al Superior en torno al Golfo de Bizkaia*.
1966 Santander: PUBLICAN - Ediciones de la Universidad de Cantabria.

1967 Ríos-Garaizar, J. 2017. A new chronological and technological synthesis for Late Middle Paleolithic of the Eastern Cantabrian
1968 Region. *Quaternary International*, 433: 50–63.

1969 Ríos-Garaizar, J., Arrizabalaga, A. & Villaluenga, A. 2012. Haltes de chasse du Châtelperronien de la Péninsule Ibérique: Labeko
1970 Koba et Ekain (Pays Basque Péninsulaire). *L'Anthropologie*, 116: 532–549.

1971 Ríos-Garaizar, J., de la Peña, P., Maíllo-Fernández, J.M. 2013. El final del Auriniense y el comienzo del Gravetiense en la región
1972 cantábrica: una visión tecno tipológica. In: de las Heras C., Lasheras J.A., Arrizabalaga Á., de la Rasilla M. (Eds.),
1973 *Pensando El Gravetiense: Nuevos Datos Para La Región Cantábrica En Su Contexto Peninsular Y Pirenaico*.
1974 *Monografías Del Museo Nacional Y Centro de Investigación de Altamira*, 23. Madrid: Ministerio de Educación, Cultura;
1975 pp. 369–382.

1976 Ríos-Garaizar, J., Iriarte, E., Arnold, L.J., Sánchez-Romero, L., Marín Arroyo, A.B., San Emetorio, A., Gómez-Olivencia, A., Pérez-
1977 Garrido, C., Demuro, M., Campaña, I., Bourguignon, L., Benito-Calvo, A., Iriarte, M.J., Aranburu, A., Arranz-Otaegi, A.,
1978 Garate, D., Silva-Gago, M., Lahaye, C., Ortega, I. 2022. The intrusive nature of the Châtelperronian in the Iberian
1979 Peninsula. *PLoS One* 17, e0265219.

1980 Rivals, F., Uzunidis, A., Sanz, M., Daura, J., 2017. Faunal dietary response to the Heinrich Event 4 in southwestern Europe.
1981 *Palaeogeogr. Palaeoclimatol. Palaeoecol.* 473, 123–130.

1982 Sanz-Royo, A., Sanz, M., Daura, J. (2020). Upper Pleistocene equids from Terrasses de la Riera dels Canyars (NE Iberian
1983 Peninsula): The presence of *Equus ferus* and *Equus hydruntinus* based on dental criteria and their implications for
1984 palaeontological identification and palaeoenvironmental reconstruction. *Quaternary International*, 566–567, 78–90.

1985 Vidal-Cordasco, M., Ocio, D., Hickler, T., Marín Arroyo, A.B., 2022. Ecosystem productivity affected the spatiotemporal
1986 disappearance of Neanderthals in Iberia. *Nat. Ecol. Evol.* 6, 1644–1657.

1987 Villaluenga, A., Arrizabalaga, A. & Ríos-Garaizar, J. 2012. Multidisciplinary approach to two Châtelperronian series: lower IX layer
1988 of Labeko Koba and X Level of Ekain (Basque country, Spain). *Journal of Taphonomy*, 10: 525–548.

1989 Wood, R.E., Arrizabalaga, A., Camps, M., Fallon, S., Iriarte-Chiapusso, M.J., Jones, R., Maroto, J., De la Rasilla, M., Santamaría,
1990 D., Soler, J., Soler, N., Villaluenga, A., Higham, T.F.G. 2014. The chronology of the earliest Upper Palaeolithic in northern
1991 Iberia: New insights from L'Arbreda, Labeko Koba and La Viña. *Journal of Human Evolution*, 69: 91–109.
1992 <https://doi.org/10.1016/j.jhevol.2013.12.017>

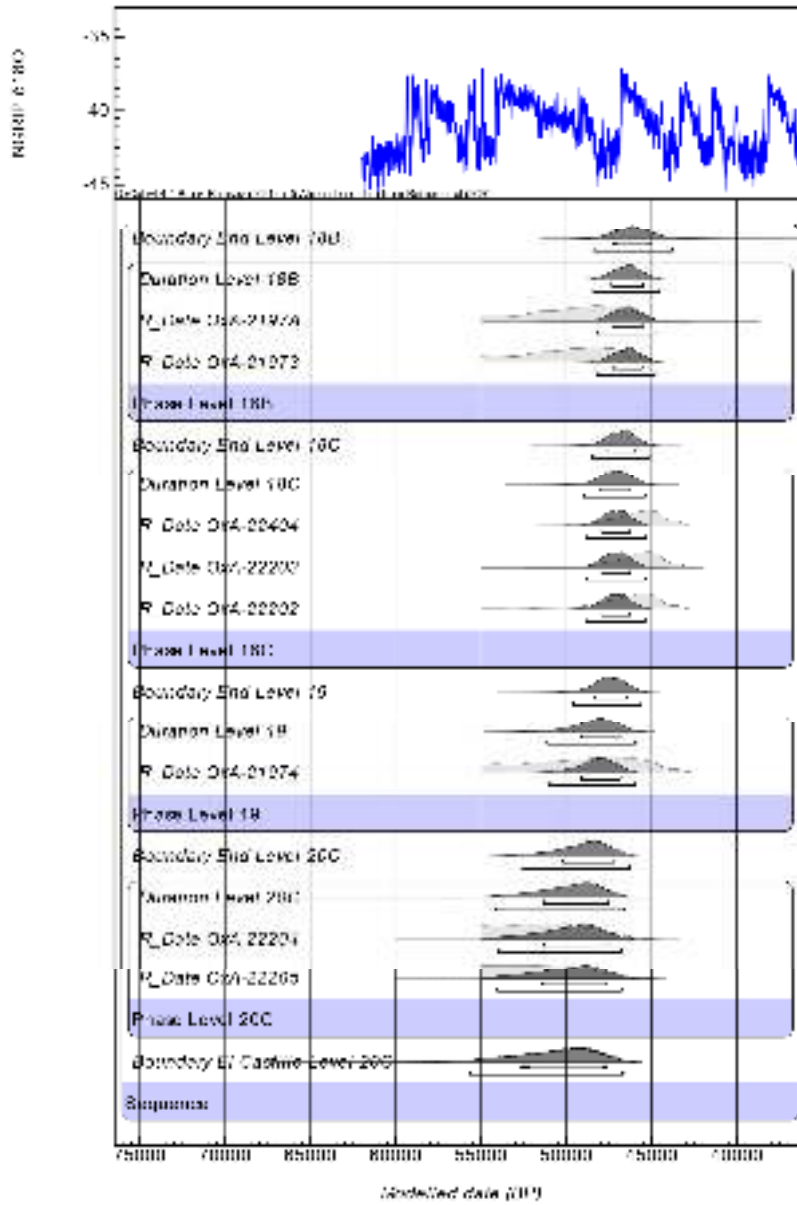
1993 Wood, R., Bernaldo de Quirós, F., Maíllo-Fernández, J.M., Tejero, J.M., Neira, A., Higham, T. 2018. El Castillo (Cantabria, northern
1994 Iberia) and the Transitional Aurignacian: Using radiocarbon dating to assess site taphonomy. *Quaternary International*,
1995 474: 56–70.

1996 Yravedra, J., & Gómez-Castanedo, A. 2010. Estudio zoológico y tafonómico del yacimiento del Otero (Secadura, Voto,
1997 Cantabria). *Espacio, Tiempo y Forma. Serie I, Nueva época. Prehistoria y Arqueología*, 3: 21–38

1998 Zilhão, J., DEerriço, F. 2003. The chronology of the Aurignacian and Transitional technocomplexes. Where do we stand? In Zilhão,
1999 J. et d'Erriço, F. eds., *The chronology of the Aurignacian and of the transitional technocomplexes. Dating, stratigraphies,*
2000 *cultural implications. Proceedings of Symposium 61 of the XIVth Congress of the UISPP*, pp. 313–349.

2001

Formatted: English (United Kingdom)



2003

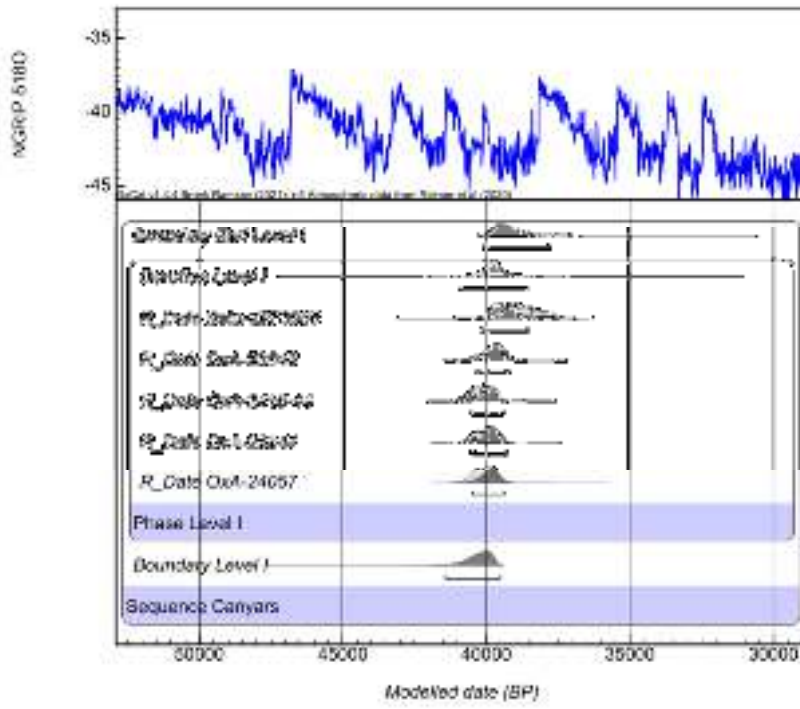
2004

2005

Figure C1. Radiocarbon dates from El Castillo modelled in OxCal4.4 against INTCAL20.

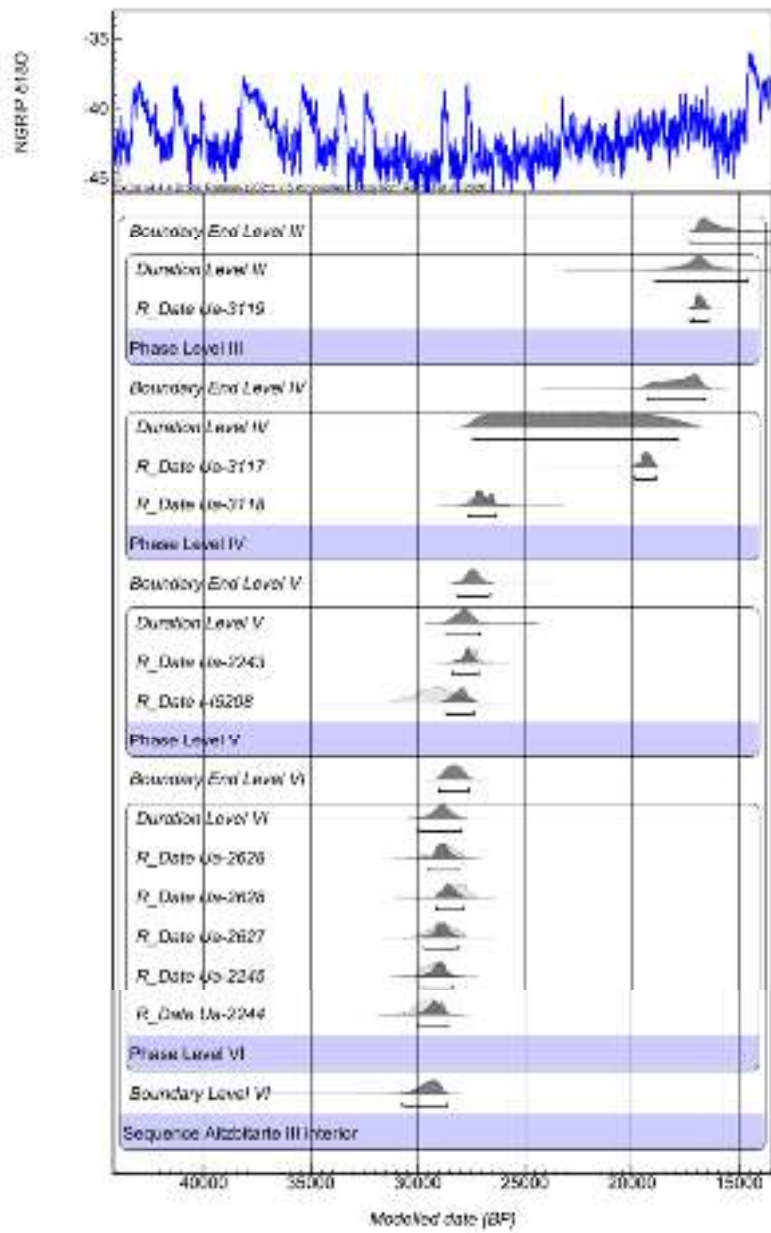
2008
2009

Figure C2. Radiocarbon dates from Labeko Koba modelled in OxCal4.4 against INTCAL20.



2010
2011
2012

Figure C3. Radiocarbon dates from Canyars modelled in OxCal4.4 against INTCAL20.



2013

2014

Figure C4. Radiocarbon dates from Aitzbitarte III-interior modelled in OxCal4.4 against INTCAL20.

2015 **Results of Bayesian Models**

El Castillo	Unmodelled (BP)			Modelled (BP)			Indices Amodel 78.8, Aoverall 82.4			
	from	to	%	from	to	%	A	L	P	C
Boundary End Level 18B				48383	43733	95.449.974				97.1
Duration Level 18B				48438	44536	95.449.974				99.8
R_Date OxA-2197A	...	45427	95.449.973	48235	44793	95.449.974	98.1		95.2	99.8
R_Date OxA-21973	...	45655	95.449.973	48240	44793	95.449.974	91.9		95.2	99.8
Phase Level 18B										
Boundary End Level 18C				48470	45117	95.449.974				99.8
Duration Level 18C				48977	45382	95.449.974				99.9
R_Date OxA-22404	49976	42918	95.449.974	48833	45383	95.449.974	82.2		95.3	99.8
R_Date OxA-22203	49451	42999	95.449.974	48819	45381	95.449.974	76.1		95.2	99.8
R_Date OxA-22202	51146	43039	95.449.974	48861	45386	95.449.974	101.2		95.4	99.8
Phase Level 18C										
Boundary End Level 19				49629	45623	95.449.974				99.7
Duration Level 19				51060	45997	95.449.974				99.7
R_Date OxA-21974	...	44367	95.449.974	50965	45998	95.449.974	120.2		95.3	99.8
Phase Level 19										
Boundary End Level 20C				52583	46286	95.449.974				99.5
Duration Level 20C				54134	46593	95.449.974				99.3
R_Date OxA-22204	...	47048	95.449.974	53958	46713	95.449.974	94		95.3	99.3
R_Date OxA-22205	...	47348	95.449.974	53965	46715	95.449.974	86.9		95.3	99.3
Phase Level 20C										
Boundary El Castillo Level 20C				55552	46609	95.449.974				95.3
Sequence										
U(0)	68.268.949	3.99E-17	4	68.268.949	5.38E-17	3.776		100		
T(5)	-2.65	2.65	95.449.974							99.9
Outlier_Model General				-2684	2502	95.449.974				100

2016

Table C1. Radiocarbon dates from El Castillo modelled in OxCal4.4 against INTCAL20.

Aitzbitarte III Interior	Unmodelled (BP)			Modelled (BP)			Indices Amodel 78.8, Aoverall 82.4			
	from	to	%	from	to	%	A	L	P	C
Boundary End Level III				17300	12910	9.544.997				98
Duration Level III				18960	14630	9.544.997				99.6
R_Date Ua-3119	17270	16390	9.544.997	17300	16430	9.544.997	100.8		95.8	99.8
Phase Level III										
Boundary End Level IV				19320	16640	9.544.997				99.3
Duration Level IV				27430	17820	9.544.997				98.9
R_Date Ua-3117	19830	18900	9.544.997	19840	18910	9.544.997	99.9		95.3	99.6
R_Date Ua-3118	27700	26430	9.544.997	27600	26360	9.544.997	98.1		95.2	99.5
Phase Level IV										
Boundary End Level V				28210	26680	9.544.997				99.7
Duration Level V				28680	27130	9.544.997				99.9
R_Date Ua-2243	28260	26610	9.544.997	28370	27190	9.544.997	88.8		95.4	99.8
R_Date I-15208	30830	27760	9.544.997	28710	27370	9.544.997	57.7		94.8	99.8
Phase Level V										
Boundary End Level VI				29010	27630	9.544.997				99.7
Duration Level VI				29990	27930	9.544.997				99.8
R_Date Ua-2628	29760	27840	9.544.997	29570	28080	9.544.997	118.2		96	99.8
R_Date Ua-2628	28760	27360	9.544.997	29150	27920	9.544.997	67		94.3	99.8
R_Date Ua-2627	29920	27870	9.544.997	29680	28110	9.544.997	120.5		96	99.8
R_Date Ua-2245	30070	28280	9.544.997	29820	28360	9.544.997	108		95.9	99.8
R_Date Ua-2244	30720	28760	9.544.997	30010	28570	9.544.997	77.7		94.9	99.7
Phase Level VI										
Boundary Level VI				30730	28650	9.544.997				96
Sequence										
U(0,4)	3.99E-17	4	9.544.997	5.38E-17	3.772	9.544.997	100			99
T(5)	-2.65	2.65	9.544.997							95.5
Outlier_Model General				-1420	1280	9.544.997				99.9

2018

Table C2. Radiocarbon dates from Labeko Koba modelled in OxCal4.4 against INTCAL20.

2019

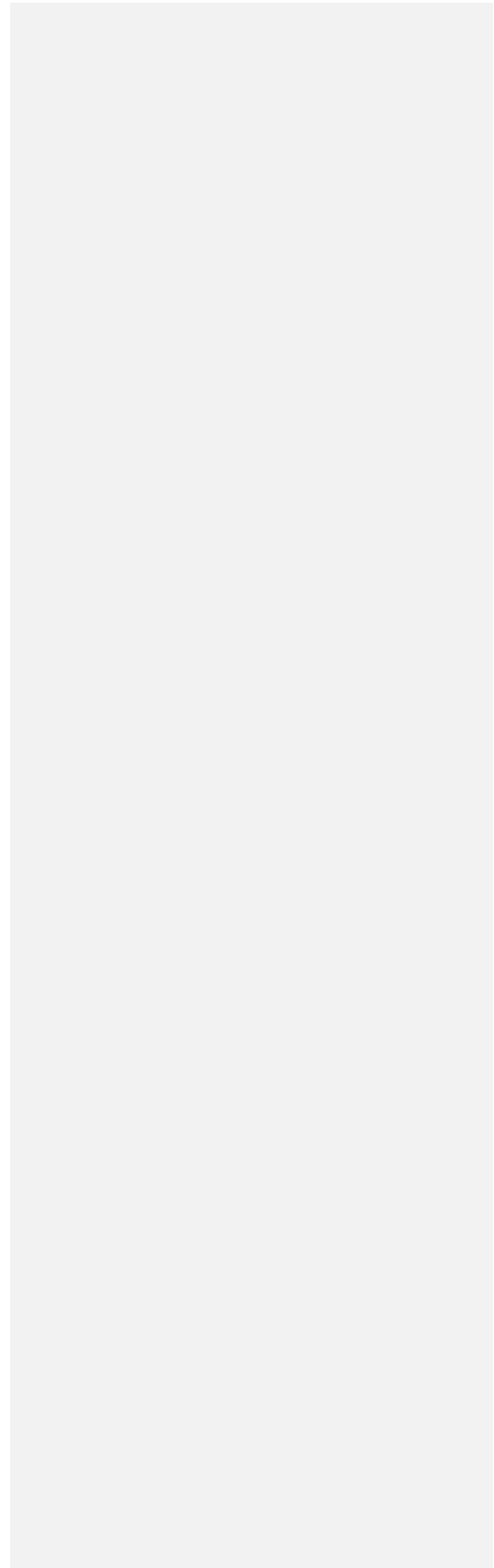
Canyars	Unmodelled (BP)			Modelled (BP)			Indices Amodel 78.8, Aoverall 82.4		
Boundary End Level I				40090	37770	95.45			95.3
Duration Level I				40890	38530	95.45			99.7
R_Date Beta-2273965	39630	37570	9.544.997	40190	38560	95.45	63.2	93.4	99.6
R_Date OxA-23643	40520	39140	9.544.997	40330	39240	95.45	114.2	96.1	99.8
R_Date OxA-2416-44	40880	39450	9.544.997	40540	39400	95.45	99.2	96	99.8
R_Date OxA-23644	40740	39300	9.544.997	40470	39340	95.45	110.5	96	99.8
R_Date OxA-24057	40790	39390	9.544.997	40490	39380	95.45	104.3	96	99.8
Phase Level I									
Boundary Level I				41450	39500	95.45			96.6
Sequence Canyars									
U(0,4)	3.99E-17	4	9.544.997	5.38E-17	3.82	95.45	100		100
T(5)	-2.65	2.65	9.544.997						99.4
Outlier_Model General				-800	1480	95.45			99.9

Table C3. Radiocarbon dates from Canyars modelled in OxCal4.4 against INTCAL20.

Labeko Koba	Unmodelled (BP)			Modelled (BP)			Indices Amodel 78.8, Aoverall 82.4			
	from	to	%	from	to	%	A	L	P	C
Boundary End Level IV				38710	32030	9.544.997				98.4
Duration Level IV				39000	33710	9.544.997				99.8
R_Date OxA-21768	39700	37030	9.544.997	39050	33820	9.544.997	75.5		80	99.8
R_Date OxA-21780	39780	36910	9.544.997	39050	33960	9.544.997	81.3		82.3	99.8
Phase Level IV										
Boundary End Level V				39470	35440	9.544.997				99.8
Duration Level V				39730	35950	9.544.997				99.8
R_Date OxA-21779	41170	38260	9.544.997	39830	36330	9.544.997	21		87.2	99.8
R_Date OxA-21767	41230	38500	9.544.997	39860	36340	9.544.997	15.5		85.5	99.8
Phase Level V										
Boundary End Level VI				40240	36360	9.544.997				99.8
Duration Level VI				41030	37860	9.544.997				99.9
R_Date OxA-21841	37710	35420	9.544.997							
R_Date OxA-21794	38040	35460	9.544.997							
R_Combine comb:23689	37350	35900	9.544.997	40620	36500	9.544.997	4.3			99.8
R_Date OxA-21778	41390	39190	9.544.997	40970	38550	9.544.997	90		94.4	99.9
Phase Level VI										
Boundary End Level VII				41490	38890	9.544.997				99.9
Duration Level VII				41910	39570	9.544.997				99.9
R_Date OxA-21840	41610	39250	9.544.997							
R_Date OxA-21793	41720	39390	9.544.997							
R_Combine comb:23688	41290	39570	9.544.997	41650	39780	9.544.997	87.3			99.9
R_Date OxA-X-2314-43	42350	40260	9.544.997	41900	40000	9.544.997	96.5		95.4	99.9
R_Date OxA-21766	42520	40530	9.544.997	41950	40020	9.544.997	80.3		94.6	99.9
Phase Level VII										
Boundary End Level IX upper				42190	40360	9.544.997				99.9
Duration Level IX upper				42750	40580	9.544.997				99.9
R_Date OxA-22559	42090	39850	9.544.997							
R_Date OxA-22653	42520	40530	9.544.997							
R_Combine comb:27311	42120	40600	9.544.997	42330	40800	9.544.997	95			99.9
R_Date OxA-21792	42370	40330	9.544.997	42380	40820	9.544.997	113.4		95.7	99.9
R_Date OxA-21777	43160	40960	9.544.997	42600	40950	9.544.997	99.5		95.6	99.9
R_Date OxA-23199	43980	41490	9.544.997	42800	40990	9.544.997	52.4		92.8	99.9
Phase Level IX upper										
Boundary End Level IX inf				43420	40970	9.544.997				99.9
Duration Level IX inf				48940	41340	9.544.997				99.8
R_Date OxA-22560	42780	40980	9.544.997	49670	41300	9.544.997	75.3		76	99.8
R_Date OxA-22562	43830	41220	9.544.997	45860	41380	9.544.997	102.8		90.9	99.8
R_Date OxA-22563	43250	41010	9.544.997	46280	41300	9.544.997	99.1		89.7	99.8
R_Date OxA-22561	43790	41130	9.544.997	45920	41340	9.544.997	102.3		90.7	99.8
R_Date OxA-22564	43370	41050	9.544.997	46060	41320	9.544.997	101		90.2	99.8
Phase Level IX inf										
Boundary Labeko Level IX inf				52660	41740	9.544.997				96.6
Sequence Labeko Koba										
N(0,2)	-4	4	9.544.997							99.4
Outlier_Model SSimple				...	840	9.544.997				97.5
U(0,4)	3.99E-17	4	9.544.997	5.38E-17	3.932	9.544.997	100			98.3
T(5)	-2.65	2.65	9.544.997							97.5
Outlier_Model General				-6130	9280	9.544.997				99.4

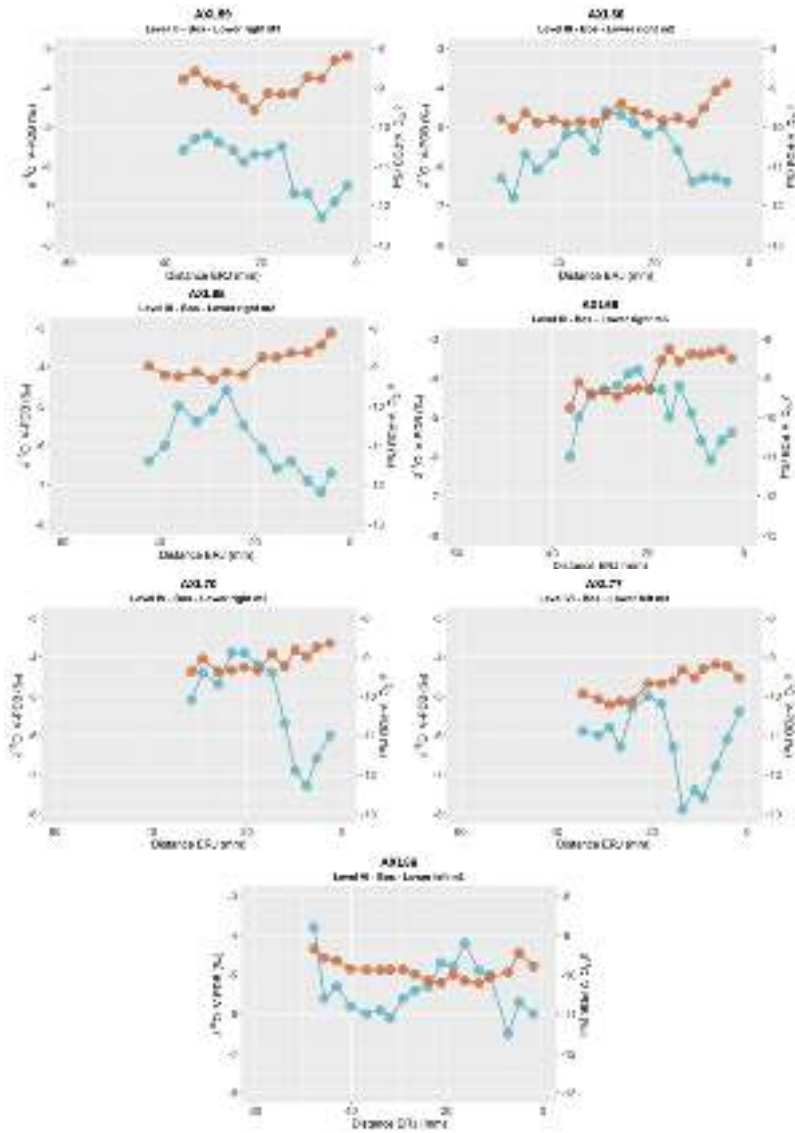
Table C4. Radiocarbon dates from Aitzbitarte III-interior modelled in OxCal4.4 against INTCAL20.

2025



2026 **Appendix CD. Intratooth curve plots**

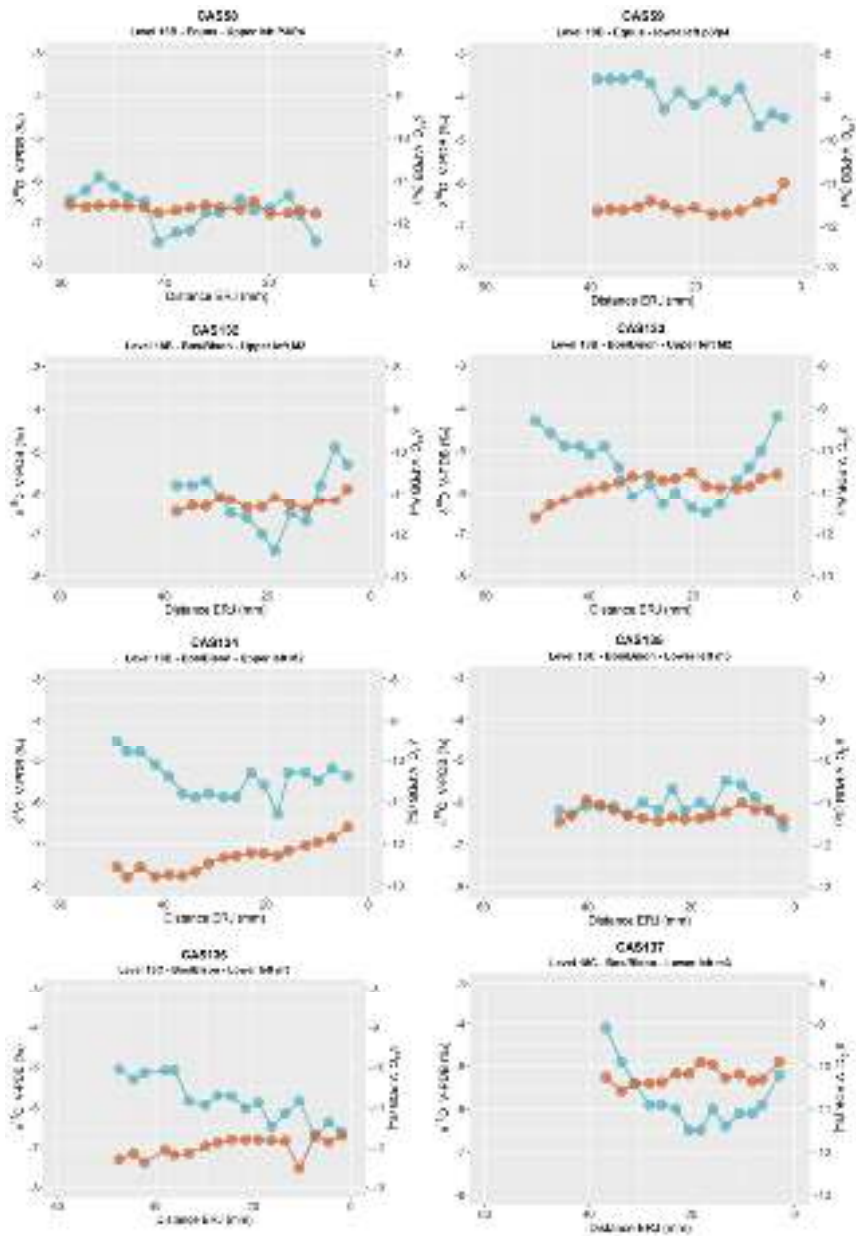
2027 Original curves derived from enamel intratooth sampling on enamel carbonate. Provided by sites. In blue,
 2028 oxygen stable isotope composition ($\delta^{18}\text{O}$), and, in brown, carbon stable isotope composition ($\delta^{13}\text{C}$). In the
 2029 x-axis, the distance from Enamel Root Junction (ERJ). Notice that the y-axis can experience some
 2030 variations between sites.



2031
 2032 **Figure DC1.** Intratooth plots of oxygen ($\delta^{18}\text{O}$) and carbon ($\delta^{13}\text{C}$) isotope composition from teeth from Axlor, considering distance
 2033 from enamel root junction (ERC).

2034

2035

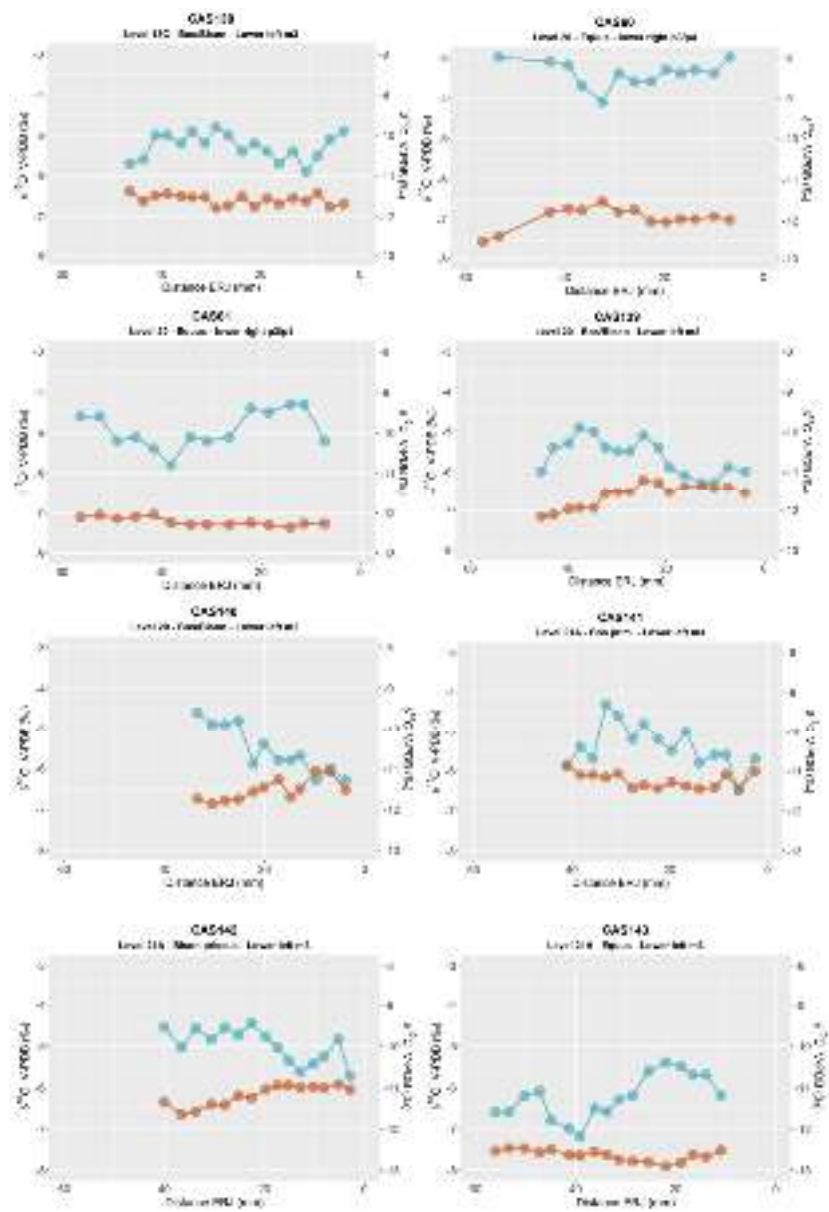


2036

2037

2038

Figure D62. Intra-tooth plots of oxygen ($\delta^{18}\text{O}$) and carbon ($\delta^{13}\text{C}$) isotope composition from teeth from El Castillo, considering the sample's distance from the enamel root junction (ERC).



2039

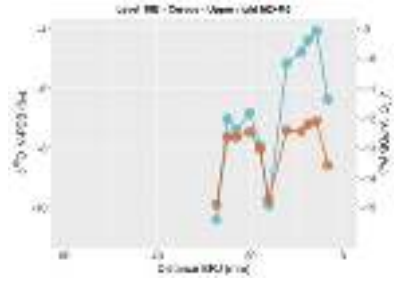
2040

2041

2042

Figure DC3. Intratooth plots of oxygen ($\delta^{18}\text{O}$) and carbon ($\delta^{13}\text{C}$) isotope composition from teeth from El Castillo, considering the sample's distance from the enamel root junction (ERC).

2043

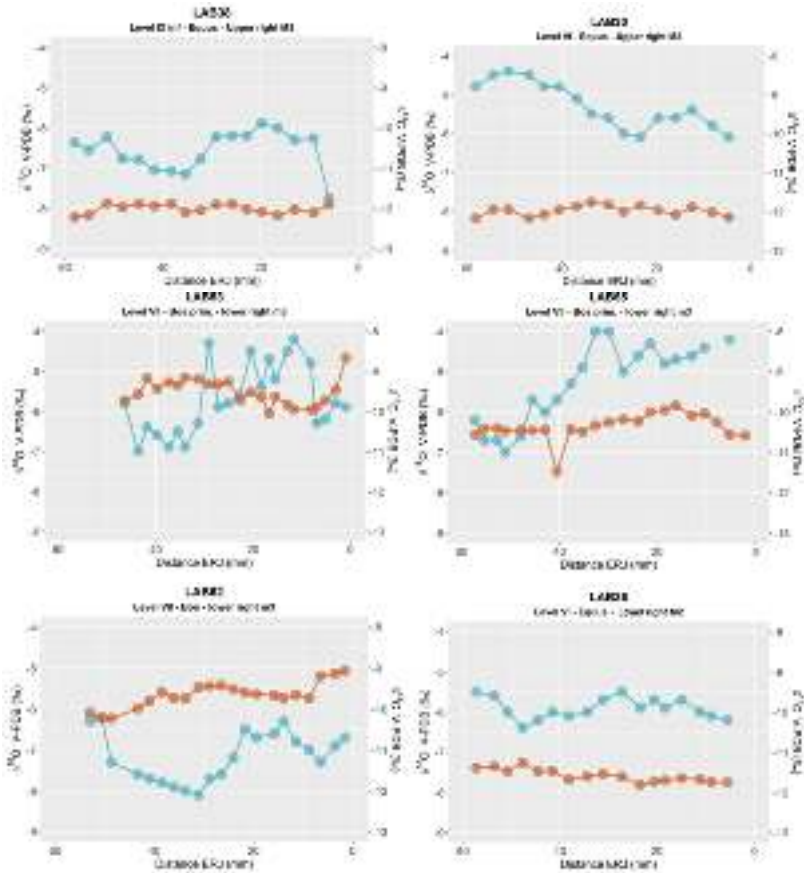


2044

2045
2046

Figure DC4. Intratooth plots of oxygen ($\delta^{18}\text{O}$) and carbon ($\delta^{13}\text{C}$) isotope composition from teeth from El Castillo, considering the sample's distance from the enamel root junction (ERC).

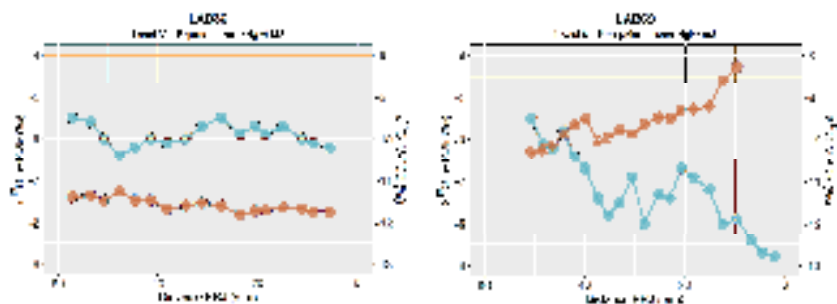
2047



2048

2049
2050

Figure DC5. Intratooth plots of oxygen ($\delta^{18}\text{O}$) and carbon ($\delta^{13}\text{C}$) isotope composition from teeth from Labeko Koba, considering the sample's distance from the enamel root junction (ERC).



2051

2052

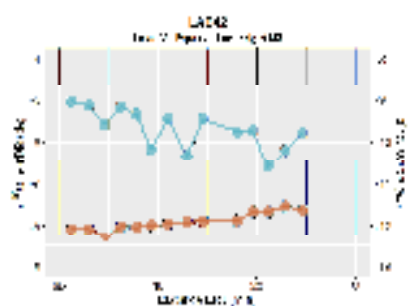
2053

2054

2055

2056

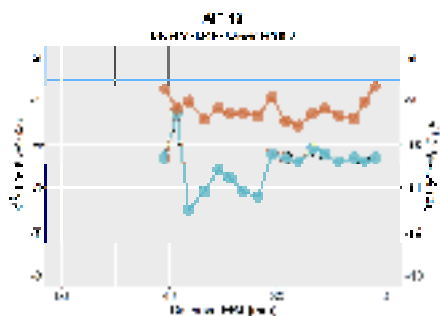
2057



2058 **Figure DC6.** Intratooth plots of oxygen ($\delta^{18}\text{O}$) and carbon ($\delta^{13}\text{C}$) isotope composition from teeth from Labeko Koba, considering
2059 the sample's distance from the enamel root junction (ERC).

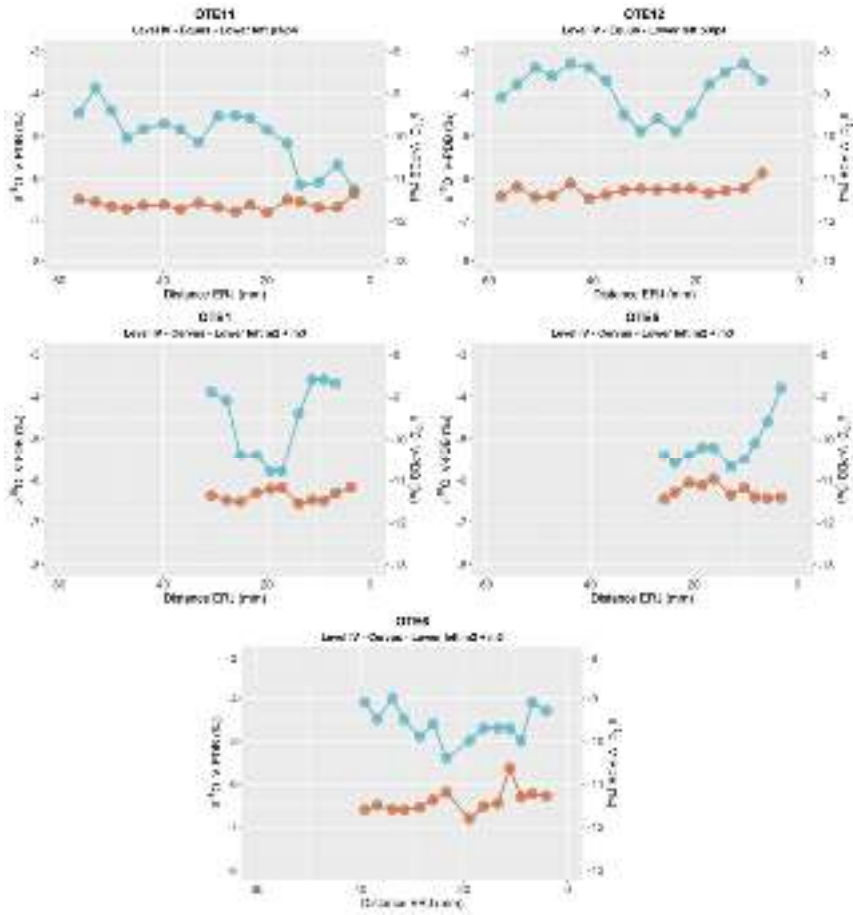
2060

2061



2062

2063 **Figure CD7.** Intratooth plots of oxygen ($\delta^{18}\text{O}$) and carbon ($\delta^{13}\text{C}$) isotope composition from teeth from Aitzbitarte III [interior](#),
2064 considering the sample's distance from the enamel root junction (ERC).

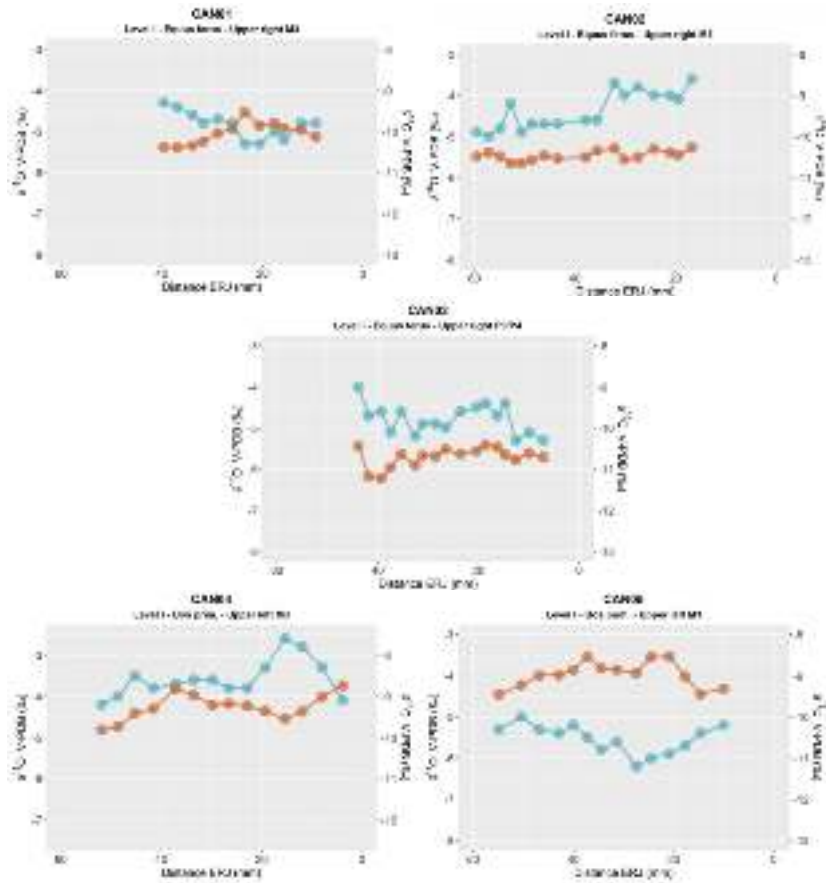


2065

2066

2067

Figure Dc8. Intratooth plots of oxygen ($\delta^{18}\text{O}$) and carbon ($\delta^{13}\text{C}$) isotope composition from teeth from El Otero, considering the sample's distance from the enamel root junction (ERC).



2068

2069

2070

2071

Figure DC9. Intratooth plots of oxygen ($\delta^{18}\text{O}$) and carbon ($\delta^{13}\text{C}$) isotope composition from teeth from Canyars considering the sample's distance from the enamel root junction (ERC).

2072 **Appendix ED. Inverse Modelling: Methodological Details and Models**

2073 The intratooth $\delta^{18}\text{O}$ profiles presented in this study were obtained through the application of inverse
2074 modelling, using an adapted version of the code published in reference (Passey et al., 2005b). This
2075 modeling approach allowed for the correction of the damping effect and the reconstruction of the original
2076 $\delta^{18}\text{O}$ input time series. The model reproduces the temporal delay between $\delta^{18}\text{O}$ changes in the
2077 animal's input and their manifestation in tooth enamel, exhibiting a consistent x-direction delay in the
2078 modelled $\delta^{18}\text{O}$ curve relative to the enamel $\delta^{18}\text{O}$ input time series. The model utilizes different species-
2079 specific parameters related to enamel formation, which vary between bovines and equids. These parameters
2080 have been established based on previous studies (Bendrey et al., 2015; Zazzo et al., 2012; Passey and
2081 Cerling, 2002; Kohn, 2004; Blumenthal et al., 2014). For *Bos/Bison* sp., the initial mineral content of enamel
2082 is fixed at 25%, the enamel appositional length is set at 1.5 mm, and the maturation length is 25 mm. For
2083 *Equus* sp., the initial mineral content of enamel is fixed at 22%, the enamel appositional length is set at 6
2084 mm, and the maturation length is 28 mm.

2085 In addition, the model requires other variables related to sampling geometry, as well as error estimates
2086 derived from mass spectrometer measurements. The distance between samples varies for each tooth, but
2087 as a general trend, the sampling depth on the tooth enamel surface in the samples of this study represents
2088 approximately 70% of the total enamel depth. The standard deviation of the measurements obtained from
2089 the mass spectrometer was typically set at 0.12%, taking into account the uncertainty associated with the
2090 standards. Finally, the models require a damping factor that determines the cumulative damping along the
2091 isotopic profile by adjusting the measured error (E_{meas}) to the prediction error (E_{pred}). In the teeth analysed
2092 in this study, the damping factor ranged from 0.001 to 0.1.

2093 The most likely model solutions were selected, and summer and winter values were extracted from the $\delta^{18}\text{O}$
2094 profiles, considering the original peaks and troughs identified in the unmodelled $\delta^{18}\text{O}$ profile. This approach
2095 was adopted to prevent the introduction of artificial peaks that the model may produce, particularly in teeth
2096 without a distinct sinusoidal shape. Flat and less sinusoidal profile are less suitable for the application of the
2097 model, given its inherent assumption of an approximately sinusoidal form. Non-sinusoidal curves can lead
2098 to complex interpretations in the model outcomes. Consequently, this methodology was not applied to
2099 analysed intratooth $\delta^{13}\text{C}$ profiles, as the examined individuals did not exhibit appreciable seasonal change.

2100

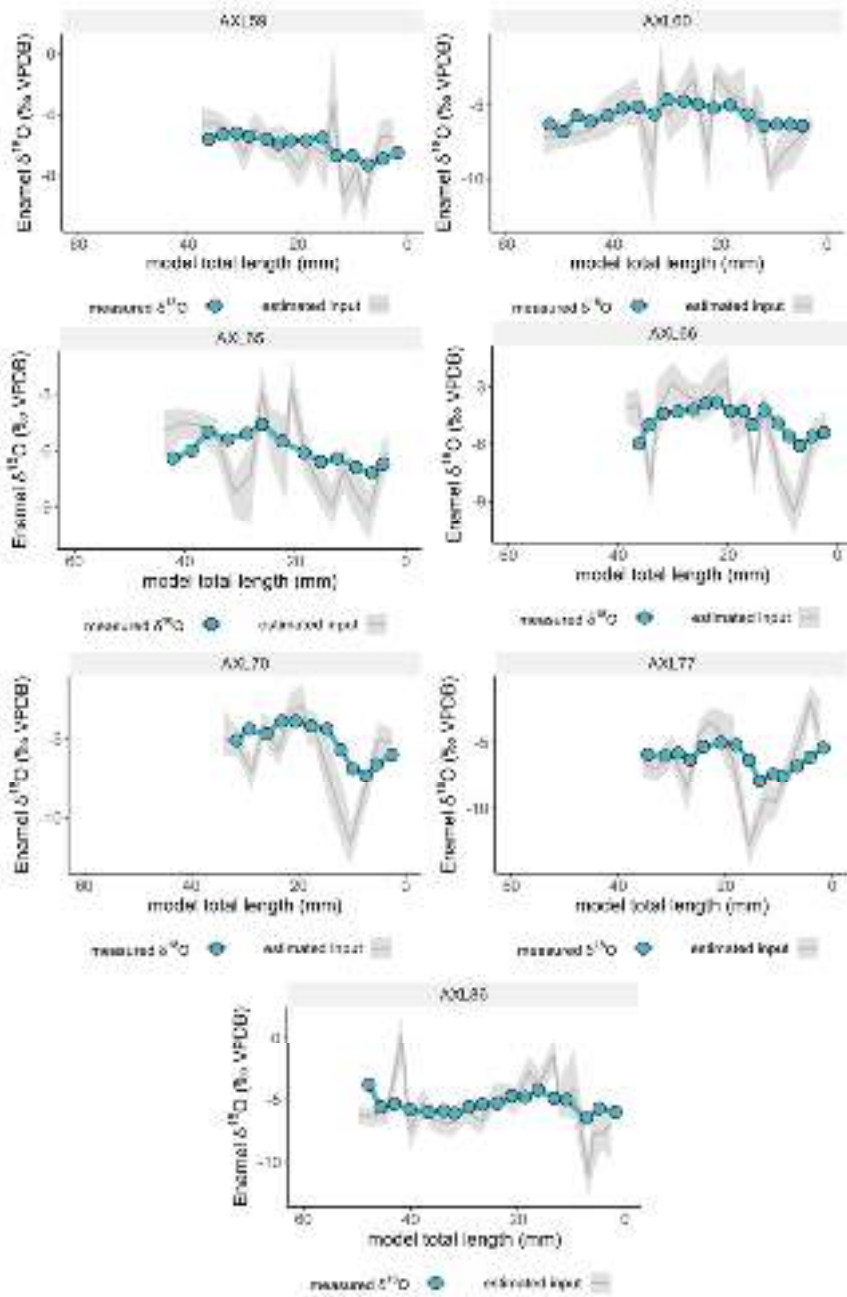
Formatted: Superscript

Formatted: Font: Italic

Formatted: Font: Italic

Formatted: Superscript

Formatted: Superscript



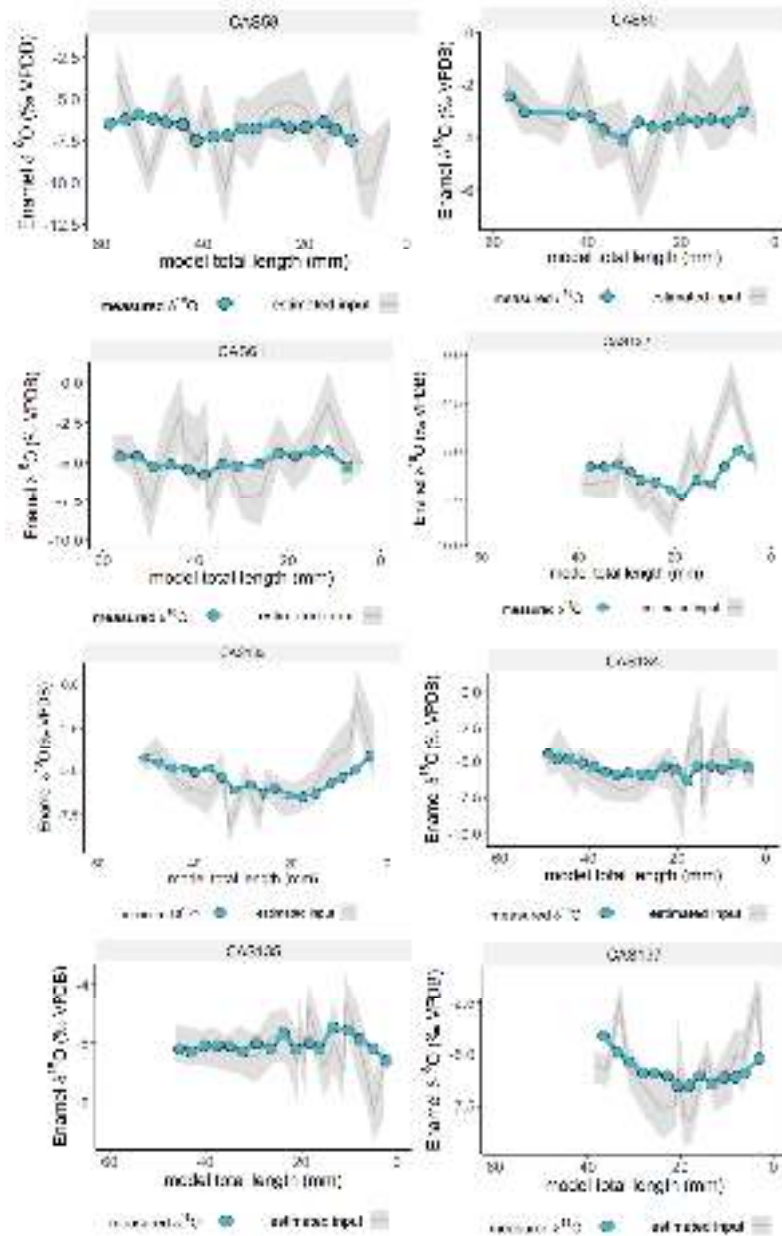
2101

2102

2103

2104

Figure ED1. Inverse models for oxygen isotope composition ($\delta^{18}\text{O}$) from teeth from Axlor, considering distance from enamel root junction. The blue line and points correspond to original data and grey line the most likely model solution, with the 95% confidence interval shown in shaded areas.



2106

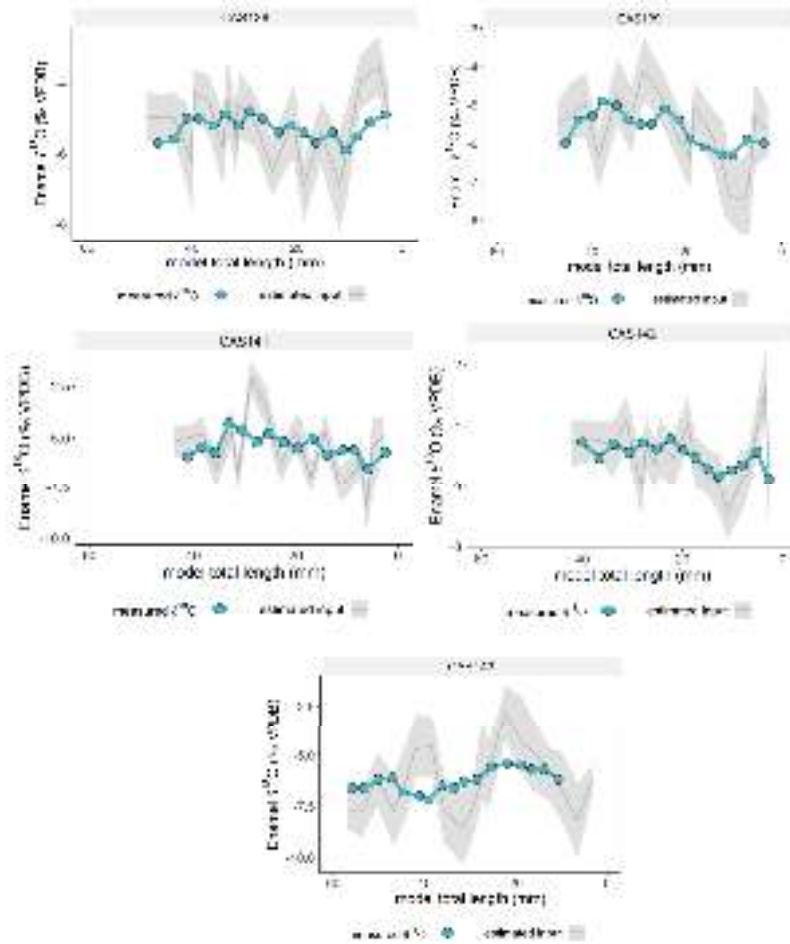
2107

2108

2109

Figure EB2. Inverse models for oxygen isotope composition ($\delta^{18}\text{O}$) from teeth from El Castillo, considering distance from enamel root junction. The blue line and points correspond to original data and grey line the most likely model solution, with the 95% confidence interval shown in shaded areas.

2110



2111

2112

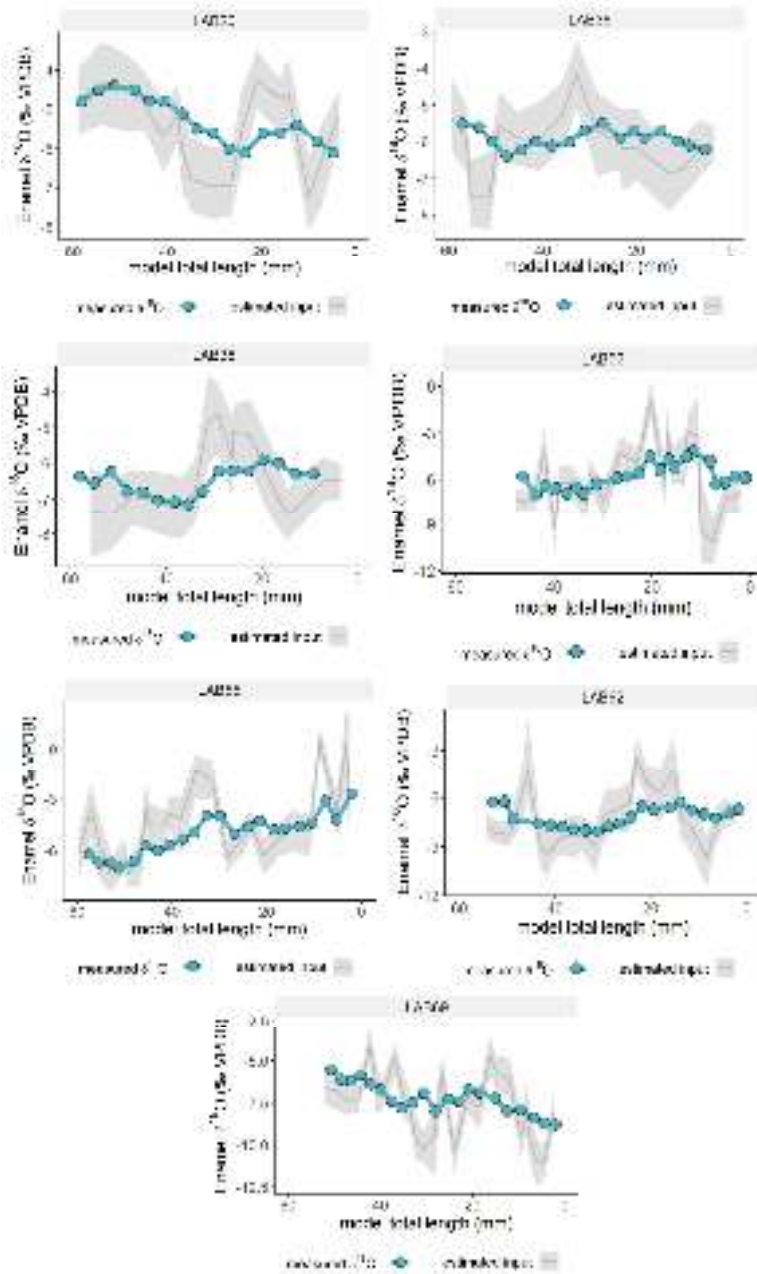
2113

2114

2115

2116

Figure EB3. Inverse models for oxygen isotope composition ($\delta^{18}\text{O}$) from teeth from El Castillo, considering distance from enamel root junction. The blue line and points correspond to original data and grey line the most likely model solution, with the 95% confidence interval shown in shaded areas.



2117

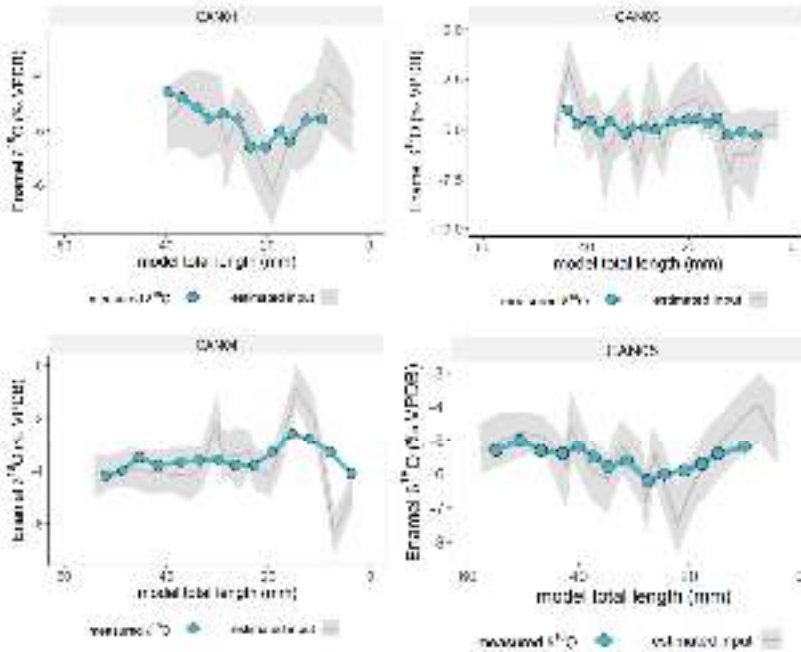
2118

2119

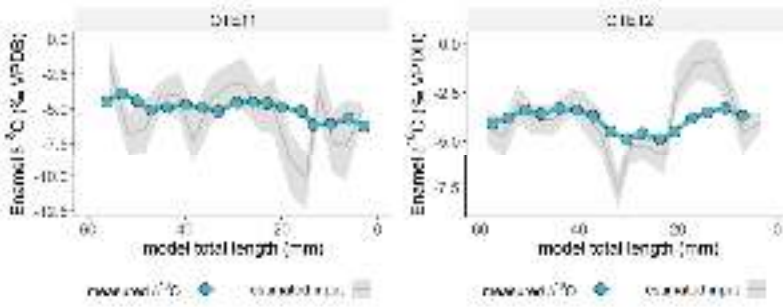
2120

Figure ED4. Inverse models for oxygen isotope composition ($\delta^{18}\text{O}$) from teeth from Labeko Koba, considering distance from enamel root junction. The blue line and points correspond to original data and grey line the most likely model solution, with the 95% confidence interval shown in shaded areas.

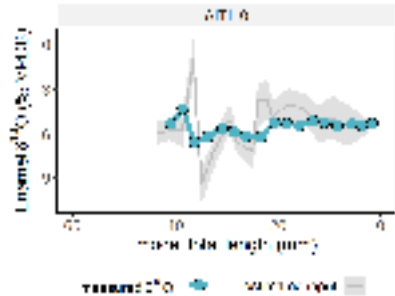
2121



2122
2123 **Figure ED5.** Inverse models for oxygen isotope composition ($\delta^{18}\text{O}$) from teeth from Canyars considering distance from enamel root junction. The
2124 blue line and points correspond to original data and grey line the most likely model solution, with the 95% confidence interval shown in shaded
2125 areas.



2126
2127 **Figure ED6.** Inverse models for oxygen isotope composition ($\delta^{18}\text{O}$) from teeth from El Otero, considering distance from enamel root junction. The
2128 blue line and points correspond to original data and grey line the most likely model solution, with the 95% confidence interval shown in shaded
2129 areas.



2130

2131

2132

2133

Figure DE7. Inverse models for oxygen isotope composition ($\delta^{18}\text{O}$) from teeth from Aitzbitarte III interior, considering distance from enamel root junction. The blue line and points correspond to original data and grey line the most likely model solution, with the 95% confidence interval shown in shaded areas.

2134

2135

References Appendix D

2136

Bendrey, R., Vella, D., Zazzo, A., Balasse, M., Lepetz, S., 2015. Exponentially decreasing tooth growth rate in horse teeth: implications for isotopic analyses. *Archaeometry* 57, 1104–1124. <https://doi.org/10.1111/arem.12151>

2137

Blumenthal, S.A., Cerling, T.E., Christ, K.L., Bromage, T.G., Kozdon, R., Valley, J.W., 2014. Stable isotope time-series in mammalian teeth: In situ $\delta^{18}\text{O}$ from the innermost enamel layer. *Geochimica et Cosmochimica Acta* 124, 223–236. <https://doi.org/10.1016/j.gca.2013.09.032>

2138

Kohn, M.J., 2004. Comment: Tooth Enamel Mineralization in Ungulates: Implications for Recovering a Primary Isotopic Time Series, by B. H. Passey and T. E. Cerling (2002). *Geochimica et Cosmochimica Acta* 68, 403–405. [https://doi.org/10.1016/S0016-7037\(03\)00443-5](https://doi.org/10.1016/S0016-7037(03)00443-5)

2139

Passey, B.H., Cerling, T.E., 2002. Tooth enamel mineralization in ungulates: implications for recovering a primary isotopic time-series. *Geochimica et Cosmochimica Acta* 66, 3225–3234. [https://doi.org/10.1016/S0016-7037\(02\)00933-X](https://doi.org/10.1016/S0016-7037(02)00933-X)

2140

Passey, B.H., Cerling, T.E., Schuster, G.T., Robinson, T.F., Roeder, B.L., Krueger, S.K., 2005. Inverse methods for estimating primary input signals from time-averaged isotope profiles. *Geochimica et Cosmochimica Acta* 69, 4101–4116. <https://doi.org/10.1016/j.gca.2004.12.002>

2141

Passey, B.H., Robinson, T.F., Ayliffe, L.K., Cerling, T.E., Sponheimer, M., Dearing, M.D., Roeder, B.L., Ehleringer, J.R., 2005. Carbon isotope fractionation between diet, breath CO_2 , and bioapatite in different mammals. *J. Archaeol. Sci.* 32, 1459–1470. <https://doi.org/10.1016/j.jas.2005.03.015>

2142

Zazzo, A., Bendrey, R., Vella, D., Moloney, A.P., Monahan, F.J., Schmidt, O., 2012. A refined sampling strategy for intra-tooth stable isotope analysis of mammalian enamel. *Geochimica et Cosmochimica Acta* 84, 1–13. <https://doi.org/10.1016/j.gca.2012.01.012>

2143

2144

2145

2146

2147

2148

2149

2150

2151

2152

2153

2154

2155